2. <u>Library loan and photocopying permit</u>

Title of Thesis: _Active Noise Control in Ducts using Adaptive_

Digital Filters

Candidate: _L.L.J. BILLET_

Three copies of the above thesis are now formally submitted for the degree
of _M Phil_ Should the Senate of the University award me either this
degree or another higher degree in respect of this thesis, I hereby agree
that from the date of the award + the thesis may be made available for
inter-library loan or for photocopying and that the abstract may be made
available for publication.

+ (or exceptionally the time stipulated under the proviso to reg. 20, viz_____

Signature:_███████_ Date: _4/11/1991_

University of Southampton

Faculty of Engineering and Applied Science

Active Noise Control in ducts using adaptive digital filters

M. Phil Thesis

by L. Billet

1992

SUMMARY

The propagation of sound in a duct can be actively controlled by introducing a secondary source driven to cancel the original sound wave produced by a primary source.

In this study we compare for the first time in the same conditions three adaptive time domain algorithms currently used for the active control of noise in ducts : the LMS (Least Mean Square) algorithm, the LMS algorithm with feedback cancellation and the infinite impulse response LMS algorithm.

Firstly we establish the theoretical basis necessary to calculate the optimal single channel controller. Secondly we study each algorithm through a practical realisation and through computer simulation using an appropriate electro-acoustic model of the real experiment. The infinite impulse response algorithm is found to be the most efficient one. Moreover we demonstrated that the imperfect frequency response of the transducers (microphone and loudspeakers) is responsible for most of the limitation of the active noise control system.

ACKNOWLEDGEMENTS

CONTENTS

LIST of FIGURES

CHAPTER I

INTRODUCTION

The Active Control of Sound is a direct consequence of the interference principle in a linear medium given by Huygens [1] in 1690 and demonstrated by Young [2] in optics at the beginning of the nineteenth century : an antiphased noise is superposed on an unwanted one. As a result, a zone of quiet can be obtained under certain conditions. In rooms, the general problem is of great complexity : the system has an important number of degrees of freedom in the spatial dimension which imply that significant attenuation is generally feasible only using multiple sources [17]. In ducts, below the cut-off frequency, the geometry of the problem is one-dimensional. Therefore, the attenuation of a broadband signal is possible using only a single source.

The relative simplicity of the physics in ducts explains the early attempts made to achieve active noise control in this domain. In 1934, P. Lueg [3] lodged a patent describing a "process of silencing sound oscillations" which already contains most of the features developed in modern systems : the oncoming sound, detected by a microphone is processed through a "controller" which drives a loudspeaker with a signal out of phase with the primary one. P. Lueg was conscious of the crucial point which is that the speed of sound is much slower than the speed with which electrical signals can propagate. Provided that the distance between the detection microphone and the secondary source is large enough, the system therefore has some time to predict the genuine secondary signal from collected information. In 1934, the state of the art of electronics was not advanced enough to enable Lueg's system to be a breakthrough in noise control.

The next significant step was not before the mid-1960's, induced by advances in technology and control theory. Jessel in 1968 [4] understood that the main utility of active noise control systems in ducts is to reduce low frequency noise. This point is of great interest since passive hardware is generally inefficient or bulky at low-frequencies and produces back pressure by obstructing the duct. Jessel and his successors [5] tried to compensate the limited capabilities of their analog controller

by using complex arrays of microphones and loudspeakers. The idea was to build directional sensors and actuators in order to minimize the coupling between the detection microphone and the secondary source. The optimal location for multiple sensors and actuators was established in an extensive theoretical study by Swinbanks [6] in 1973. Attenuation obtained with these multipole systems was excellent with pure tones but limited with broadband noise.

In the beginning of the 1980's, it was possible to implement the controller as a digital filter. Ross [7][8] described the physical system as a superposition of electric transfer functions, calculated the optimal transfer function of the controller and implemented it as a digital filter. Roure [9] introduced an acoustic model of the duct and the electroacoustic system and extended Ross's theoretical results to a formula which shows that the controller is independent of the reflection conditions at both ends. These frequency-domain methods [10] gave excellent results but suffered from a lack of flexibility : the controller was build into a fixed configuration which is a inconvenient in a fluctuating environment. At the same time several people were looking at the idea of an adaptive controller updated directly from the time domain signals [11] and in 1980 Chaplin made a successful system to cancel exhaust noise based upon a trial and error method [12]. Given the increasing power of digital signal processors and the results from adaptive filters theory developed by Widrow et al. [13] time domain methods became more and more popular and finally became more popular than frequency-domain methods.

Nowadays, one of the most successful algorithms for updating the controller is the "Least Mean Square" algorithm or LMS algorithm. The fact that even some people once devoted to frequency domain methods such as Roure in the LMA, Marseille, have turned to the LMS algorithm [14] signifies that it has started to become a kind of standard in active control. Both its simplicity and robustness make it so popular.

The LMS algorithm however has led to a large number of variations in the implementation of the controller; the controller can be an FIR [13] or an IIR filter [15], an echo canceller can be introduced to solve the problem of the feedback loop between the detection microphone and the secondary source [16]. All these structures have been tested independently but they have never been compared in the same experimental conditions. This point is going to be one of the major goals of this study. It is the first time that the three methods given above are implemented in the same experiment. In this way their performance will be judged more objectively.

Moreover, most of the previous studies have used simplistic models in computer simulations or theoretical calculations. In this report, we will try to analyse very

carefully the limiting factors in a single channel noise control system such as the length of the digital filters, the imperfection of the transducers, through intensive and realistic computer simulation.

The structure of the thesis is as follow :

Chapter II contains a theoretical analysis in the frequency domain. Following the work of Ross and Roure we deduce the optimal controller from a deterministic point of view.

Chapter III is an experimental validation of Roure's acoustic model developed in chapter II.

Chapter IV determines the optimal least squares controller under certain constraints : causality, imperfect secondary source, finite length and structure of the controller.

Chapter V is a description of the three LMS-like algorithms.

Chapter VI, which presents the major contribution of the thesis, contains the experimental and simulation results which enable us to compare the algorithms detailled in chapter V.

Chapter VII draws the general conclusions of this report and gives suggestion for further work.

CHAPTER II

THEORY

II.1 Description of a single channel system

The active noise control system described in this report and built at the signal processing and control group is depicted on **figure 2.1**. On a piece of pipe are mounted two loudspeakers and two microphones. The left hand speaker is supposed to represent the disturbing source (usually a pump or a fan in full scale realizations). In our case this primary source is fed with a white noise to simulate the most unpredictable signal. The controller W is connected to the detection microphone on the left and to the secondary loudspeaker on the right. This system works in a way similar to Lueg's (see introduction). The main difference is the addition of a microphone at the right hand or "downstream" end. This microphone collects the residual signal which can be used to update the controller as we shall see later.

Although the coupling between the secondary actuator and the detection sensor can be significantly reduced by using arrays of microphones and loudspeakers, we decided to build and study a single channel system for various reasons:

-We wanted to test the performance of the LMS algorithm in the most critical condition, i.e. with a high level of feedback corrupting the reference signal.

-The use of multiple microphone sensors and multipole actuators is a delicate problem. It requires perfectly matched microphones and good quality loudspeakers. Our choice was to demonstrate the feasibility of active noise control with cheap, relatively low-quality transducers.

The controller is aimed to minimize the signal at the error sensor. Several approaches have been proposed using different assumptions about the acoustics and the signal. We are going to follow Ross's approach who derives the frequency response of the controller.
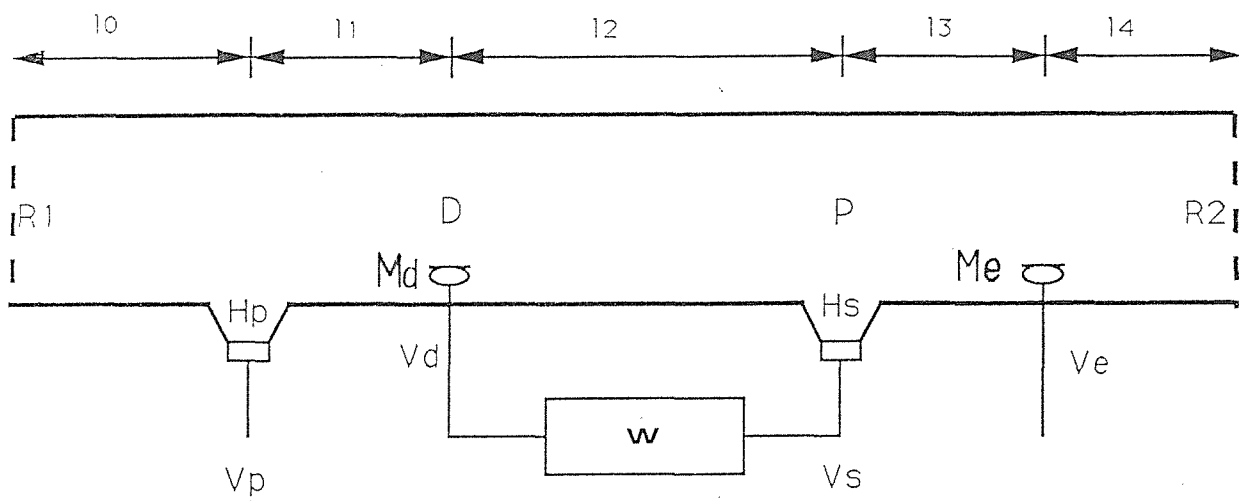
Up is the Primary signal
Us is the Secondary signal
Ud is the Detection microphone signal
Ue is the Error microphone signal

Figure 2.1 Description of the Active Noise Control System in duct used at the ISVR

II.2 Superposition principle

Ross' method relies upon the principle of superposition. All the electrical signal Ve, Vs, Vp, Vd (**figure 2.1**) are supposed to be linearly related. As a consequence the global system is characterized by a set of electrical transfer functions defined as follow :

$$A(j\omega) = \left[\frac{V_e(j\omega)}{V_p(j\omega)}\right]_{vs=0} \qquad B(j\omega) = \left[\frac{V_d(j\omega)}{V_p(j\omega)}\right]_{vs=0} \qquad (2.1)$$

$$C(j\omega) = \left[\frac{V_e(j\omega)}{V_s(j\omega)}\right]_{vp=0} \qquad F(j\omega) = \left[\frac{V_d(j\omega)}{V_s(j\omega)}\right]_{vp=0} \qquad (2.2)$$

This formulation enable us to represent the system as a block-diagram (**figure 2.2**) which shows clearly a feedback loop F between the controller output and its input. The description above is extremely general since there is no need to think of any transducer. The system is seen from its inputs and outputs only. However, to apply the principle of superposition we have to assume that all components in the system (acoustic, electrical and electroacoustic) are linear. This is true provided that the transducers are used in a suitable dynamic range. Provided that the frequency of the signals is below the cut-off frequency of the duct, the waves remain plane, so, driving the single error signal to zero will suppress the downstream propagating acoustic wave.

In this case we can write

$$Ve(j\omega) = A(j\omega).Vp(j\omega) + C(j\omega).Vs(j\omega) \qquad (2.3)$$

and

$$Vs(j\omega) = W(j\omega).(B(j\omega).Vp(j\omega) + F(j\omega).Vs(j\omega)) \qquad (2.4)$$

with W(jω) the non time varying controller transfer function.
And we deduce

$$Vs(f) = \frac{W(j\omega).B(j\omega).Vp(j\omega)}{1 - W(j\omega).F(j\omega)} \qquad (2.5)$$
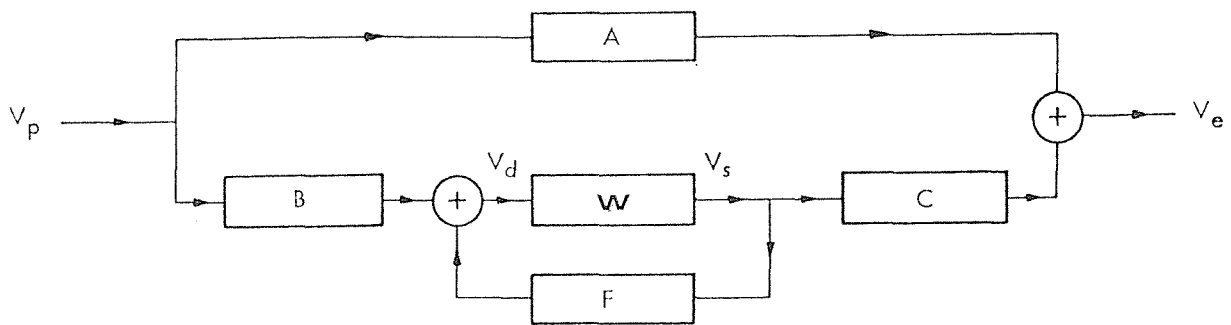
Figure 2.2 Block diagram resulting from the superposition principle.

(2.3) and (2.5) lead to

$$Ve(j\omega) = \frac{A(j\omega) - A(j\omega).W(j\omega).F(j\omega) + C(j\omega).W(j\omega).B(j\omega)}{1 - W(j\omega).F(j\omega)}.Vp(j\omega) \qquad (2.6)$$

(provided that $1 - W(s).F(s)$ has no roots in the right hand s plane)
The cancellation downstream is perfect if $\qquad Ve(j\omega) = 0$ for all ω

which, according to (2.6) is equivalent to

$$A(j\omega) - A(j\omega).W_{ideal}(j\omega).F(j\omega) + C(j\omega).W(j\omega).B(j\omega) = 0 \text{ for all } \omega$$

assuming that

$$1 - W_{ideal}(j\omega).F(j\omega) \neq 0$$

leads to the following result

$$W_{ideal}(j\omega) = \frac{A(j\omega)}{A(j\omega).F(j\omega) - B(j\omega).C(j\omega)} \qquad (2.7)$$

The ideal controller transfer function can be derived from the individual transfer function A, B, C, F. Practically A, B, C, F can be estimated by random or swept sine excitation. Therefore it is possible to calculate an estimate of the ideal frequency response of the controller. If we want to implement the controller as a digital filter we can inverse Fourier transform this estimate to obtain a time domain impulse response. This is roughly the method employed by Ross and Roure to build their controller. It happens to work quite well but it is subject to some limitation:

-Since the condition to determine the controller is the perfect cancellation of the residual error, both signal and transfer function are supposed to be known with an infinite degree of accuracy. No uncorrelated measurement noise is assumed to be present in the microphone signals.

-The controller transfer function is supposed to be invertible by Fourier transform. In practice this may be not true and even if a stable inverse exists it may be non-causal. The impulse response has therefore to be truncated in order to be implemented as a digital filter.

-The transfer functions have to be measured prior to cancellation which prevents the system reacting to any fluctuation.

In order to limit these inconvenience an adaptive and recursive procedure was suggested to modify the controller transfer function [8] [9] [18] . The frequency response of the controller is derived from the previous estimate and a measure of the residual sound spectrum. The new filter at the next step is then

$$W_{i+1}(j\omega) = U(j\omega)W_i(j\omega) \tag{2.8}$$

where $U(j\omega)$ is some function of the residual field and $W_i(j\omega)$ is the transfer function of the actual controller. Even if this method improves the performance of the system it still requires an inverse Fourier transform and a time windowing at each step. The effect of these transformations are extremely difficult to formalize and therefore the convergence properties of this algorithm are not well understood.

In the case where the calculated controller $W(j\omega)$ is not identical to the ideal one, because of measurement error for instance, the error signal is not driven to zero. The reduction can be expressed as in [35]

$$\Delta(j\omega) = \frac{error(system\ on)}{error(system\ off)}$$

$$\Delta(j\omega) = \frac{Ve(j\omega)}{A(j\omega)Vp(j\omega)} \tag{2.9}$$

from (2.6)

$$A(j\omega) = \frac{A(j\omega) - W(j\omega).(A(j\omega)\ F(j\omega) - C(j\omega).B(j\omega))}{A(j\omega)\ (1 - W(j\omega).F(j\omega))}$$ (2.10)

and from (2.7)

$$A(j\omega) = \frac{A(j\omega) - A(j\omega)\dfrac{W(j\omega)}{W_{ideal}(j\omega)}}{A(j\omega)\ (1 - W(j\omega).F(j\omega))}$$ (2.11)

so that

$$A(j\omega) = \frac{1 - \dfrac{W(j\omega)}{W_{ideal}(j\omega)}}{1 - W(j\omega).F(j\omega)}$$ (2.12)

If $W(j\omega) = W_{ideal}(j\omega)$ we find as expected that the cancellation is perfect.

II.3 Calculation of the individual transfer functions via an Electro-acoustic model

II.3.1. Notation

In order to extend Ross' results, Roure has described the individual transfer functions defined above in terms of the physical features of the duct and its transducers. Such a model has two qualities:

It leads to a remarkably simple expression of the ideal controller frequency response.

It is realistic enough to give a good basis for a computer simulation of great utility.

In Roure's paper both loudspeakers and microphones are defined by their electrical transfer functions and directivities. Since we have decided to study the

most simple case (monopole loudspeakers and simple omni-directional sensors) all directivities will be equal to unity and therefore invisible in the calculation. The convention will be as follow:

Hp(jω) = Primary source transfer function = pressure in anechoic duct per unit input voltage

Hs(jω) = Secondary source transfer function, defined by analogy with Hp(jω)

Md(jω) = Detection microphone transfer function = output voltage per unit pressure in the duct.

Me(jω) = Error microphone transfer function, defined by analogy with Md(jω)

The second assumption of the model is that sound waves travel without dispersion and attenuation along the duct. If the waves are plane, i.e. if the frequency is below the cut-off frequency, this is a reasonable assumption. As a consequence, given any point in the duct whose coordonate is x the sound pressure has the following general expression :

$$p(x,\omega) = P_+(\omega)e^{-j(kx-\omega t)} + P_-(\omega)e^{-j(kx+\omega t)} \tag{2.13}$$

$P_+(\omega)$ is the amplitude of the wave travelling to the right and $P_-(\omega)$ is the amplitude of the wave travelling to the left. Since the waves are non-dispersive k and ω are related to by

$$k = \omega/c$$

Where c is the frequency independent wave speed assumed in this case to equal 340 ms^{-1}.

Finally, the sound waves are supposed to be reflected and attenuated by a complex frequency dependent reflection coefficients $R_1(j\omega)$ on the left and $R_2(j\omega)$ on the right hand of the duct.

Once we have defined the electroacoustic-model we can calculate the different individual transfer functions. There are several different ways of calculating these expressions. The usual one is to do it in the frequency domain using the standard steady waves travelling theory (for a detailed description see ref [18], appendix I). Although these methods lead surely to the solution, we prefer to use its dual counterpart, a time domain calculation. Such a method gives a better understanding of the phenomena occurring in the duct.

II.3.2. Time Domain Expression

In this paragraph lower case letters will denote the impulse responses corresponding to transfer functions denoted by capital letters. Let us calculate $a(t)$, the impulse response between the primary source and the error microphone. Experimentally it could be obtained by applying an impulse in v_p and by measuring the corresponding signal $v_e(t)=a(t)$.

We are going to proceed the same way in our calculation.

Imagine we apply an impulse in v_p :

$$v_p(t)=v_0.\delta(t) \tag{2.14}$$

where v_0 is a constant and equal to 1 volt.

Since the loudspeaker is a monopole source its output $h_p(t)$ splits into two impulses travelling upstream and downstream (**figure 2.3**) $h^+_p(t)$ and $h^-_p(t)$

Consider the $h^+_p(t)$ impulse with reference to the lengths and reflection coefficients defined in **figure 2.1**. It first reaches the error microphone by travelling the distance $l_1+l_2+l_3$ and a second time after being reflected back by the end R_2 (distance $l_1+l_2+l_3+2l_4$) Similarly the impulse $h^-_p(t)$ is first reflected by R_1, reaches the microphone after the distance $2l_0+l_1+l_2+l_3$ is reflected by R_2 and finally arrives at the microphone after $2l_0+l_1+l_2+l_3+2l_4$.

The **figure 2.4** shows these four different types of reflection which lead us to the following first order expression for $a(t)$ assuming that the absorption due to the walls of the duct is negligible. ([*] is the convolution operator)

$$a'(t) \quad = \quad m_e(t)*\left(h_p(t - \frac{l_1+l_2+l_3}{c}) + \underset{II}{R_1(t)*h_p(t - \frac{2l_0+l_1+l_2+l_3}{c})} \right)$$
$$\underset{I}{}$$

$$+\underset{III}{R_2(t)*h_p(t - \frac{l_1+l_2+l_3+2l_4}{c})} + \underset{IV}{R_1(t)*R_2(t)*h_p(t - \frac{2l_0+l_1+l_2+l_3+2l_4}{c})} \right) \tag{2.15}$$

Where $m_e(t)$ is the impulse response of the error microphone.

Each of the four terms I II III IV correspond to each of the four reflections previously discussed. This is the main pattern. However the impulses do not stop
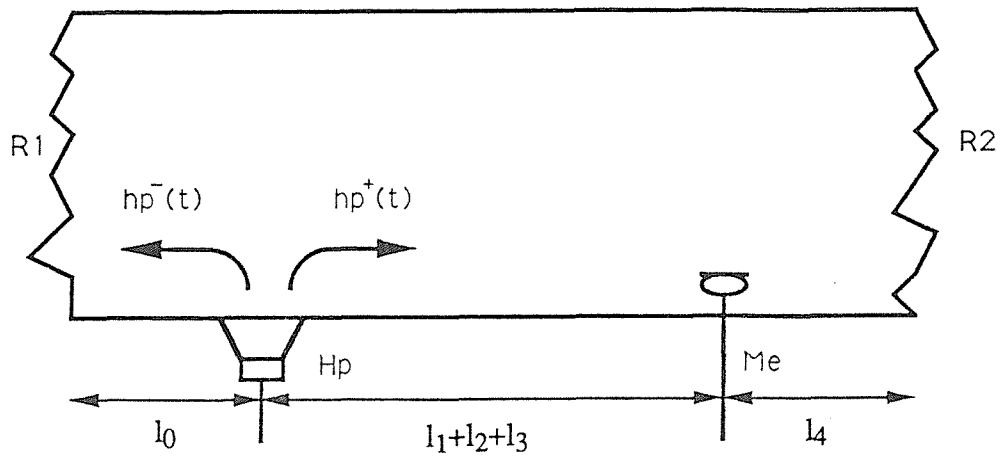
Figure 2.3 An impulse generated at Hp splits into $hp^+(t)$ and $hp^-(t)$
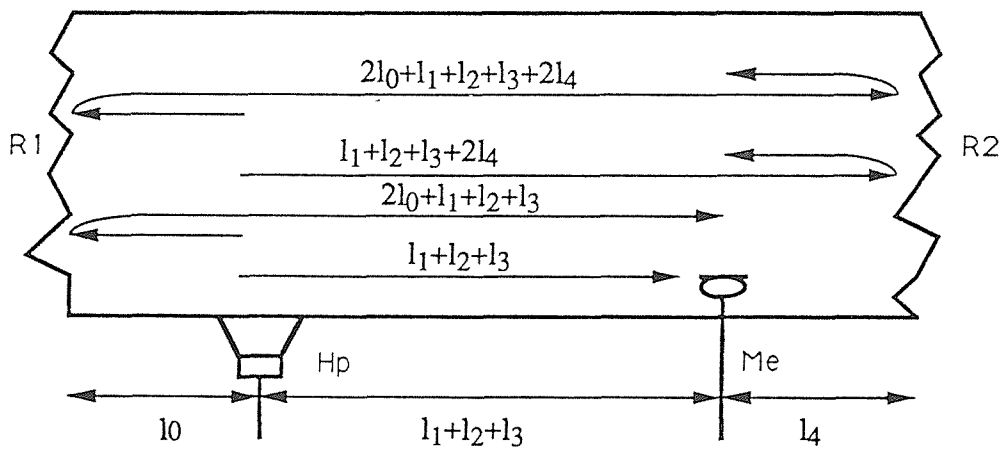
Figure 2.4 The four differents paths between Hp and Me

after one or two reflections. They continue to travel in the duct with the following characteristic : they pass the microphone periodically every $2l/c$ second (where $l = l_0 + l_1 + l_2 + l_3 + l_4$) attenuated each time by the factor $R_1 R_2$ (two reflections). The effect of such reflected contributions can be mathematically expressed by the convolution of the term $a'(t)$ by

$$\sum_{n=0}^{\infty} (R_1(t) * R_2(t))^{(n)} \delta\left(t - \frac{2nl}{c}\right)$$

Where $^{(n)}$ denotes the n-th convolution power.
hence we obtain

$$a(t) = \left(h_p\left(t - \frac{l_1 + l_2 + l_3}{c}\right) + R_1(t) * h_p\left(t - \frac{2l_0 + l_1 + l_2 + l_3}{c}\right) + R_2(t) * h_p\left(t - \frac{l_1 + l_2 + l_3 + 2l_4}{c}\right) \right.$$
$$\left. + R_1(t) * R_2(t) * h_p\left(t - \frac{2l_0 + l_1 + l_2 + l_3 + 2l_4}{c}\right) \right) * m_e(t) * \sum_{n=0}^{\infty} (R_1(t) * R_2(t))^{(n)} \delta\left(t - \frac{2nl}{c}\right) \qquad (2.16)$$

with $*$ as the convolution operator

Similarly we can obtain the time domain expression for $b(t)$, $c(t)$, $f(t)$ as follows :

$$b(t) = \left(h_p\left(t - \frac{l_1}{c}\right) + R_1(t) * h_p\left(t - \frac{l_1 + 2l_0}{c}\right) + R_2(t) * h_p\left(t - \frac{l_1 + 2l_2 + 2l_3 + 2l_4}{c}\right) \right.$$
$$\left. + R_1(t) * R_2(t) * h_p\left(t - \frac{l + l_0 + l_2 + l_3 + l_4}{c}\right) \right) * m_d(t) * \sum_{n=0}^{\infty} (R_1(t) * R_2(t))^{(n)} \delta\left(t - \frac{2nl}{c}\right) \qquad (2.17)$$

$$c(t) = \left(h_s\left(t - \frac{l_3}{c}\right) + R_1(t) * h_s\left(t - \frac{2l_0 + 2l_1 + 2l_2 + l_3}{c}\right) + R_2(t) * h_s\left(t - \frac{l_3 + 2l_4}{c}\right) \right.$$
$$\left. + R_1(t) * R_2(t) * h_s\left(t - \frac{l + l_0 + l_1 + l_2 + l_4}{c}\right) \right) * m_e(t) * \sum_{n=0}^{\infty} (R_1(t) * R_2(t))^{(n)} \delta\left(t - \frac{2nl}{c}\right) \qquad (2.18)$$

$$f(t) = \left(h_s\left(t - \frac{l_2}{c}\right) + R_1(t) * h_s\left(t - \frac{2l - l_2 - 2l_3 - 2l_4}{c}\right) + R_2(t) * h_s\left(t - \frac{2l - l_2 - 2l_0 - 2l_1}{c}\right) \right.$$
$$\left. + R_1(t) * R_2(t) * h_s\left(t - \frac{2l - l_2}{c}\right) \right) * m_d(t) * \sum_{n=0}^{\infty} (R_1(t) * R_2(t))^{(n)} \delta\left(t - \frac{2nl}{c}\right) \qquad (2.19)$$

(2.17), (2.18), (2.19) share of course the same features with (2.16) that is a main pattern of four reflections repeated every $2l/c$ second.

II.3.3. Frequency Domain Expression

These time domain expressions (2.16), (2.17), (2.18), (2.19), are useful to describe the wave displacement in the duct. However we need also the frequency domain expressions to deduce the ideal controller. These are easily obtained from the time domain formulas. We will illustrate this with $a(t)$.

$A(j\omega)$, the Fourier transform of $a(t)$, is the product of two terms.
The first one, Fourier transform of $a'(t)$ is equal to

$$A'(j\omega) = H_p(j\omega).M_e(j\omega)(.e^{-jk(l_1+l_2+l_3)}+R_2(j\omega)e^{-jk(l_1+l_2+l_3+2l_4)}$$

$$+R_1(j\omega)e^{-jk(2l_0+l_1+l_2+2l_3)}+R_1(j\omega)R_2(j\omega)e^{-jk(2l_0+l_1+l_2+2l_3+2l_4)}) \qquad (2.20)$$

where $k = 2\pi f/c$ is the wave number

The second term is the Fourier transform of $\displaystyle\sum_{n=0}^{\infty}(R_1(t)*R_2(t))^{(n)}\delta(t-\frac{2nl}{c})$ which

gives

$$\sum_{n=0}^{\infty}(R_1(jw)R_2(jw))^{n}e^{-2jnkl} \qquad (2.21)$$

Since $R_1(j\omega)$ and $R_2(j\omega)$ are <1 (the terminations are assumed linear and passive) (2.21) can be considered as the expansion of a geometric progression, and factorized into $\dfrac{1}{1-R_1(j\omega)R_2(j\omega)e^{-2jkl}}$

Hence from (2.20) and (2.21) and omitting the $j\omega$ dependence to simplify the expressions we deduce

$$A(j\omega) = \frac{H_p.M_e.e^{-jk(l_1+l_2+l_3)}\left(1+R_2.e^{-2jkl_4}\right)\left(1+R_1.e^{-2jkl_0}\right)}{1-R_1.R_2.e^{-2jkl}} \qquad (2.22)$$

The same process applied to b(t), c(t), f(t) gives us

$$B(j\omega) = \frac{H_p.M_d.e^{-jkl_1}\left(1+R_2.e^{-2jk(l_2+l_3+l_4)}\right)\left(1+R_1.e^{-2jkl_0}\right)}{1-R_1.R_2.e^{-2jkl}} \qquad (2.23)$$

$$C(j\omega) = \frac{H_s.M_e.e^{-jkl_3}\left(1+R_2.e^{-2jkl_4}\right)\left(1+R_1.e^{-2jk(l_0+l_1+l_2)}\right)}{1-R_1.R_2.e^{-2jkl}} \qquad (2.24)$$

$$F(j\omega) = \frac{H_s.M_d.R_1.R_2.e^{-jkl_3}\left(1 + \frac{1}{R_1}.e^{-2jk(l_0+l_1)}\right)\left(1 + \frac{1}{R_2}.e^{-2jk(l_3+l_4)}\right)}{1-R_1.R_2.e^{-2jkl}}$$

$$(2.25)$$

II.4 Ideal controller derivation

At this stage we can substitute (2.22), (2.23), (2.24), (2.25) into (2.5). A good deal of simplification then occurs leading to an expression for the ideal controller in terms of the acoustic variables :

$$W_i(j\omega) = \frac{-e^{-jkl_2}}{H_s(j\omega)M_d(j\omega)(1 - e^{-2jkl_2})} \qquad (2.26)$$

Dividing numerator and denominator by e^{-jkl_2}

$$W_i(j\omega) = \frac{-1}{2j.H_s(j\omega)M_d(j\omega).\sin(kl_2)} \qquad (2.27)$$

This remarkably simple result also developed in [26], requires several remarks.

II.4.1. Duct independence

The expression of the controller is only dependent on the properties of the system between the detection sensor and secondary source. It is completely independent, for instance, of the reflection coefficients and the nature of the primary source. An intuitive demonstration of this striking property will be given in a few moments.

II.4.2. Loudspeaker inversion

The expression (2.26) contains the inverse of the loudspeaker H_S and of the detection microphone M_d. So far we have implicitly assumed the existence of such an inverse. However this may not exist in practice. Effectively, if the loudspeaker possesses a zero on the imaginary axis (which is very likely since $Hs(0) = 0$ for almost any loudspeaker) the inverse therefore possesses a pole situated on the imaginary axis ($1/Hp(0) \rightarrow \infty$). Thus, a true inverse of the loudspeaker can very well have no meaning at all.

However we shall see in practice that a perfect inverse is not necessary to achieve some cancellation but we must not underestimate this problem ; in several cases it is responsible for a serious instability.

II.4.3 Stability of the controller

Even if the stability of the loudspeaker inverse is taken for granted, the other term in (2.27) is sure to lead to an unstable impulse response (at least in the usual sense that is bounded input -> bounded output)

The term $sin(kl_2)$ in the denominator of equ. (2.27) is equal at several frequencies. Let us take an example. If $l_2 = 1.224m$ (the experimental value). since $k = 2\pi f/c$ and $c = 340m/s$ the sine becomes zero for each frequency multiple of 139 Hz. If we assume that the frequency range of interest is from say 0 to 1000 Hz, $W_i(f)$ becomes infinite about 8 times. **Figure 2.5** shows the transfer function of the controller for a feedback path length $l_2 = 1.224m$, assuming that the transducers are perfect.

Because this transfer function contains some infinite values we cannot use the Fourier transform to obtain the time domain expression of the controller. The z transform however enable us to overcome these difficulties and leads to a time domain formulation for W_{ideal} (see Appendix B.1).

This expression is

$$w_{ideal}(t) = (h_s^{(-1)}(t) * m_e^{(-1)}(t)) * \sum_{n=0}^{\infty} \delta(t - \frac{l_2}{c} - \frac{2nl_2}{c}) \qquad (2.28)$$

This impulse response can be generated by the following combination of filters (see **figure 2.6**). The first delay corresponds to the direct path while the recursive filter acts like a feedback canceller. The first samples of the ideal controller impulse response are also given **figure 2.7**. Since this impulse response is of infinite energy the instability of the ideal controller appears more obvious. At least it is consistent with the conclusions derived from the frequency domain.

However, even if the ideal controller is unstable, this does not imply than the overall response of the system constituted of the direct path, the feedback path and the controller is of infinite energy. Some pole-zero cancellations are likely to take place. A demonstration of this fact is given further.

Moreover, in practice the walls of the duct are not perfectly rigid, and some dissipation also occurs due to viscous and thermal effects at the duct wall, introducing a loss factor in the formula (2.28) thus becoming

$$w_{ideal}(t) = (h_s^{(-1)}(t) * m_e^{(-1)}(t)) * \sum_{n=0}^{\infty} \mu^n \delta(t - \frac{l_2}{c} - \frac{2nl_2}{c}) \qquad (2.29)$$

with $\mu < 1$. This impulse response decays exponentially with μ.

II.4.4. About the infinite resonances of the controller

We have seen with (2.26) than the spectrum of the ideal controller is made of a set of unbounded peaks regularly spaced and we can therefore predict that only a controller able to reproduce such peaks will achieve a good cancellation at all the frequencies. But where do these peaks come from ? In fact they are linked to the monopole nature of the secondary source. The pressure field generated by a monopole source is spatially symmetric. If the system works perfectly, the secondary source forces a "pressure release" (zero pressure) in front of it which causes perfect reflection.

Modulus (dB)
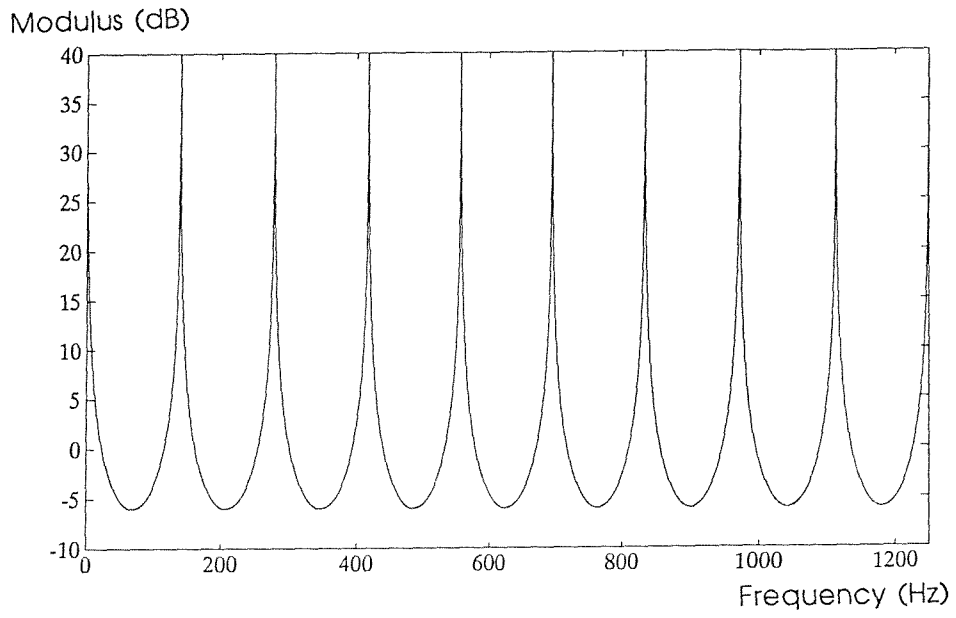
Figure 2.5 Ideal Controller spectrum for l2=1.224 m
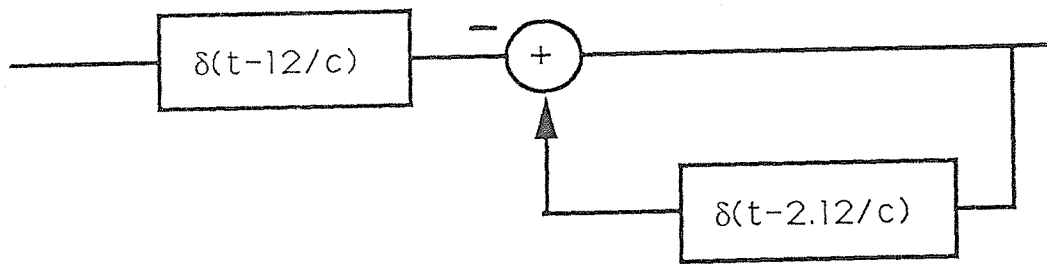
Figure 2.6 Time-domain structure of the ideal controller
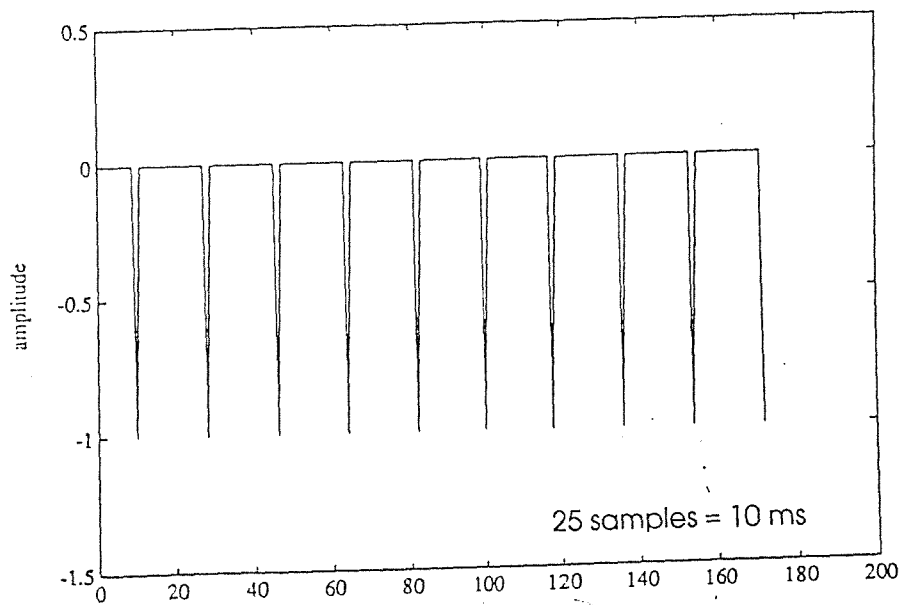
Figure 2.7 Impulse response of the idealcontroller : first samples

- 19 -

Then the secondary source acts effectively as a sound reflector which means that the pressure field upstream is made up of two waves travelling in opposite direction.

Suppose the unwanted noise is

$$p_1(t) = P_0.\cos(-kx+\omega t)$$

the secondary source is at x=0.
Consequently the reflected pressure is

$$p_2(t) = -P_0.\cos(kx+\omega t)$$

$$p(t) = p_1(t) + p_2(t) = -2.P_0.\sin(kx).\sin(\omega t) \qquad (2.30)$$

the pressure field upstream is a standing wave whose node of vibration are every $\lambda/2$ i.e. every c/2f.

From (2.30) we find a node at x=0 and for $\omega = 0$ whatever x. Moreover we have a node of vibration at the detection microphone for all frequencies multiple of f = $c/2l_2$. So at all these frequencies the detection microphone is unable to detect any signal. In order to drive the secondary loudspeaker the controller has therefore to multiply such a signal by an infinite gain. The infinite gain of the ideal controller is a direct consequence of the monopole structure of the secondary source and the fact that the detection microphone is omni-directional. With two detection microphones we would not have this inconvenience. It is always possible to position the two microphones in a way such that they are never located simultaneously at a node of pressure (for a limited bandwith). However a system with two detection microphones is more complicated: it requires a controller for each detector and so doubles the complexity of the active noise control system.

II.4.5. Pictorial interpretation of the expression for the ideal controller

We are going to follow the history of an impulse generated upstream by a primary source and processed through a controller whose structure is shown in **figure 2.6.** The **figure 2.8.a** shows the impulse coming from the left and represented by a small triangle : the delta symbol in the filter blocks mean a pure delay of l_2/c. The impulse is first detected by the detection microphone and after a change of sign (the circled line on the figure), is delayed into the first filter (the direct one) (**figure**

2.8.b). When the original impulse reaches the loudspeaker it produces an impulse out of phase which cancels downstream. However, the loudspeaker is a monopole source, and creates therefore a residual impulse on the left. (**figure 2.8.c**) During this period the impulse through the controller is travelling in the recursive part of the filter. The next step is the detection of the residual impulse by the microphone which leads to an internal cancellation between the recursive and the non-recursive filter (**figure 2.8.f**). Eventually the residual impulse is reflected back and then attenuated which leaves us back at step 1 (**figure 2.8.g**). This cycle goes on and on until the residual impulse vanishes after many reflections (depending on the reflection coefficient value).

This little demonstration shows that even with a controller which is unstable the impulse of the system to the sequence of impulses generated in the duct can be of finite energy.

2.8.a

2.8.b
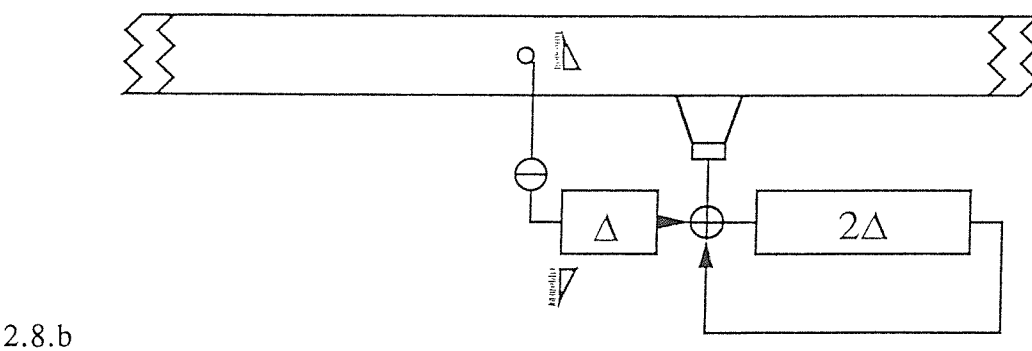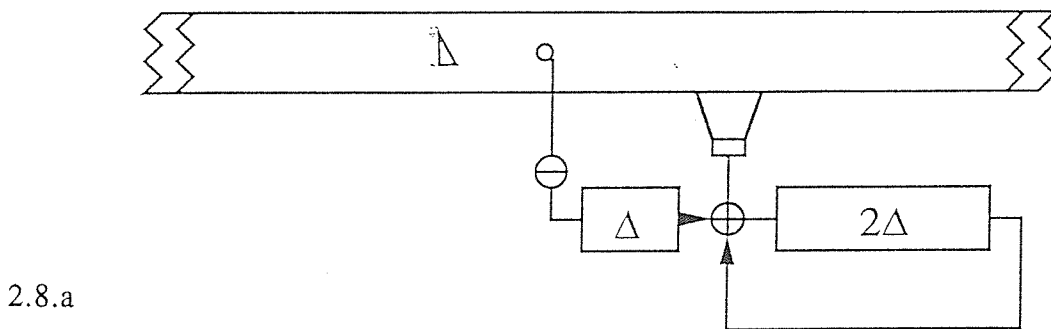
Figure 2.8 Operation of the ideal controller

2.8.f
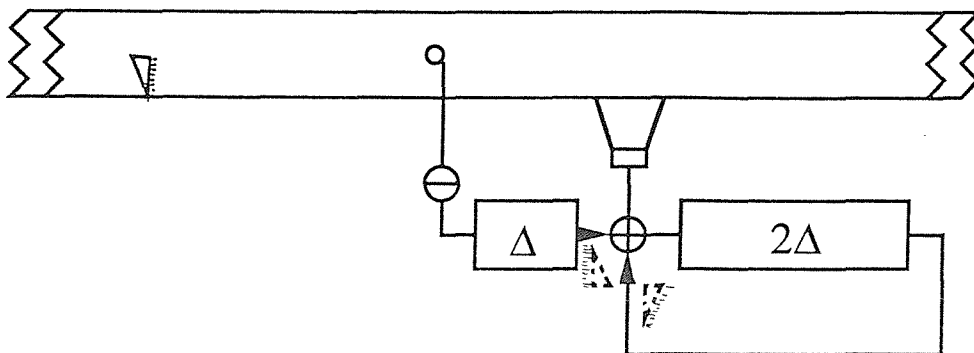
2.8.g
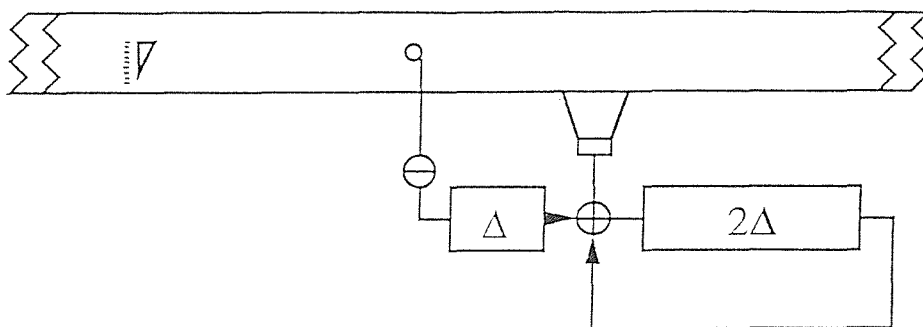
Figure 2.8 Operation of the ideal controller (continued)

2.8.c

2.8.d

2.8.e
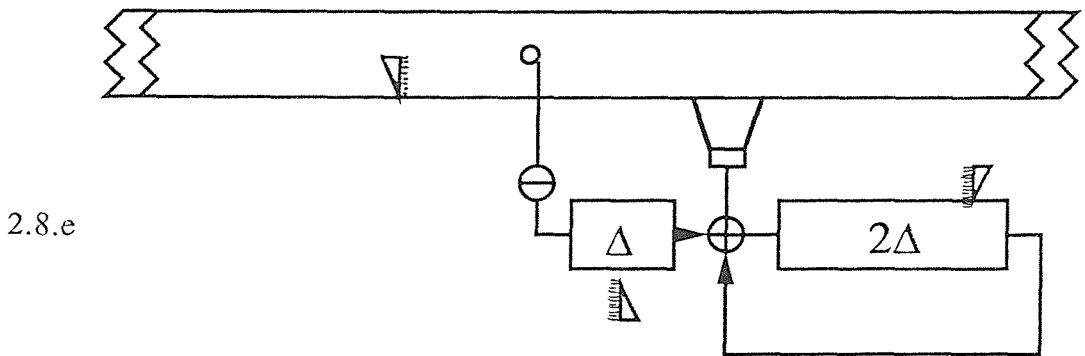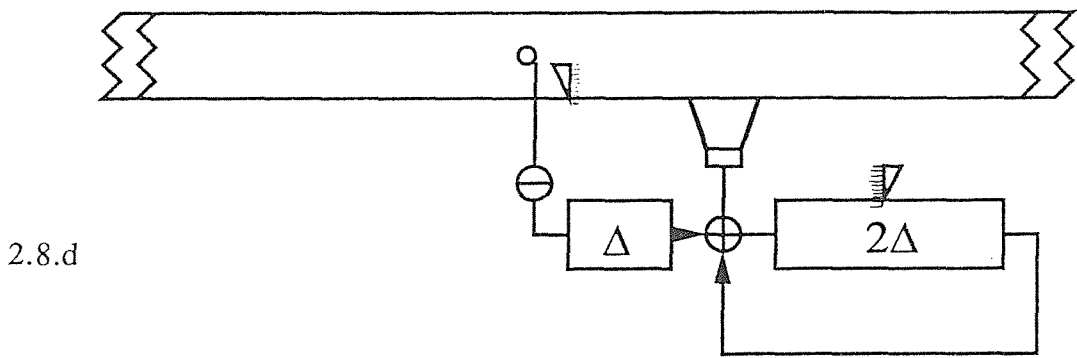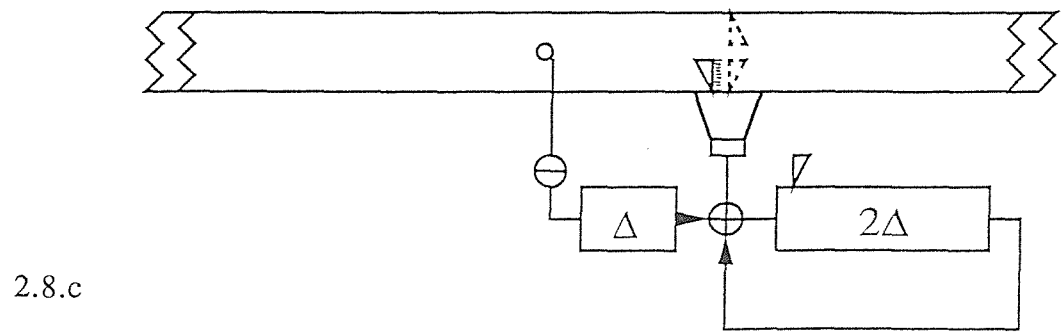
Figure 2.8 Operation of the ideal controller (continued)

Chapter III

Application of theory to the experimental duct

This chapter is an experimental validation of the model described in chapter II. Such a validation is necessary because we intend to make intensive use of a computer simulation in order to study the LMS algorithm. Firstly we will describe the experimental equipment and secondly we will see how to estimate the missing parameters of the model. Finally we will compare the impulse responses and transfer functions obtained experimentally and calculated using the formulas (2.16) to (2.19).

III.1. Physical description of the A.N.C equipment

The experiment is described in **figure 3.1.** The PC computer acts as a host computer for a LOUGHBOROUGH DSP TMS320 card and a 12 bits analogue-to-digital converter (LOUGHBOUROUGH Sound Image cards PCS25 and PC4i2o). The microphones and louspeakers and their amplifiers are linked to a connector box linked itself to the D/A-A/D converter. The low-pass filters act as anti-aliasing and reconstructing filters. The PC is only used to display useful data on the screen. Consequently the TMS processor performs all the important tasks such as active noise cancellation and various transfer function identification.

Following the notational convention of **Figure (2.1)** we have for the experimental duct :

$$l_0 = 0.816m$$
$$l_1 = 0.272m$$
$$l_2 = 1.224m$$
$$l_3 = 0.816m$$
$$l_4 = 0.272m$$
$$l = 3.400m$$

The diameter of the pipe is 11.5cm
The primary loudspeaker is a REALISTIC 4" WOOFER
The secondary loudspeaker is a RS 6.5" BASS LOUDSPEAKER
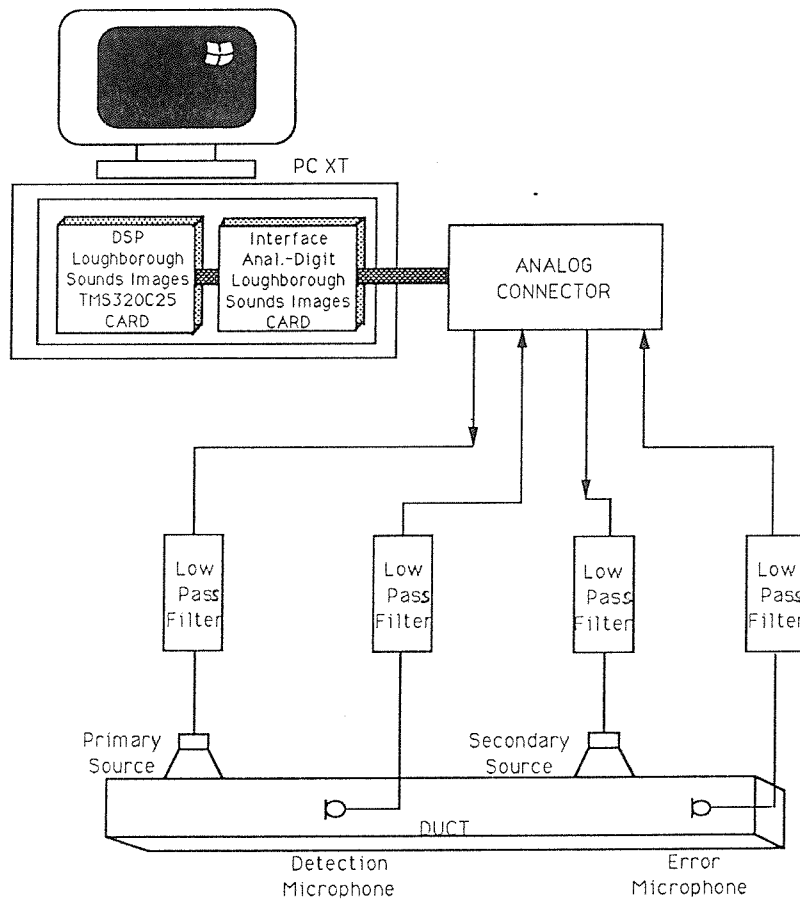
Figure 3.1 Active Noise Control System : Hardware Description.

Both microphones are cheap omnidirectional electret microphones (WM-063)
Anti-aliasing filters are KEMO VBF 23 filters.

III.2. Computer simulation model

In order to simulate the real world constituted by the duct and its associated
transducers, a simplified version of Roure's acoustical model has been
implemented numerically on a PC computer. We have programmed various black
boxes, corresponding to the different electrical transfer functions. Each black box
has an unique input and output. When a sampled value is presented at the input
another a resulting sampled value is produced at the output. **Figure 3.2** shows the
structure of one of theses black boxes which is directly derived from equation (2.16),
(2.17), (2.18), or (2.19). The box denoted by Hp correspond to the combination of a
loudspeaker, a microphone and two low-pass filters. In the numerical model Hp
is an FIR filter. Delay1 to Delay4 represent the four different paths that a wave can
take to go from a given loudspeaker to a given microphone. R_1 and R_2 are the
reflection coefficients. Though the delays can be determined by measuring the
length of the pipe elements, we have to use more sophisticated methods to estimate
Hp and the reflection coefficients. We will consider these techniques below.

III.3. Measurements of the transducer transfer functions

The transducers are an important part of the ANC system. They are responsible
for a lot of imperfections and limitations in the performance.
In order to make the numerical model as close as possible to the real experiment
we have to be particularly careful in modelling it. In fact what we need to measure
is more than just both loudspeaker transfer functions. It has to include the
microphones, the anti-aliasing filter and the converters as well. From now, when
we speak of a "transducer" it will mean an hypothetical electrical transfer
function defined as follows : the transfer function of a system constituted from a
low-pass filter connected to a loudspeaker mounted on the middle of an infinite
duct; a microphone is situated very close to the loudspeaker membrane in such a
way that there is no delay between them; finally the microphone is connected to a
low-pass filter.
Figure 3.3 describes the experiment employed to estimate such a transfer function.
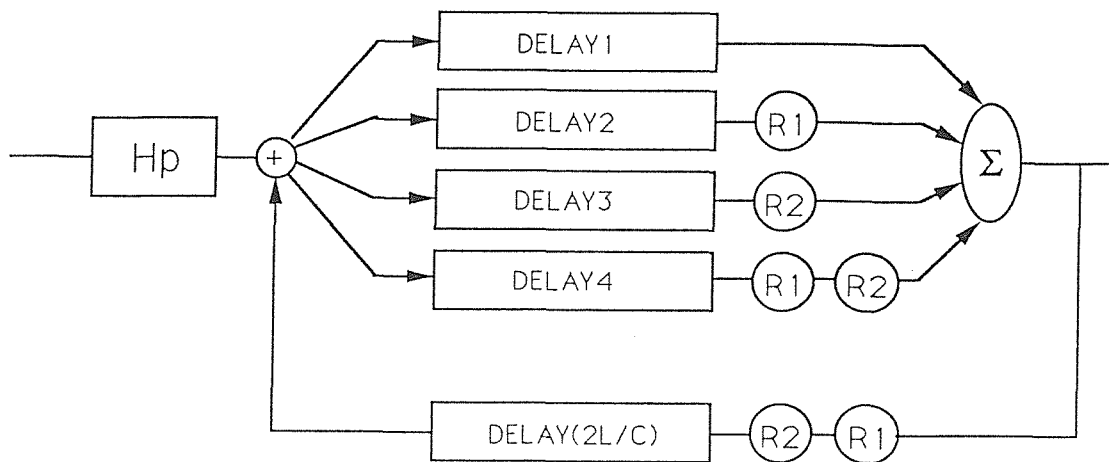
Figure 3.2 Internal structure of a typical black box
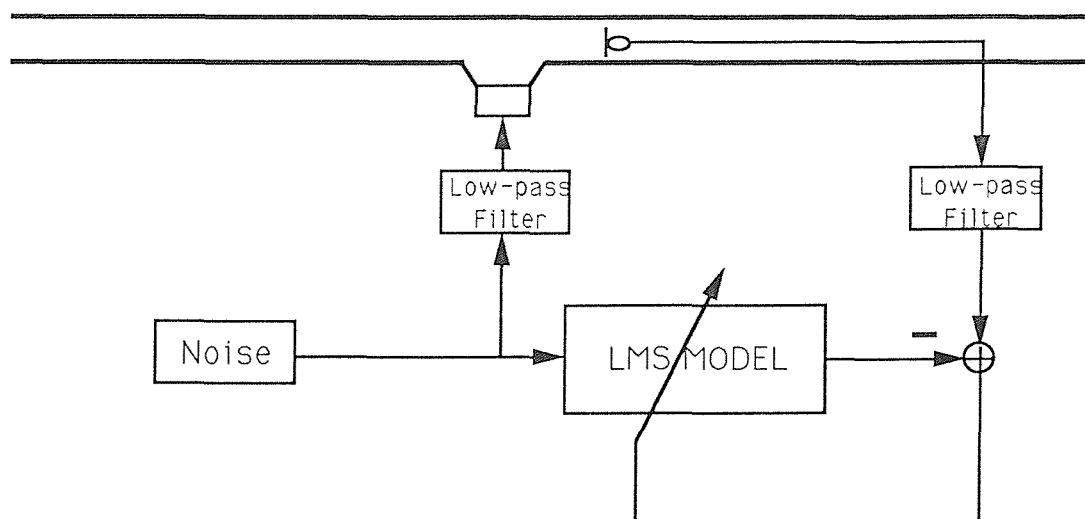
Figure 3.3 Measurement of the loudspeaker impulse response : principle

Two long pieces of pipe (6 m each) are placed on each side of the loudspeaker. A microphone is situated at 27.2 cm from the loudspeaker. At this distance the sound waves generated by the loudspeaker are plane. The extra delay corresponding to 27.6 cm is exactly two sample periods if the sampling frequency is 2500Hz. It will be eliminated by the suppression of the first two samples from the measured impulse response. The impulse response between the input x and the output y is identified using an adaptive Least Mean Square algorithm implemented on the TMS320. (See Chapter V to find more details about this algorithm). Even if the pipe is very long the measured impulse response contains some artefact due to the first echos. After elimination of these echos by a time domain windowing, we obtain the measured impulse response of the transducer path.

Since the microphones are identical there are only two different transducer paths. One contains the primary speaker the other one contains the secondary speaker. **Figure 3.4** gives the two different impulse response obtained experimentally. We can see on **Figure 3.5** a plot of the corresponding transfer functions. We recognize the resonance characteristic of a loudspeaker and at high frequencies, the effect of anti-aliasing and reconstructing filters responsible for an important attenuation and phase shift.

III.4.   Measurement of the reflection coefficients

In equations (2.22) to (2.25) the reflection coefficients are assumed to be frequency dependent. It is well known that in practice the modulus of the reflection coefficients decays with the frequency. However, in order to avoid too much a complexity in the numerical model, we have decided to consider the reflection coefficients as scalar quantities (frequency independent). The validity of this assumption will be proved a posteriori by comparison between simulated and measured transfer functions.

A way to determine these reflection coefficients is to measure $R_1(j\omega)$ and $R_2(j\omega)$, the frequency response of both ends. Then mean square values can be obtained by integration. The experimental setup to measure the frequency response is illustrated in **figure 3.6.**

A loudspeaker is located at one end of a long pipe (6 m). The reflection coefficient of the other end is the one we want to determine. A microphone is situated at the middle of the pipe. This location has been chosen in order to maximize the delay between two consecutive echos detected by the microphone. Using a least mean square identification algorithm implemented in the TMS microprocessor we have
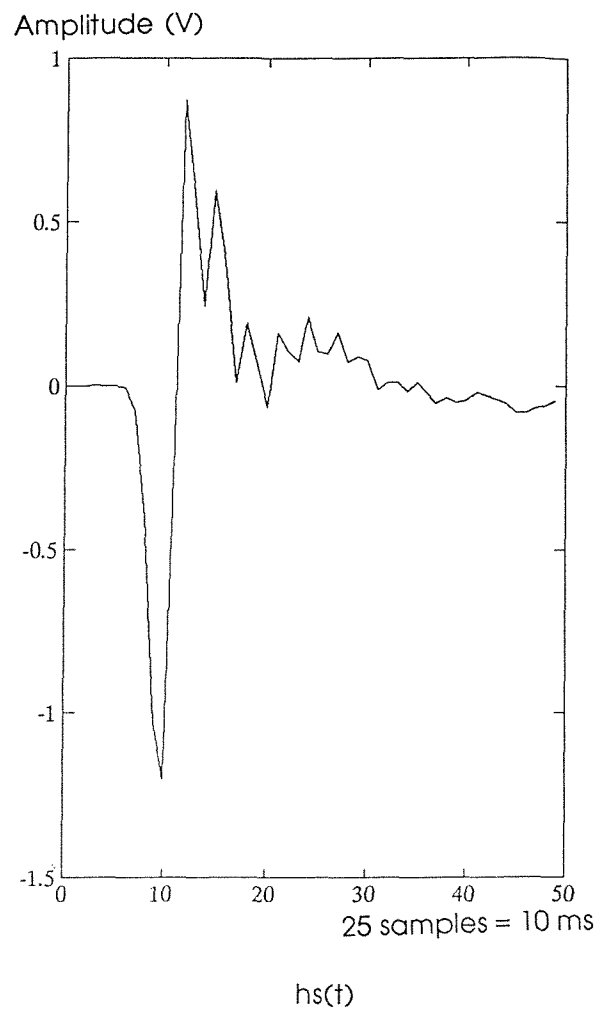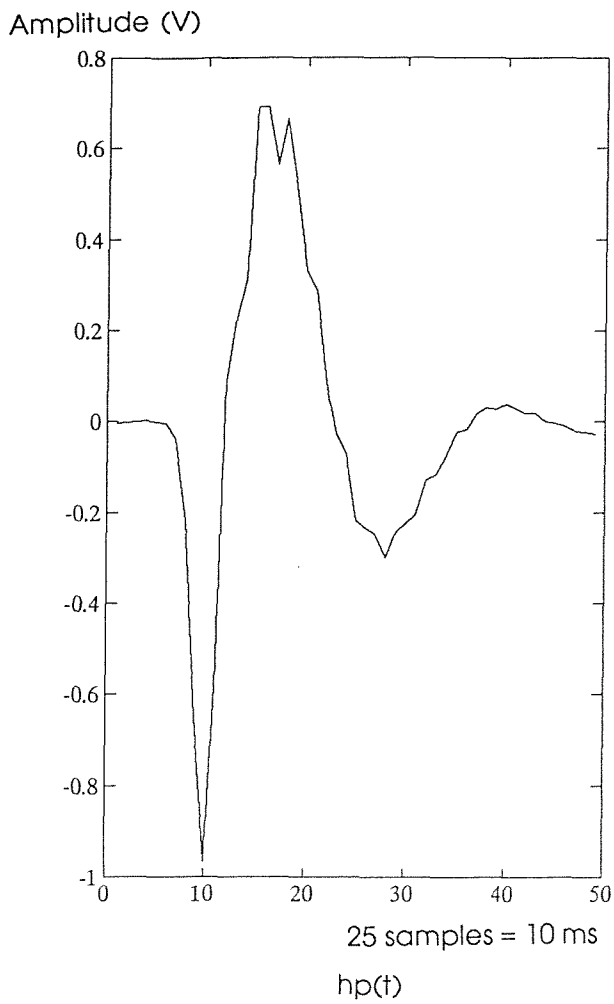
Figure 3.4 Impulse response of the transducer path
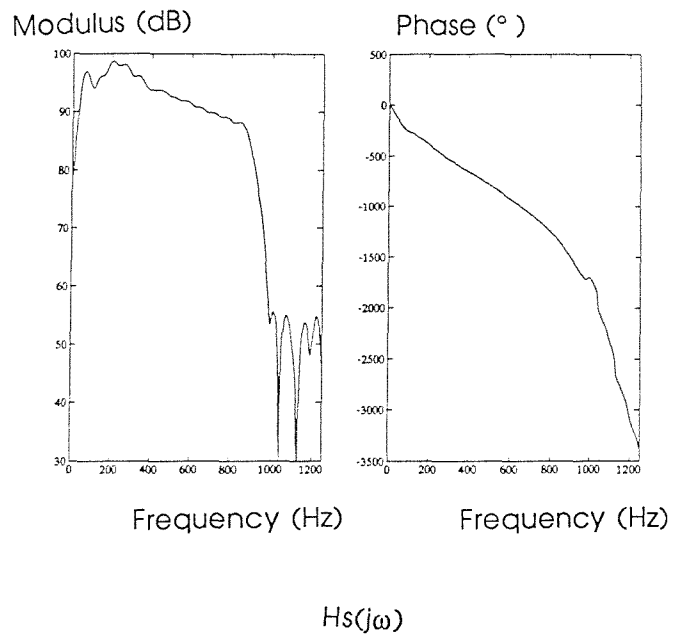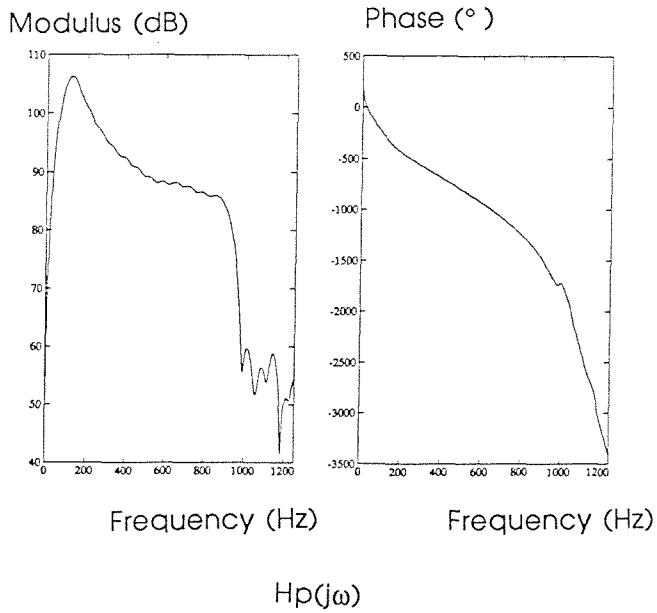
Figure 3.5 Modulus and phase of the transducer path transfer function
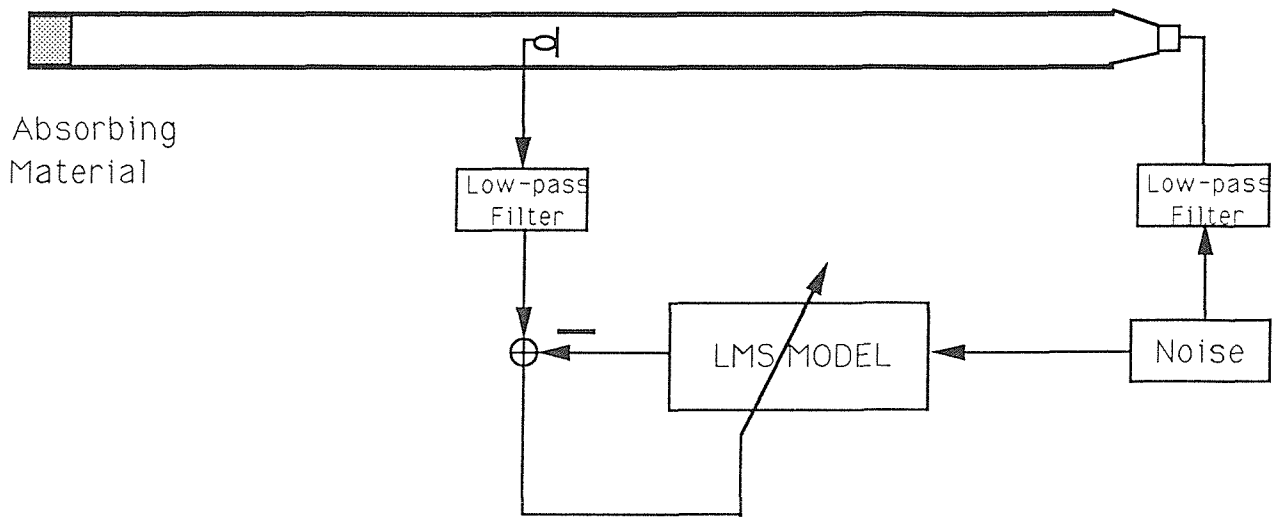
Figure 3.6 Measurement of the reflection coefficients : principle

modulus (linear scale)
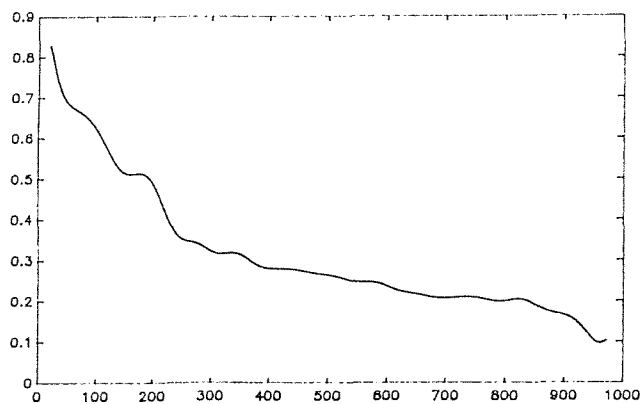
modulus (linear scale)

Frequency (Hz)
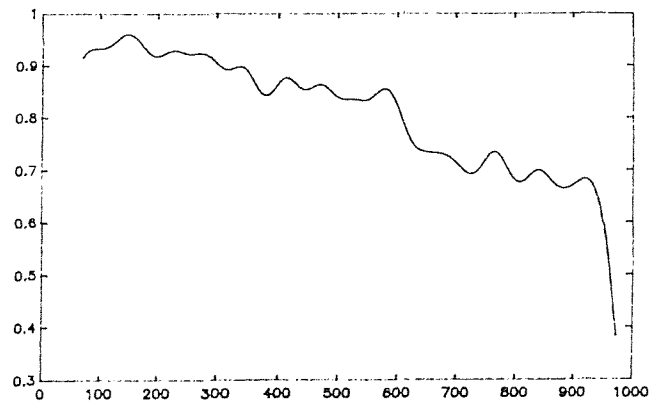
Frequency (Hz)

Figure 3.7 Reflection coefficients R1 and R2 : frequency response.

determined the impulse response between the loudspeaker and the microphone. As expected this impulse response was made of several bursts, and the first two , due to the direct path and first reflection were correctly separated. They have been isolated using appropriate windowing and Fourier transformed. The transfer function of the end was therefore easy to calculate by dividing the reflection Fourier transform by the direct path Fourier transform. **Figure 3.7** shows the moduli of these transfer functions. The curve on the left represents the left end. This end is closed with a 40 cm long piece of foam. Above 300 Hz the reflection coefficient does not vary too much. Below this frequency this is not true. The coefficient falls quickly from 0.83 to 0.35. The resulting mean square value is 0.39. On the right we have a plot of the right end transfer function. This end is open and therefore not absorbant. This is confirmed on the diagram. The coefficient decays steadily from nearly 1.0 to 0.7. The mean square value is 0.83. The study of free end in a pipe [19] shows that the reflected wave is out of phase with the incoming one. In the computer model this is taken into account by giving to R_2 a negative value. To summarize, the values we will use in our computer model by now are :

$$R_1 = \quad 0.39$$
$$R_2 = -\ 0.83$$

III.5. Comparison between the model and the experiment

The experimentally measured responses of the transducers and reflectors were used in the computation of the model previously described in equ. (2.16) to (2.19) to give the overall duct impulse responses used in the computer simulation, $\hat{a}(t), \hat{b}(t),$ $\hat{c}(t), \hat{f}(t)$. On the other hand a direct measurement on the duct produces $a(t), b(t),$ $c(t), f(t)$. These impulse responses have been experimentally identified with an LMS technique. The experimental setup was similar to the transducer identification. Comparison between $a(t)$ and $\hat{a}(t)$, $b(t)$ and $\hat{b}(t)$, $c(t)$ and $\hat{c}(t)$, $f(t)$ and $\hat{f}(t)$, show some strong similarities (see **figure 3.8**).

In particular, the decay rate is almost identical for both calculated and measured impulse responses. This proves the approximation of the reflection coefficients to be a sensible one. The similarity observed in the time domain occurs equally in the frequency domain (see **figure 3.9**). The various resonances are nearly the same and the damping seems to be correctly estimated.

III.6. Conclusion

In chapter II we have developed a theoretical expression for the ideal controller. These theoretical results have been extended by the introduction of electroacoustic models of the individual responses in the duct. In chapter III a simplified version of these models has been described. Then, the impulse and frequency response of the model has been computed and compared to experimental results. The good match between experimental results and simulated ones leads to several remarks :

-the assumptions of linearity and non dispersivity are proven a posteriori since they are verified by the experiment

-the assumption of frequency independent reflection is not too strong. The time domain results show a realistic decay and the frequency domain plots show a acceptable modulus coincidence.

-consequently such a model will be a reliable tool to study the behavior of different controller structures in various conditions.
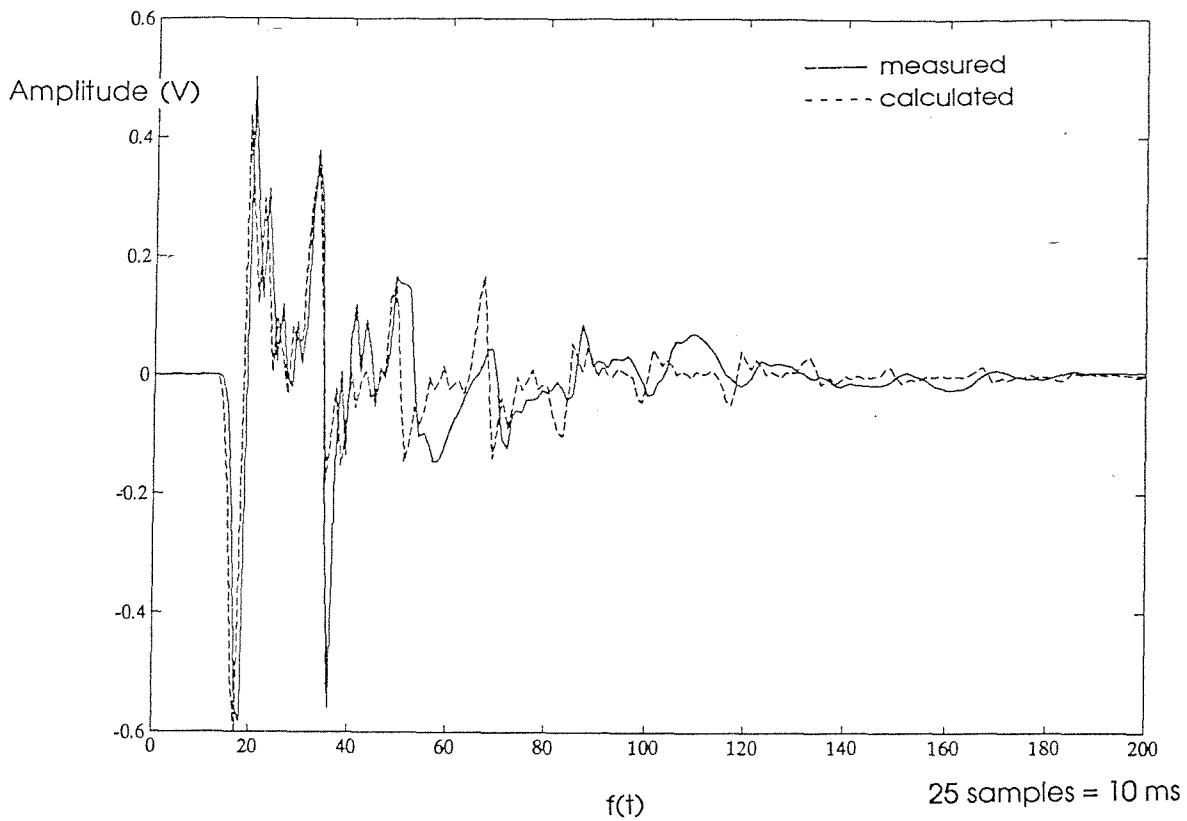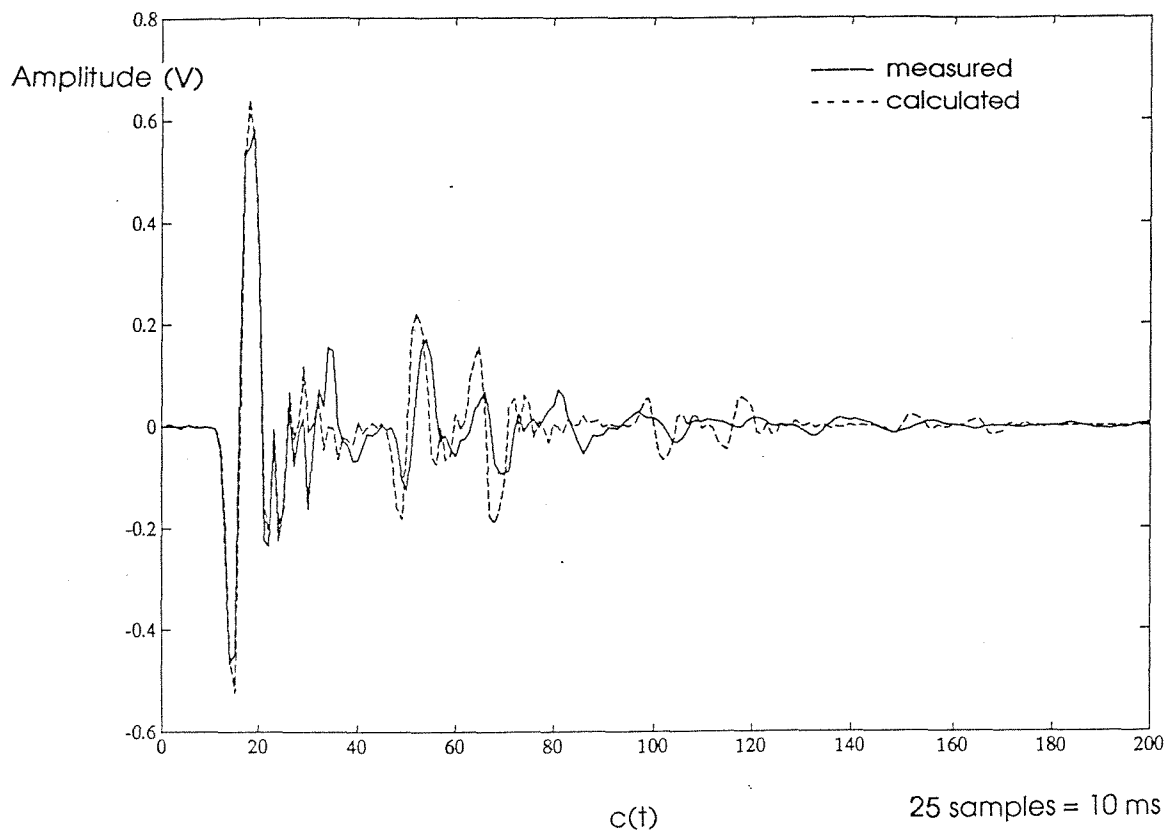
Figure 3.8 Comparison between the impulse responses predicted by the model and the impulse responses measured in the duct..

a(t)

25 samples = 10 ms

b(t)

25 samples = 10 ms
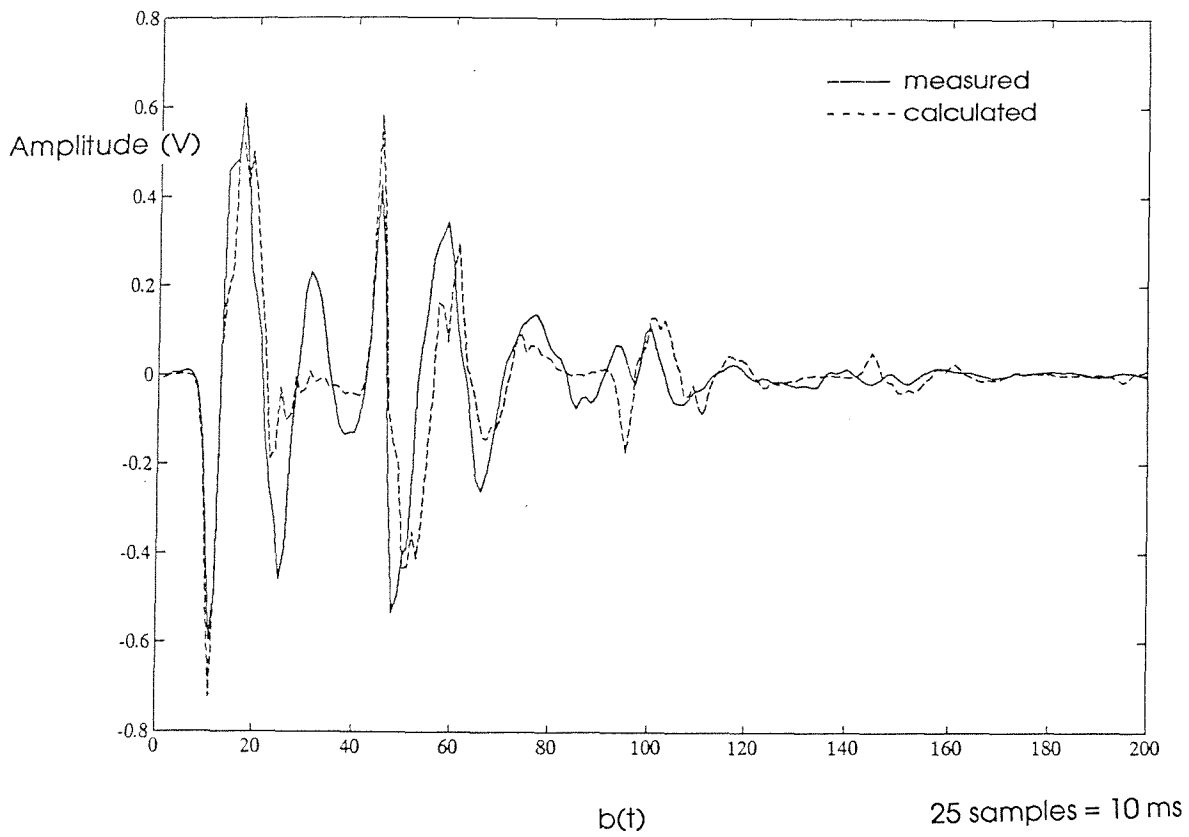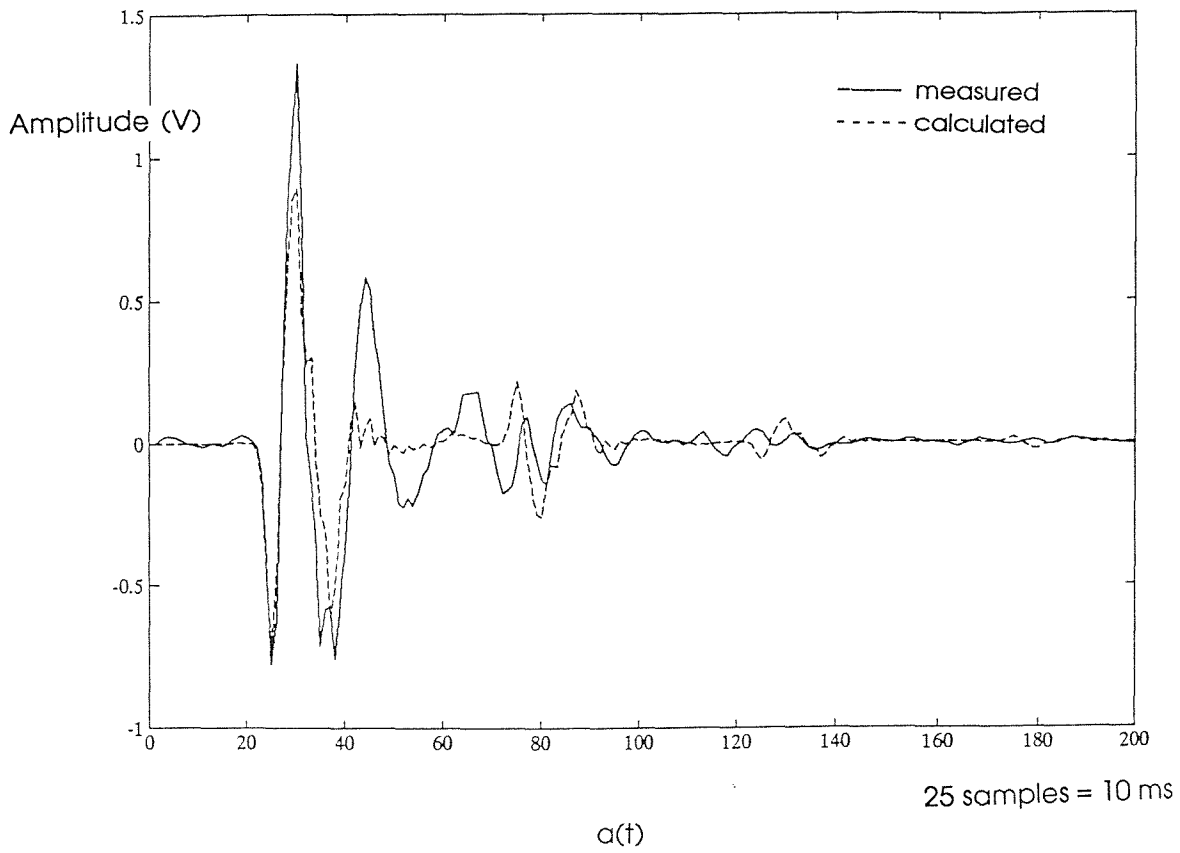
Figure 3.8　　Comparison between the impulse responses predicted by the model and the impulse responses measured in the duct..
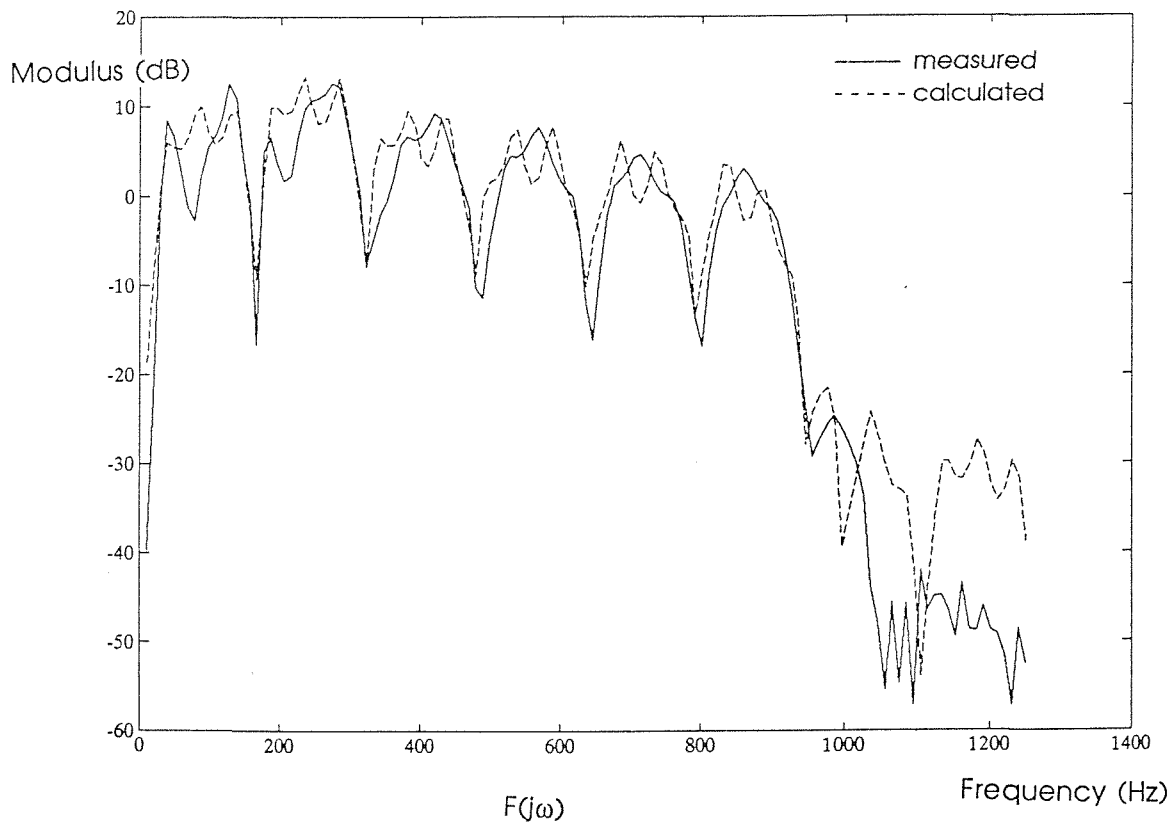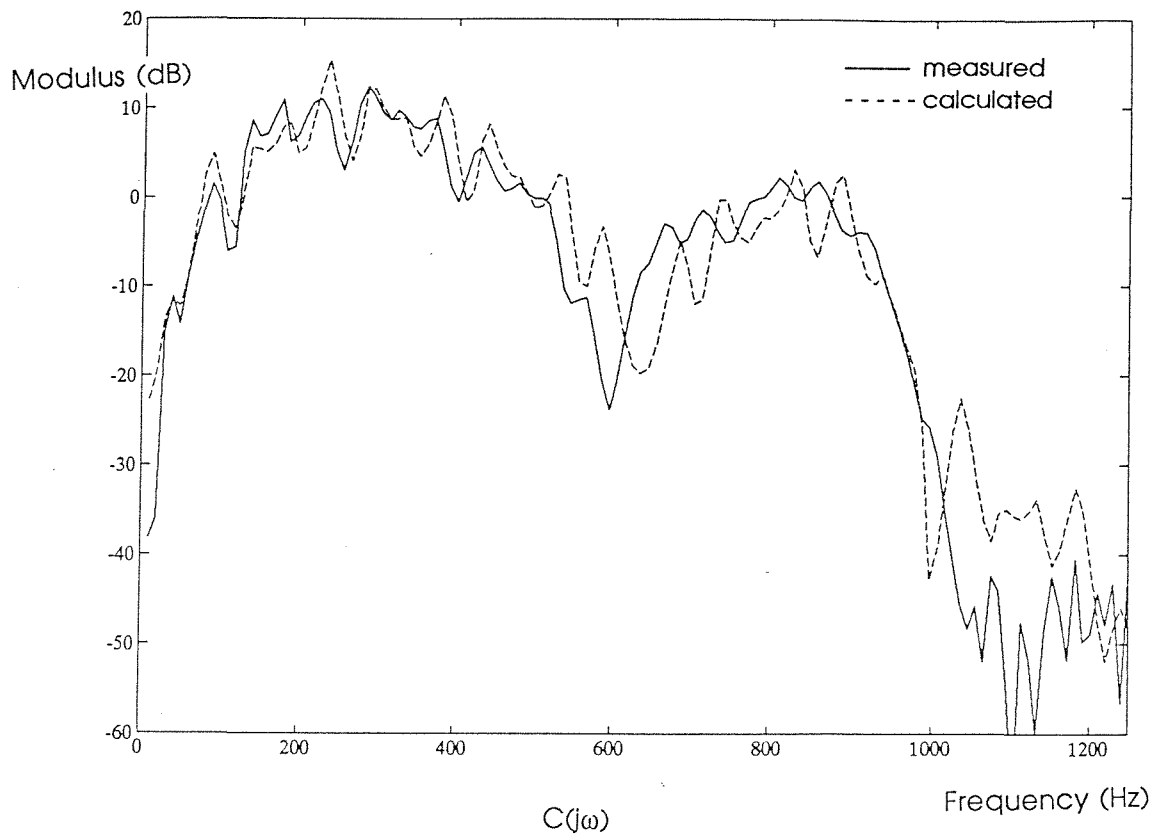
Figure 3.9 Comparison between the transfer functions predicted by the model and the transfer functions measured in the duct..
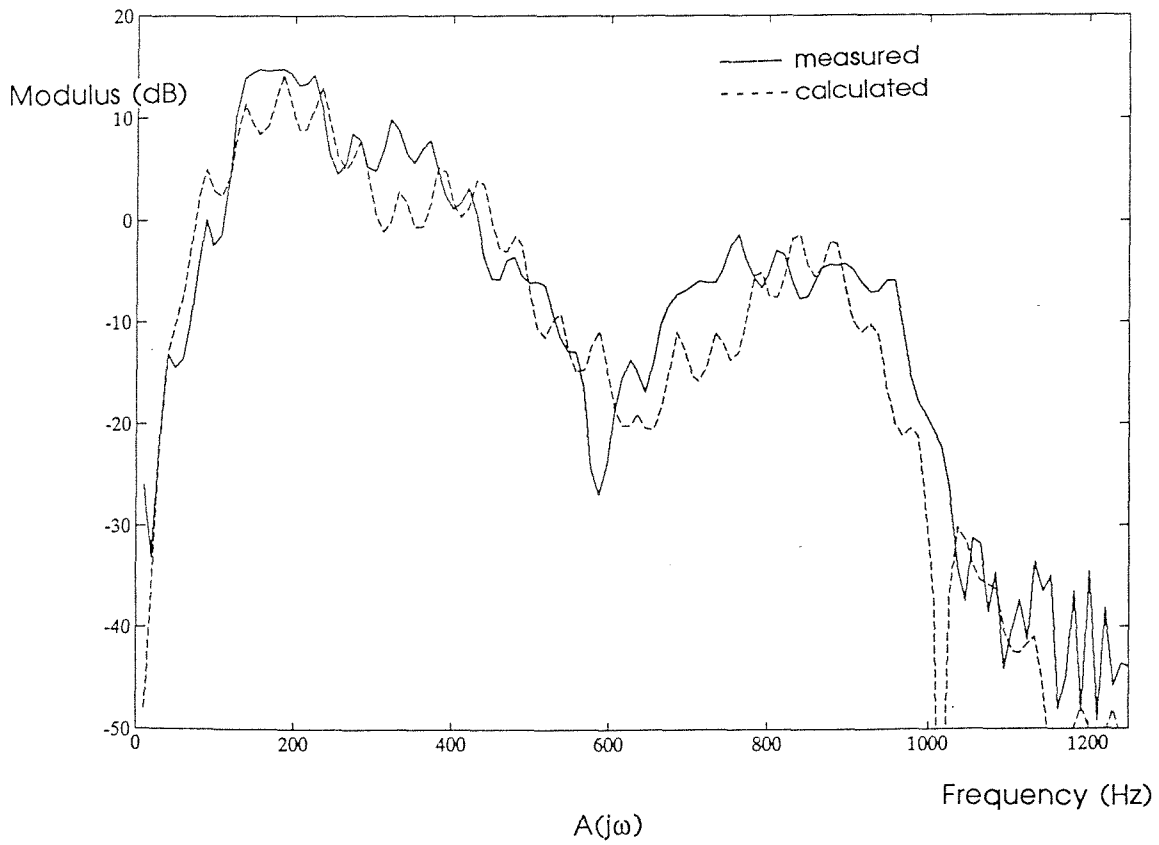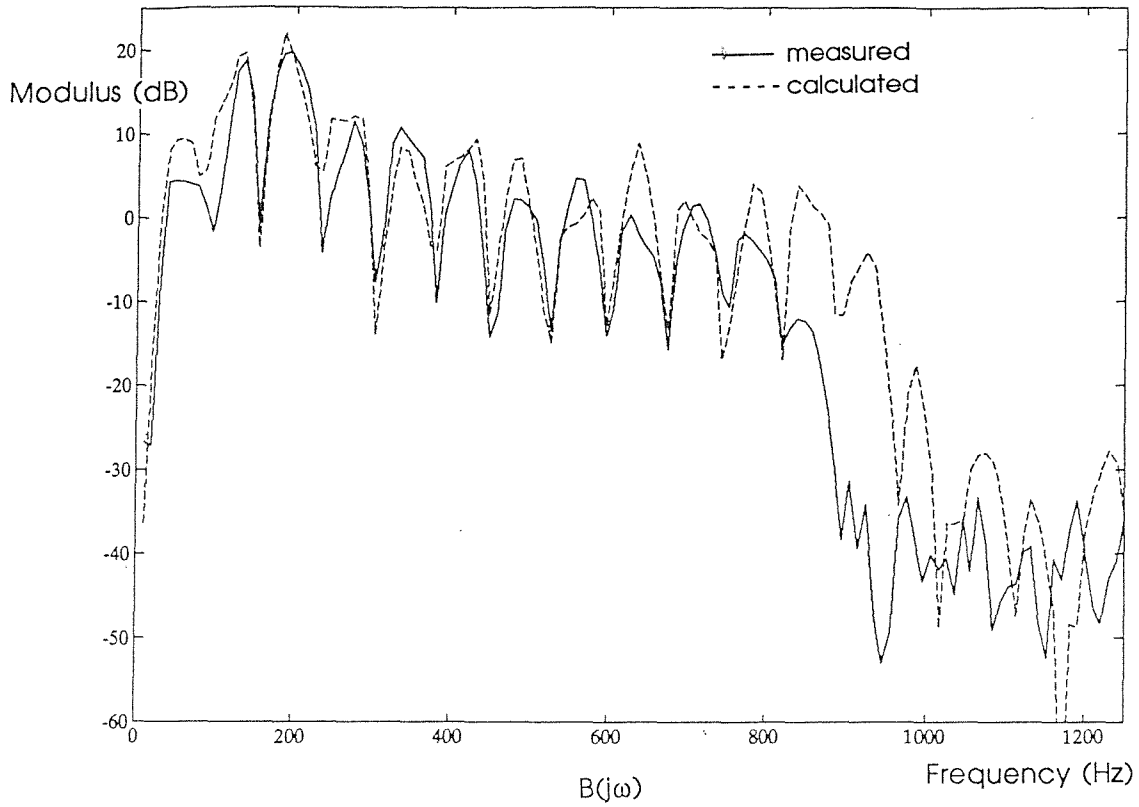
Figure 3.9 Comparison between the transfer functions predicted by the model and the transfer functions measured in the duct..

CHAPTER IV

The optimal least square controller

In chapter II the expression for the ideal controller was derived, using a purely deterministic calculation. Since this expression was been derived from the condition e(t) = 0, the attenuation is supposed to be perfect. In practice the noise reduction is limited for several reasons :

1) the physical realisation may use a finite impulse response controller.
2) the filters must be causal.
3) measurement noise is present on signals from both detection and error microphones.

The final limitation has been dicussed by Roure [9] but will not be addressed here, we concentrate on the limitation imposed by using a causal finite length filter.

In the formula

$$W_{ideal}(j\omega) = \underbrace{\frac{1}{H_s(j\omega)M_d(j\omega)}}_{\text{I}} \cdot \underbrace{\frac{-e^{-jkl_2}}{1 - e^{-2jkl_2}}}_{\text{II}}$$

(4.0)

term II is causal but has an infinite impulse response and is therefore related to the condition 1) whereas term I is more likely to be non-causal and related to condition 2). Since theses terms are independent we can study their influence separately.

IV .1 Least mean square inverse of the response of the transducer

IV.1.1 Condition of stability

If we assume that input and output signals are sampled, the detection microphone (M_d) and the secondary loudspeaker (H_S) can be considered to be coupled together to form a single system whose z-transform is

$$Trans(z) = M_d(z).H_S(z)$$

We want to find a filter whose z-transform is the inverse of the z-transform $Trans(z)$.

Assuming that n is large enough, it is always possible to approximate $Trans(z)$ by a rational polynomial of z.

$$Trans(z) = \frac{a_0 + a_1 z^{-1} + ... + a_n z^{-n}}{1 + b_1 z^{-1} + ... + b_n z^{-n}} \qquad (4.1)$$

This expression can be factorized into a set of first order polynomials

$$Trans(z) = \frac{A.(s_1 z^{-1}-1)(...)(s_n z^{-1}-1)}{(p_1 z^{-1}-1)(...)(p_n z^{-1}-1)} \qquad (4.2)$$

The first idea to find an inverse to such a transfer function would be to say that the required filter is simply defined by

$$Inv(z) = \frac{(p_1 z^{-1}-1)(...)(p_n z^{-1}-1)}{A.(s_1 z^{-1}-1)(...)(s_n z^{-1}-1)} \qquad (4.3)$$

The poles become zeros and vice-versa. However we know from digital linear systems theory that a causal filter is stable only if all the poles of its transfer function lie inside the unit circle of the z-plane (see [20] for more details). If some poles do not lie within the unit circle it is still possible to relate a stable filter to the transfer function. Unfortunately such a filter will not be causal.

We now consider the response of a practical transducer (that is mainly of a loudspeaker). We know that it is a causal and stable system. Its poles are

consequently inside the unit circle. But we know nothing about its zeros. Some of them may well be outside the unit circle which would imply poles outside for the inverse. **Figure 4.1** shows the impulse response obtained by inverse Fourier transforming the inverse of the frequency response of the secondary transducer, whose measurement was discussed in §III.3, taken over 2048 points. The important non causal part suggests that the inverse of such a transducer is very likely to have poles outside the unit circle. In fact, since a loudspeaker can generate no pressure in an anechoic duct at a frequency of 0 Hz, we know already that a zero is located on z=1, that is exactly on the unit circle. Moreover, Trans(z) is not only the transfer function of the loudspeaker but takes into account the detection microphone, the sampling system, the anti-aliasing and reconstructing filters, generally, both filters of a very high order with consequently many poles and zeros

IV.1.2 Yule-Walker equations

Fortunately, there is a distance between the detection microphone and the secondary source. The problem we have to deal with is thus somewhat easier than just calculating a causal inverse of the transducer. This correspond to taking the term $-e^{-jkl_2}$ (which correspond to a pure delay if no loss is present in the duct) from numerator of term II in equation (4.0) to term I. The delay allows us to have access to some of the non-causal part of the inverse. The situation is described on **figure 4.2**. The signal x(n) is delayed by p samples before being compared to the signal y(n). In practice the W filter is situated on the left of hs but since they are linear filters, we can commute them for convenience of calculation. From now the notation will be as follow :

scalars are denoted by plain letters   :   x

vectors are denoted by bold letters   :   **x**

matrices are denoted by bold bracketed capital letters :   **[M]**

vectors elements and matrices elements are written x_i and $[M]_{ij}$.

Moreover if x(n) is a sampled signal we define a regressing vector of order N :

$$\mathbf{x}(n) = [x(n), x(n-1), x(n-2), \ldots\ldots, x(n-N-1)]^T$$

Now, suppose that W is an FIR filter described by the tap delay vector

$$\mathbf{w} = [w_0, w_1, w_2, \ldots\ldots, w_{N-1}]^T$$

We want to determine **w** in such a way that the expectation of the square of the error vector is minimum.

The error at time n is

$$e(n) = d(n)-y(n) = d(n)+w^T r(n) \qquad (4.4)$$

We want to minimize the expectation of the square of the error that is

$$E\{e^2(n)\} = E\{(d(n) + w^T r(n))^2\} \qquad (4.5)$$

$$E\{e^2(n)\} = E\{d^2(n)\} + 2E\{d(n)r^T(n)\}w + w^T E\{r(n)r^T(n)\}w \qquad (4.6)$$

$$E\{e^2(n)\} = E\{d^2(n)\} + 2c_{rd}{}^T w + w^T[A_{rr}]w \qquad (4.7)$$

where c_{rd} is the cross-correlation vector between the desired response and the output signal and $[A_{rr}]$ is the autocorrelation matrix of the signal r(n)

Equation (4.7) describes the error function $E[e^2(n)]$ as a quadratic function of the coefficients of the filter W. Such a function has a unique minimum given by the condition :

$$\frac{\partial}{\partial w_i} E[e^2(n)] = 0 \quad \text{for } 0 \le i \le N-1$$

which can also be written as

$$E[2.e(n).\frac{\partial}{\partial w_i} e(n)] = 0 \quad \text{for } 0 \le i \le N-1$$

which from (4.7) gives

$$[A_{rr}]w = -c_{rd} \qquad (4.8)$$

This system known as the Wiener-Hopf, Yule-Walker or Normal equations [21], can be solved to give the optimal FIR filter of given length in the mean-square sense :

$$w_{opt} = -[A_{rr}]^{-1}c_{rd} \qquad (4.9)$$
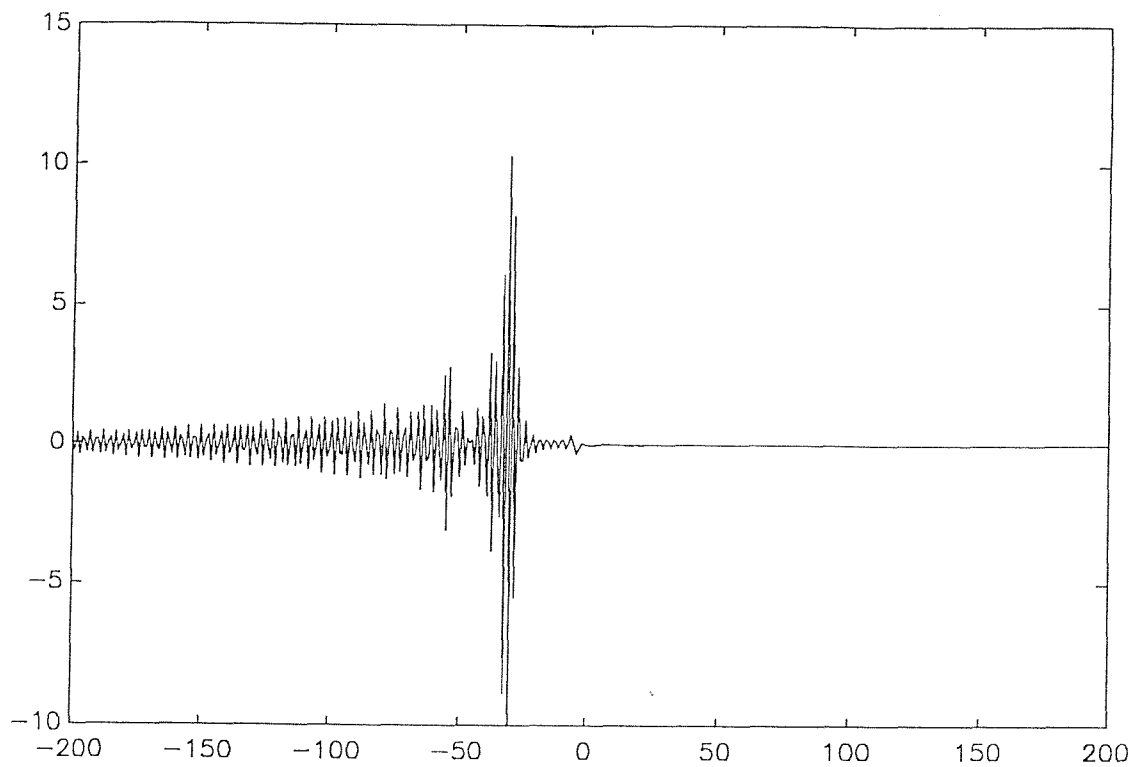
Figure 4.1 Inverse of the secondary transducer obtained by inverse Fourier transforming the measured 1/(Hs.Md) taken over 2048 points. The non-causal component demonstrates that (Hs.Md) is non-minimal phase.
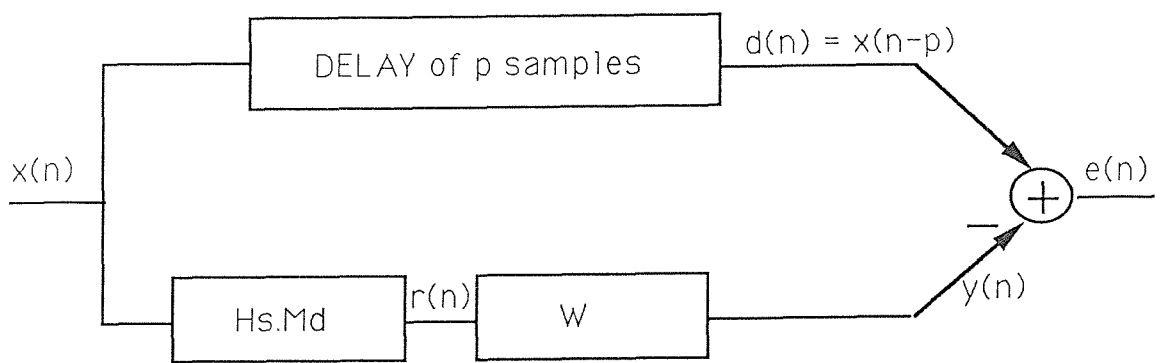
Figure 4.2 Least square identification of the inverse of the louspeaker : principle

IV.1.3 Optimal inverse for different length of the direct path

Consider two sampled signals $x(n)$ and $y(n)$ whose z transforms are $X(z)$ and $Y(z)$. The expressions of power spectral and cross-spectral density are :

$$S_{xx}(z) = E\{X(1/z).X(z)\}$$
$$S_{xy}(z) = E\{X(1/z).Y(z)\}$$

Where $E\{\}$ means expectation or average over ensemble.
Taking the inverse-z-transform of both members leads us to the autocorrelation and intercorrelation functions $a_{xx}(n)$ and $a_{xy}(n)$. Using the properties of the z transform :

$$Z^{-1}(X(z).Y(z)) = Z^{-1}(X(z)) * Z^{-1}(Y(z))$$
$$Z^{-1}(X(1/z)) = x(-n)$$

we have :

$$a_{xx}(n) = E\{x(-n)*x(n)\}$$
$$a_{xy}(n) = E\{x(-n)*y(n)\}$$

Imagine now that the input signal $x(n)$ depicted on **figure 4.2** is a white noise with unity variance, the autocorrelation function of $r(n)$ is given by

$$a_{rr}(n) = E\{r(n)*r(-n)\} \tag{4.10}$$

moreover

$$r(n) = x(n)*trans(n) \tag{4.11}$$

with $trans(n)$ as the transducer impulse response.

So, the autocorrelation function can be written as :

$$a_{rr}(n) = E\{x(-n)*trans(-n)*x(n)*trans(n)\} = E\{trans(-n)*trans(n)*x(-n)*x(n)\} \tag{4.13}$$

x(n) is a white noise, it implies

$$E\{x(-n)*x(n)\} = \delta(n)$$

and therefore, since trans(n) is a deterministic signal,

$$a_{rr}(n) = trans(n)*trans(-n)*\delta(n) = trans(n)*trans(-n) \qquad (4.14)$$

Then, the autocorrelation matrix $[\mathbf{A}]_{rr}$ in (4.9) has elements which can be calculated from the transducer impulse response.

Similarly, since in this case the desired signal is the delayed reference $d(n) = x(n-p)$, then

$$c_{rd}(n) = E\{x(-n)*trans(-n)*x(n-p)\} \qquad (4.15)$$

$$c_{rd}(n) = E\{trans(-n-p)*x(-n)*x(n)\} = trans(-n-p)*\delta(n) \qquad (4.16)$$

$$c_{rd}(n) = trans(-n-p) \qquad (4.17)$$

This last relation is most interesting. The cross-correlation function is simply the impulse response of the loudspeaker reversed in time and shifted by p samples to the right. Now let us come back to the Yule -Walker equations. The autocorrelation matrix contains information about the transducer power spectral density , but no information about its phase. The cross-correlation vector on the other hand contains information about the system phase. How much information does it contain? Since trans(n) is causal it means that trans(-n) = 0 for n>p where p is modelling delay in **figure 4.2**. Then, using (4.17), we deduce that $c_{rd}(n) = 0$ for n>p. Moreover since W is also causal the samples $c_{rd}(n)$ for n < 0 will not be considered. This implies that the cross correlation vector contains information about the first p samples of the impulse response of the loudspeaker. If p = 0 for instance there is no information in the cross -correlation vector and therefore it is impossible to predict the genuine output if x(n) is white and the system is non-minimum phase. If p>m, length of the transducer impulse response, the cross correlation vector contains all the information about the transducer and the attenuation should be significant. A rule of thumb should be to ensure that p > m. It is of course possible that in doing this we largely over estimate the minimum value of p particularly if

the loudspeaker is mainly an autoregressive system. To determine the genuine value for p one can imagine shortening the transducer impulse response by compensating the pole of the system using an AR estimation. Once compensated, the impulse response of the modified transducer would only consist of its non-minimal phase components. However this complicates substantially the active noise control system.
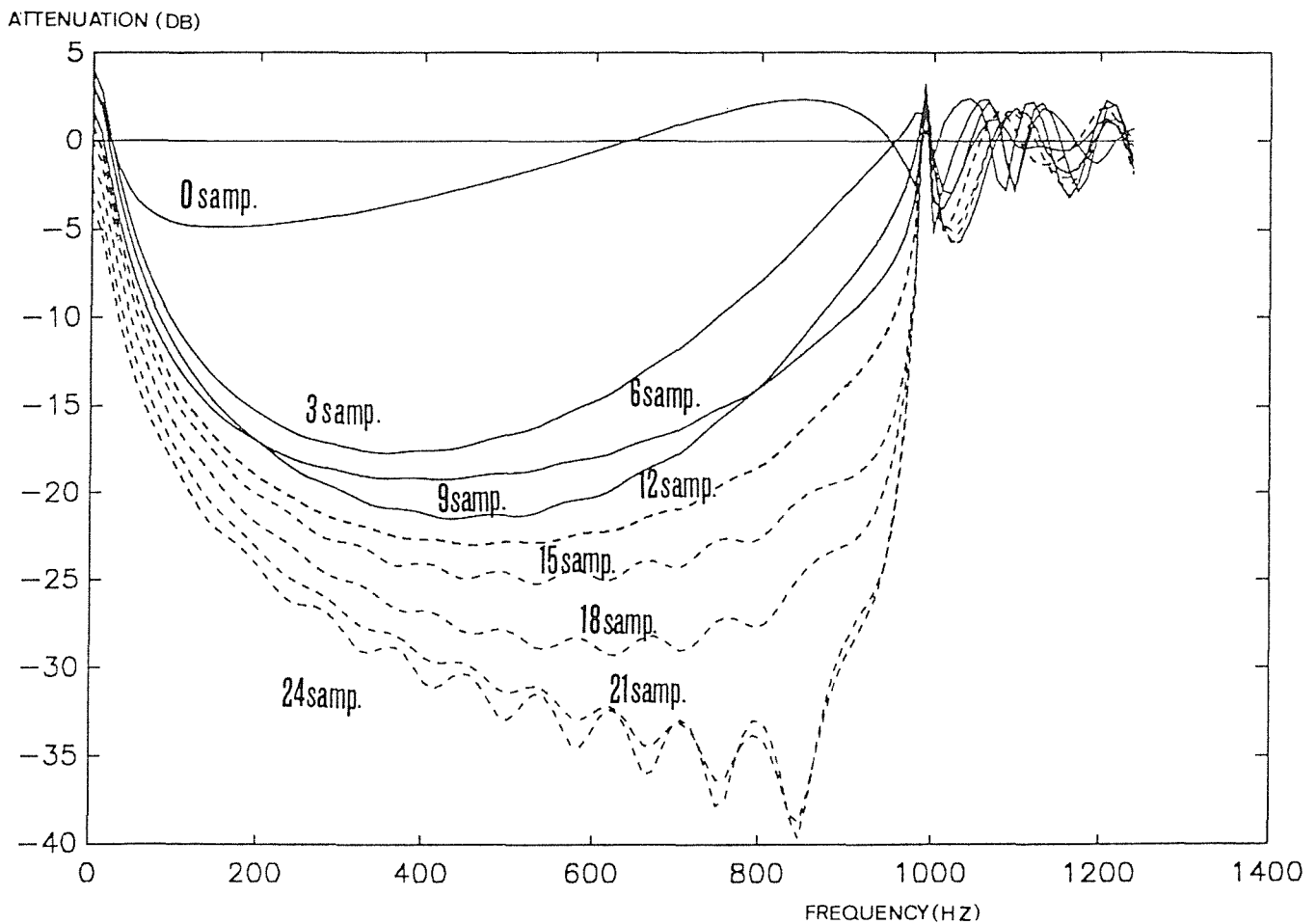
ATTENUATION (DB)

Figure 4.3 Limitation in the attenuation due to the loudspeacker for diverse length of the direct path.

Figure 4.3 shows the predicted attenuation i.e. the spectrum of the minimum possible error sequence in **figure 4.2,** for different values of the delay parameter p. The loudspeaker is the one used in our experiment (impulse response given on **figure 3.4**) and the number of coefficients of the W filter is 250. The results agree well with the conclusions drawn above. There is nearly no attenuation for p=0 and when p $\cong$ m (m $\cong$ 25 is the length of the significant part of hs(n) in **figure 3.4**) the performance levels off.

Moreover we can see that the potential attenuation of the active control system is severely limited at low frequencies from 200 Hz and below because of the non-minimal phase properties of the loudspeaker. The singularity at high frequencies can be explained by considering the responses of the anti-aliasing and reconstructing filters, whose slopes are too steep to be inverted. This high frequency behaviour, however, does not matter too much ; the active control system is not designed to operate at such frequencies.

In the experiment the distance between the detection microphone and the secondary source is 1.224m and corresponds to a delay of 9 samples at the sample rate of 2500 samples per second. From **figure 4.3** we can predict that the attenuation for the real system will not be better than 20dB with non deterministic signals. Consequently the loudspeaker is very likely to be the limiting factor in our experiment. Of course it is still possible to increase the delay between the detector and the actuator, a delay of 21 samples giving nearly 30bB in the middle of the frequency band. To obtain such a large delay, however, the section of duct between the detection sensor and the secondary source need to be 3m long, which is not always possible in a practical system.

IV.2   Least square controller if Trans(jω) = 1

In this section we study three alternative structure for the controller. We assume for now that the responses of the two transducer are perfectly uniform. For each controller structure we will determine the optimal controller in the least mean square sense and hence predict its optimal performance for various filter lengths.

IV.2.1 Feedback cancellation structure

The feedback cancellation structure is shown in **Figure 4.4** . The controller is made of two components : a feedforward filter, W and a feedback one, F'. The interest of such a structure is easy to understand. If the feedback canceller is exactly opposite to the feedback path, the coupling between the secondary source and the detection microphone is removed. The system input signal is not corrupted and the controller acts as a purely feedforward one. This structure has been used in telephone networks and is called an echo canceller [22]. More details about this realisation will be given in the next chapters.

In this paragraph we consider the echo canceller to be perfect. The system, represented on **Figure 4.5** , is now simplified : the feedback path has disappeared and the linearity and time invariance has enabled us to swap the error path and the controller.

YULE-WALKER EQUATIONS

The problem of finding the FIR filter W which minimizes the mean square of the error can be treated in the same manner as previously since the error surface is obviously quadratic. Given the convention of **figure 4.5** and according to the theory presented in the previous section, the optimal filter W is the solution of the Yule-Walker equations

$$[A_{rr}]w_{opt} = -c_{rd} \qquad (4.18)$$

$$w_{opt} = -[A_{rr}]^{-1}c_{rd} \qquad (4.19)$$

where $[A]_{rr}$ is the autocorrelation matrix of r(n) which is now the reference signal x(n) filtered by the responses corresponding to B and C ; c_{rd} is the cross-correlation vector between r(n) and d(n) where d(n) is x(n) filtered by **A**.

Assuming that x is again white noise and proceeding similarly to (4.11) we have.

$$a_{rr}(n) = E\{b(-n)*c(-n)*x(-n)*b(n)*c(n)*x(n)\} = a_{bb}(n)*a_{cc}(n) \qquad (4.20)$$

and

$$c_{rd}(n) = E\{b(-n)*c(-n)*x(-n)*a(n)*x(n)\} = b(-n)*c(-n)*a(n) \qquad (4.21)$$
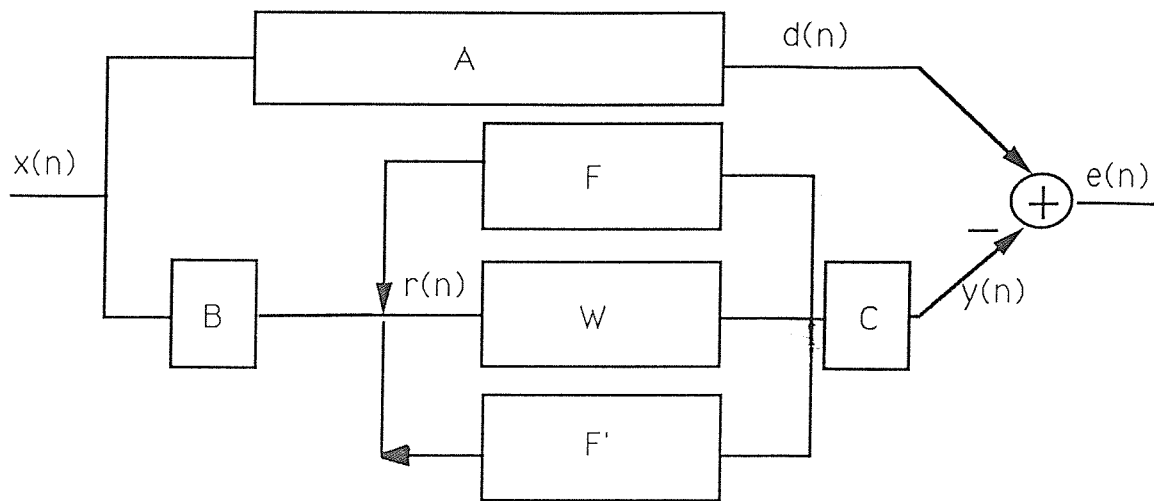
Figure 4.4 Feedback cancellation structure
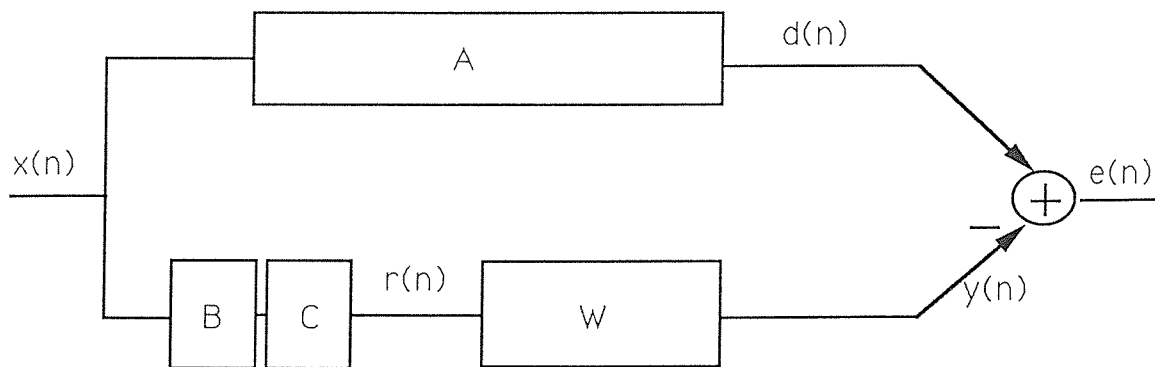
Figure 4.5 Least square identification assuming the echo canceller is perfect
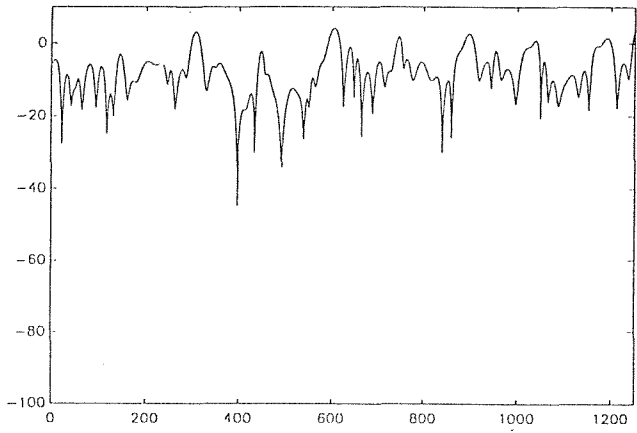
75 coefs
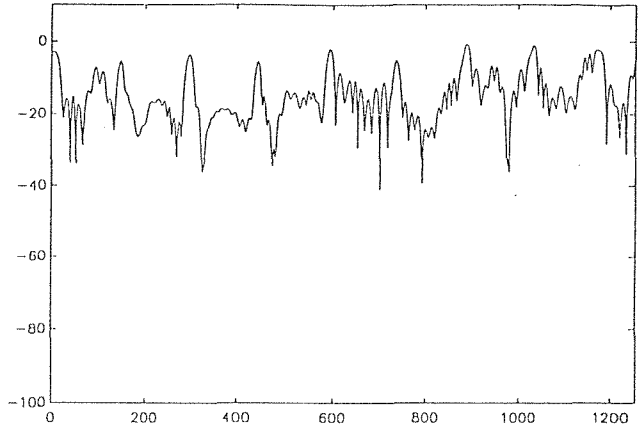
150 coefs
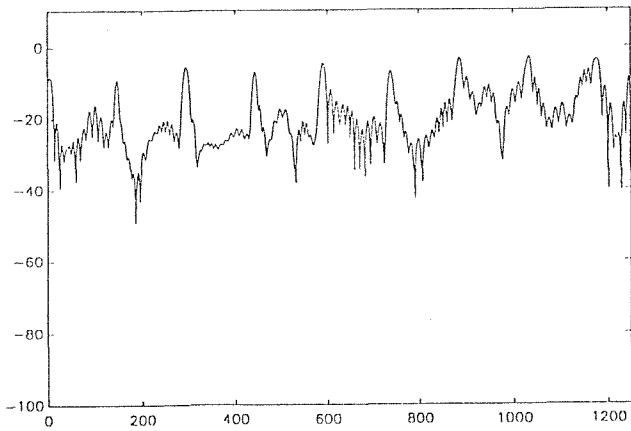
200 coefs
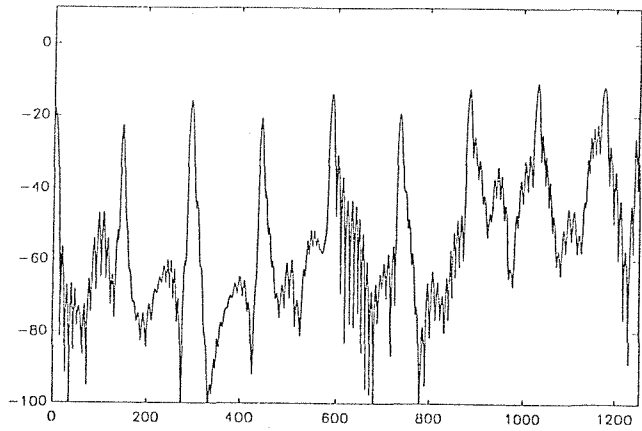
250 coefs

Figure 4.6 Attenuation predicted in the purely feedforward case. R1=0.38
R2= -0.83. The secondary source is assumed to have a perfectly flat response

Using the models described in chapter II for a(n), b(n), c(n) it is therefore possible to calculate the autocorrelation vector and to solve for the controller response numerically. We have chosen for the reflection coefficients the approximate values they have in the real experiment. **Figure 4.6** shows the attenuation predicted for various numbers of coefficients. When the controller has less than 75 coefficients the attenuation is very poor. Above 150 coefficients it can be more than 20dB for some frequencies. 250 coefficients lead to satisfactory results (this number is currently used in the real experiment). However we notice the presence of peaks in the spectrum. Such peaks limit the global attenuation to 20dB for the feedback cancellation system with 250 coefficients.

COHERENCE FUNCTION

Now consider again (4.18) and suppose that W is a non causal FIR filter of unconstrained length. In practice the number of coefficients of W must be much larger than the number of coefficients of the autocorrelation and crosscorrelation functions, supposed to be of finite duration. Under these conditions it is easy to show that (4.18) is equivalent to

$$w_{opt}(n) * c_{rr}(n) = -c_{rd}(n) \qquad \text{for } -\infty < n < \infty \qquad (4.22)$$

taking the Fourier transform of both sides of this equation, we have

$$W_{opt}(j\omega).S_{rr}(j\omega) = -S_{rd}(j\omega) \qquad (4.23)$$

and so

$$W_{opt}(j\omega) = -\frac{S_{rd}(j\omega)}{S_{rr}(j\omega)} \qquad (4.24)$$

Where S_{rr} is the power spectral density function of r(n) and S_{rd} is the cross-spectral density function of r(n) and d(n).

The result expressed in (4.24) is known as the Wiener filter [23] and gives the optimal unconstrained controller. It is satisfactory to note that we have obtained this result from the time domain Yule-Walker equations extended to the unconstrained case.

Moreover, as previously, we can define the frequency domain error function as

$$S_{ee}(j\omega) = E\{ E(j\omega)^*.E(j\omega) \}$$

i.e.

$$S_{ee}(jw) = E\{ [D(j\omega) + W(j\omega).R(j\omega)]^*. [D(j\omega) + W(j\omega).R(j\omega)] \} \qquad (4.25)$$

so that

$$S_{ee}(jw) = S_{dd} + W^*.S_{rd} + W.S_{rd}^* + WW^*.S_{rr} \qquad (4.26)$$

When the controller is off, the error power spectral density is

$$S_{ee}(off) = S_{dd}$$

When the optimal filter is used, the spectral density of the error is given by substituting (4.24) into (4.26) which gives :

$$S_{ee}(on) = S_{dd} - \frac{S_{rd}.S_{rd}^*}{S_{rr}}$$

Therfore the best attenuation we can achieve with an unconstrained filter is

$$\frac{S_{ee}(on)}{S_{ee}(off)} = 1 - \frac{S_{rd}.S_{rd}^*}{S_{rr}S_{dd}} = 1 - \gamma^2_{rd} \qquad (4.27)$$

The γ^2 function is called the coherence function and is available on most spectrum analyzers. The result (4.27) is a classical one in optimal control (see [23]). It shows that the best possible reduction using a unconstrained feedforward control system is limited in a simple way by the coherence between the measurable signals from the detection and error sensors. In the simulations considered here, however, no measurement noise is assumed and so the coherence between r(n) and d(n) is perfect ($\gamma^2_{rd} = 1$) and the residual error for a completely unconstrained filter is thus zero, as expected.

IV.2.2 Simple FIR structure

Suppose now that we remove the echo canceller. The controller then consists only of a simple transversal filter W.

Finding the optimal finite length controller is not so easy in this case. The feedback introduces several problems ; the first one is that the error surface is no longer a quadratic function of the controller coefficients. We can prove this fact by working from the frequency domain analysis.

In chapter II we have established the following formula

$$Ve(j\omega) = \frac{A - A.W.F + C.W.B}{1 - W.F}.Vp(j\omega) \qquad (4.28)$$

After expansion of the denominator into $1+WF+(WF)^2+(WF)^3+...$(assuming $|WF|<1$ for all ω, which is generally the case with practical realisations), we have :

$$Ve(j\omega) = (A - AWF + CWB).(1+WF+(WF)^2+(WF)^3+.....)Vp(j\omega) \qquad (4.29)$$

an inverse Fourier transform leads to :

$$v_e(n) = \big(a(n) - w(n)*(a(n)*f(n)-b(n)*c(n)\big) * \big(\delta(n)+w(n)*f(n)+(w(n)*f(n))^{(2)}+.....\big)*v_p(n) \qquad (4.30)$$

As $v_e(n)$ is an infinite order polynomial of the transversal filter coefficients, the square of the error, $(v_e(n))^2$, is also an infinite polonomial of the coefficients $w(i)$ and so the error surface cannot be quadratic. Such a non quadratic error surface can have several minimum values. Therefore the condition that the gradient of the expectation of the error equal to zero is not necessarily a sufficient one to find the optimal solution. However, given the complexity of the problem,we will investigate the consequences of fulfilling this condition.

The following lines describe a suboptimal algorithm, derived from the Yule-Walker equation, which converges to a minimum value of the error surface when the controller is a simple FIR filter.

First of all, we know from expression (2.26) that the ideal controller is independent of the error path and from the reflection coefficients. To simplify the calculation we will thus suppose that $C(j\omega) = 1$, $B(j\omega) = 1$ and $R_1 = R_2 = 0$, so that $F(j\omega)$ is a pure delay.

Given these approximations the system can be represented as in **figure 4.7**
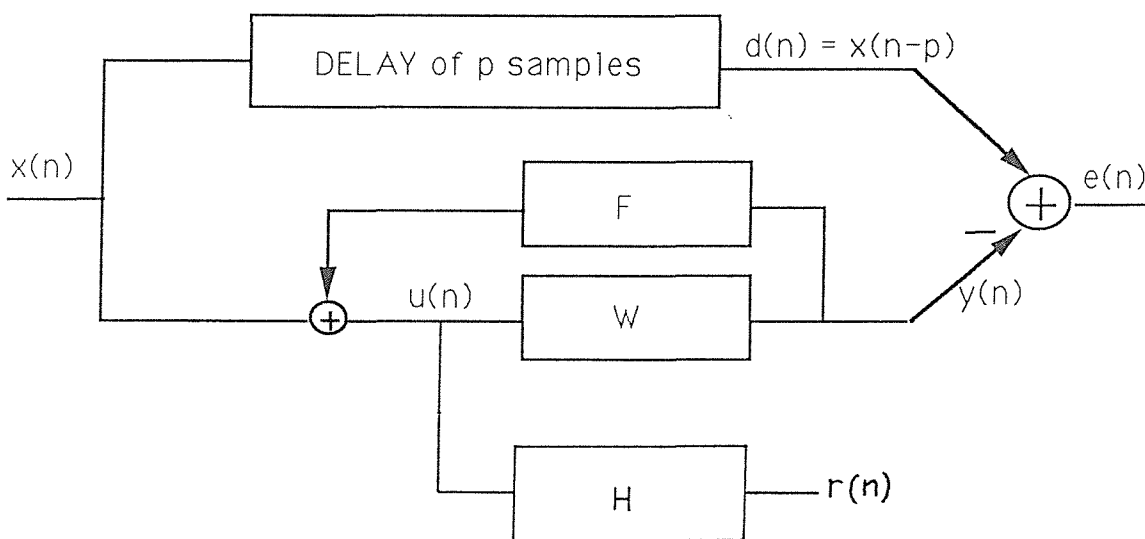
Figure 4.7 Least square identification (with a simplified error path) in presence of the feedback path.

-52-

TIME DOMAIN OPTIMIZATION

As previously we want to find the transversal filter W such as

$$\frac{\partial}{\partial w_i} E\{e^2(n)\} = 0 \quad \text{for } 0 \leq i \leq N-1$$

We can start from

$$E\{e^2(n)\} = E\{d^2(n)\} + 2c_{ud}{}^T w + w^T [A_{uu}] w$$

and differentiate it. However this leads to some tedious calculation since $\frac{\partial}{\partial w_i}[A_{uu}]$ can only be expressed in a recursive manner.

Fortunately, there is also another method using the instantaneous gradient. In (appendix B.2) is derived the expression of the gradient of the instantaneous error.

$$\left(\frac{\partial e(n)^2}{\partial w_i}\right) = e(n).(h(n)*u(n-i))$$

where $h(n)$ is the filter whose z transform is

$$H(z) = \frac{1}{1 - F(z).W(z)}$$

where $F(z)$ represents the feedback path. In this case we assume $F(z) = z^{-p}$.(feedback path delay equal to primary path delay)
Since

$$\frac{\partial}{\partial w_i} E\{e^2(n)\} = E\left\{\frac{\partial}{\partial w_i} e^2(n)\right\} \quad (4.31)$$

we have

$$\frac{\partial}{\partial w_i} E\{e^2(n)\} = E\{e(n).(h(n)*u(n-i))\} = E\{[d(n)+w(n)*u(n)].[h(n)*u(n-i)]\}$$

$$(4.32)$$

Let the signal $u(n)$ filtered by H be $r(n)$,

$$\frac{\partial}{\partial w_i}E\{e^2(n)\} = E\{d(n).r(n-i)\} + E\{\sum_{j=0}^{N}(w_j.u(n-j).r(n-i))\} \tag{4.33}$$

$$\frac{\partial}{\partial w_i}E\{e^2(n)\} = c_{rd}(i) + \sum_{j=0}^{N}(w_j.E\{u(n-j).r(n-i)\}) \tag{4.34}$$

$$\frac{\partial}{\partial w_i}E\{e^2(n)\} = c_{rd}(i) + \sum_{j=0}^{N}(w_j.c_{ru}(i-j)) = 0 \qquad \text{for all i} \tag{4.35}$$

Where $c_{rd}(n)$ is the cross-correlation function between $d(n)$ and $r(n)$ and $c_{ru}(n)$ is the cross-correlation function between $u(n)$ and $r(n)$.

(4.35) can now be expressed in a matrix terms:

$$[A_{ru}]w = -c_{rd} \tag{4.36}$$

$[A_{ru}]$ is a (Ntimes N) non symmetric matrix defined as follows :

$$[A_{ru}]_{ij} = c_{ru}(i-j) \tag{4.37}$$

c_{rd} is the cross-correlation vector between $r(n)$ and $d(n)$.

(4.36) is a relation similar to the Yule-Walker equation but this time the sytem is a non linear one since because of the feedback path, both $[A_{ru}]$ and c_{rd} depend on w in a non linear way.

Suppose however, that we give to the controller some value w_0 . We can calculate $[A_0{}_{ru}]$ and $c_0{}_{rd}$, crosscorrelation matrix and cross correlation vector related to w_0. Using (4.36) we can deduce w_1 which should be closer to the optimal controller than the initial guess.

$$w_1 = -[A_0{}_{ru}]^{-1}c_0{}_{rd} \tag{4.38}$$

We can then calculate the new crosscorelation matrix and vector and iterate (4.38) until the controller converges to the "optimal" solution.

$$w_{n+1} = -[A_{n\ ru}]^{-1}c_{n\ rd}$$ (4.39)

The **figure 4.8** shows the attenuation obtained by iterating (4.39) for various controller lengths and starting with $w_0 = 0$. Typically, 10 iterations are required for convergence. The excitation $x(n)$ is white and the number of tap delays varies from 64 to 210 . The attenuation increases with the number of coefficients but is limited at some regularly spaced frequencies. We know that these frequencies correspond to those for which a node of pressure is present at the detection sensor. Because of its FIR structure, the controller is not able to supply the infinite gain required at these frequencies,.

FREQUENCY DOMAIN OPTIMIZATION

Assuming as in IV.2.1 that the controller impulse response is not constrained to be causal and of larger duration than the crosscorrelation function, we can deduce from (4.36) an expression similar to (4.22).

$$w_{opt}(n)*c_{ru}(n) = -c_{rd}(n)$$ (4.40)

Fourier transforming both terms leads to

$$W_{opt}(j\omega).S_{ru}(j\omega) = -S_{rd}(j\omega)$$ (4.41)

moreover

$$S_{ru} = \frac{-S_{uu}}{(1 - W_{opt}.F)^*}$$ (4.42)

$$S_{uu} = \frac{S_{xx}}{(1 - W_{opt}.F)^*(1 - W_{opt}.F)}$$ (4.43)

and

$$S_{rd} = \frac{S_{xd}}{(1 - W_{opt}.F)^*(1 - W_{opt}.F)} \qquad (4.44)$$

substituing (4.42), (4.43), (4.44) into (4.41) we obtain, after eliminations at both sides.

$$W_{opt}(j\omega) = -\frac{S_{xd}(j\omega)}{S_{xx}(j\omega)}.(1 - W_{opt}(j\omega).F(j\omega)) \qquad (4.45)$$

hence

$$W_{opt}(j\omega) = -\frac{S_{xd}(j\omega)}{S_{xx}(j\omega)\left(1 - .F(j\omega)\frac{S_{xd}(j\omega)}{S_{xx}(j\omega)}\right)} \qquad (4.46)$$

Suppose that x(n) is white and there is no measurement noise in the system, since the reflexion coefficients are supposed equal to zero, both direct path and feedback path transfer functions are equal to $e^{-j\gamma l_2}$

Then

$$\frac{S_{xd}(j\omega)}{S_{xx}(j\omega)} = e^{-j\gamma l_2} \qquad (4.47)$$

Substituting (4.47) into (4.46) and replacing F(jω) by $e^{-j\gamma l_2}$ gives

$$W_{opt}(j\omega) = -\frac{e^{-j\gamma l_2}}{1 - .e^{-2j\gamma l_2}} \qquad (4.48)$$

This result is not surprising : it has already been found in chapter II (equation 2.26) using a deterministic calculation. It proves the consistency of the two approaches : the deterministic one and the stochastic one.

Proceeding as in the previous chapter we can define a frequency domain error function :

$$S_{ee}(j\omega) = E\{ E(j\omega)^*.E(j\omega) \}$$

$$S_{ee}(jw) = E\{ [D(j\omega) + W(j\omega).U(j\omega)]^* . [D(j\omega) + W(j\omega).U(j\omega)] \} \qquad (4.49)$$

$$S_{ee}(jw) = S_{dd} + W^*.S_{ud} + W. S_{ud}^* + WW^*. S_{uu} \qquad (4.50)$$

hence

$$S_{ee}(jw) = S_{dd} + \frac{W^*}{(1 - W.F)^*} S_{xd} + \frac{W}{(1 - W.F)}. S_{xd}^*$$

$$+ \frac{WW^*}{(1 - W.F)(1 - W.F)^*} S_{xx} \qquad (4.51)$$

from (4.45) we deduce

$$W_{opt}. = -\frac{S_{xd}(j\omega)}{S_{xx}(j\omega)}.(1 - W_{opt}(j\omega).F(j\omega)) \qquad (4.52)$$

Substituting (4.52) into (4.51) gives

$$S_{ee}(on) = S_{dd} - \frac{S_{xd}.S_{xd}^*}{S_{xx}}$$

and

$$S_{ee}(off) = S_{dd}$$

then

$$\frac{S_{ee}(on)}{S_{ee}(off)} = 1 - \frac{S_{xd}.S_{xd}^*}{S_{xx} S_{dd}} = 1 - \gamma^2_{xd} \qquad (4.53)$$

The optimal attenuation depends again on the coherence between the excitation signal and the reference signal. It is satisfying to notice that the theoretical optimum does not depend on the controller structure.
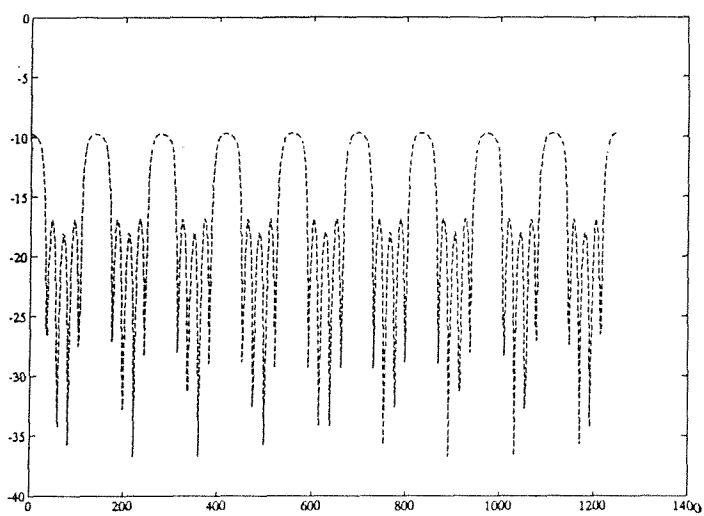
64 coefs
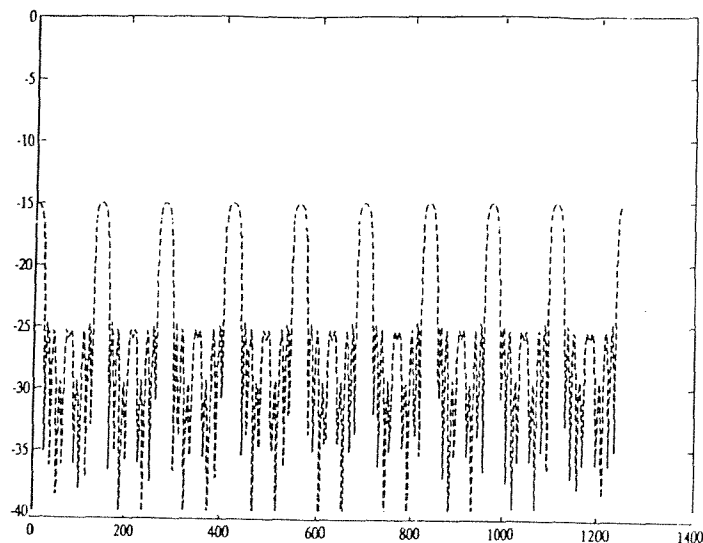
100 coefs
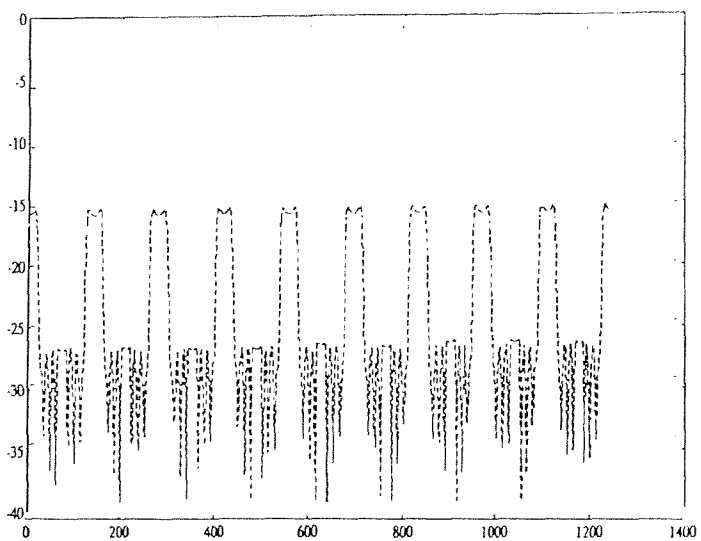
150 coefs
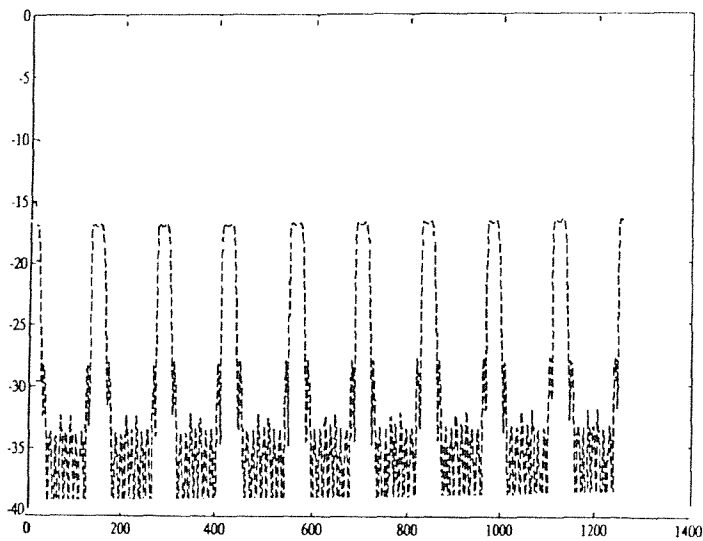
210 coefs

Figure 4.8 Maximum attenuation predicted in presence of the feedback path for different FIR controller lengths.

IV.2.3 IIR structure

This structure is shown in **figure 4.9** with error path (C) reordered for clarity. The controller comprises a two part filter (W, V) :W identifies the zeros whereas V identifies the poles of the ideal controller

The transfer function of such a controller is

$$T(j\omega) = \frac{W(j\omega)}{1 - V(j\omega)} \tag{4.54}$$

The main interest of this filter combination lies on the similarity of structure between the IIR controller and the optimal deterministic controller described in chapter II.
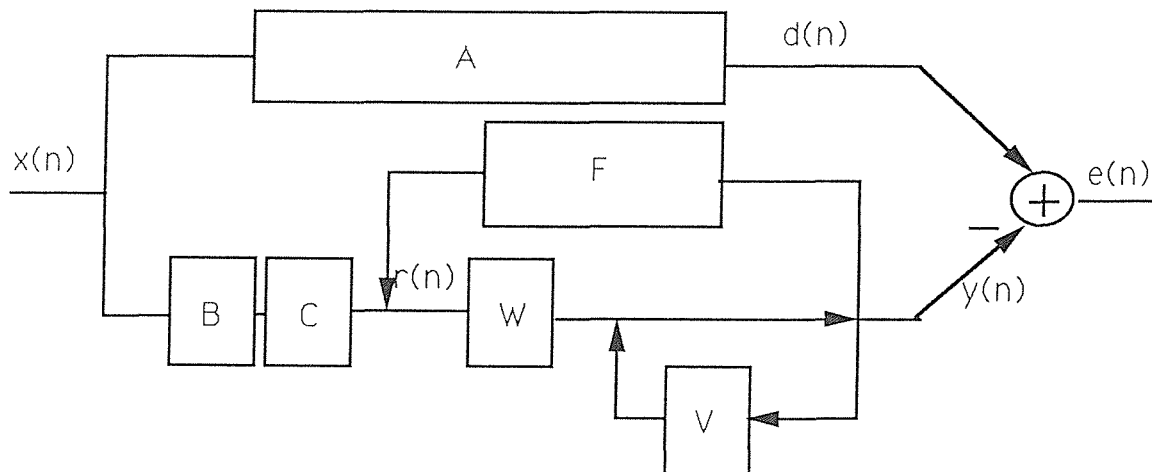
Figure 4.9 Structure of an IIR controller

Assuming that the excitation signal and the reference signal are perfectly correlated we can deduce immediatly from (2.26) and (4.54) the optimal transfer functions of V and W.

$$\frac{W(j\omega)}{1 - V(j\omega)} = \frac{-e^{-jkl_2}}{1 - e^{-2jkl_2}}$$

gives

$$W_{opt}(j\omega) = - e^{-jkl_2} \qquad\qquad (4.55)$$

$$V_{opt}(j\omega) = e^{-2jkl_2} \qquad\qquad (4.56)$$

If excitation and reference signal are not correlated, the search for the optimal recursive controller leads to extremely tedious calculation. The case will not be examined here since we shall study extensively the recursive structure in the next controller implementation.

IV.2.4 Summary

The first part of this chapter shows that the problem of inverting the response of the electroacoustical transducers and anti-aliasing filters limits the attenuation to about 20dB. In the second part we find that 20dB is also the best attenuation that a FIR controller of 250 coefficients can achieve with a perfect transducer. Whereas it is still possible to improve the second problem by increasing the number of transversal tap delays or by using a recursive controller, the first problem might be difficult to solve. Effectively as we have noticed, the response of the transducers and filters is non minimal phase and cannot be inverted perfectly by a causally constrained controller. Therefore, significant improvement in active noise control realisation will require improvement in transducer technology.

CHAPTER V

Adaptive time domain algorithms

Now that we have developed the basic theory for the ideal optimal controller, we wil consider different realisations of adaptive active noise control methods. Adaptive methods are often to be prefered in practice to exact least squares methods (i.e. direct solution of the Yule-Walker Equations) because of the smaller computational burden and the capacity for adaptive methods to track variations in signal statistics. All the methods described below are strongly linked to the well known LMS algorithm. We will thus first describe the main features of this algorithm.

V.1. The LMS algorithm

V.1.1. The use of the LMS algorithm for system identification

The LMS algorithm was been developed in the 1960's and the 1970's by Widrow and others in order to design robust and easy to compute adaptive filters. An very complete description of this algorithm and its properties is given in reference [24]. In this paragraph we will review the basic features of the LMS algorithm.

Since the LMS algorithm is widely used in system identification, we will concentrate on this application. **Figure 5.1** shows the principle of any identification process. Both the input and output of a plant (A) are known. A filter W is used to calculate a prediction of the plant output. At each sample, the W filter is updated according to some criterion applied on the prediction error e. In the case of the LMS algorithm the criterion is to minimize the Least Mean Square error, hence the name.
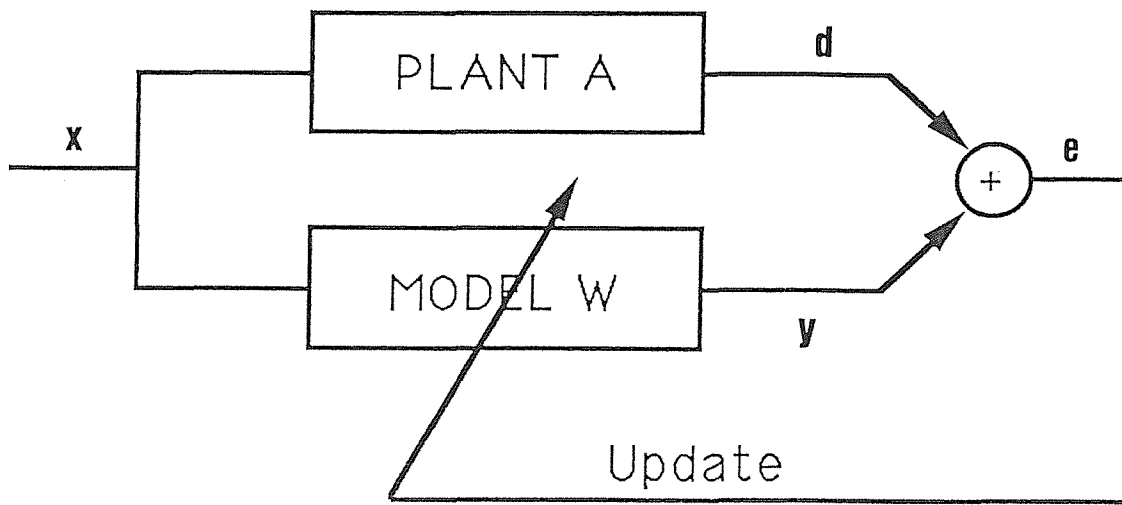
Figure 5.1 System identification using an adaptive filter
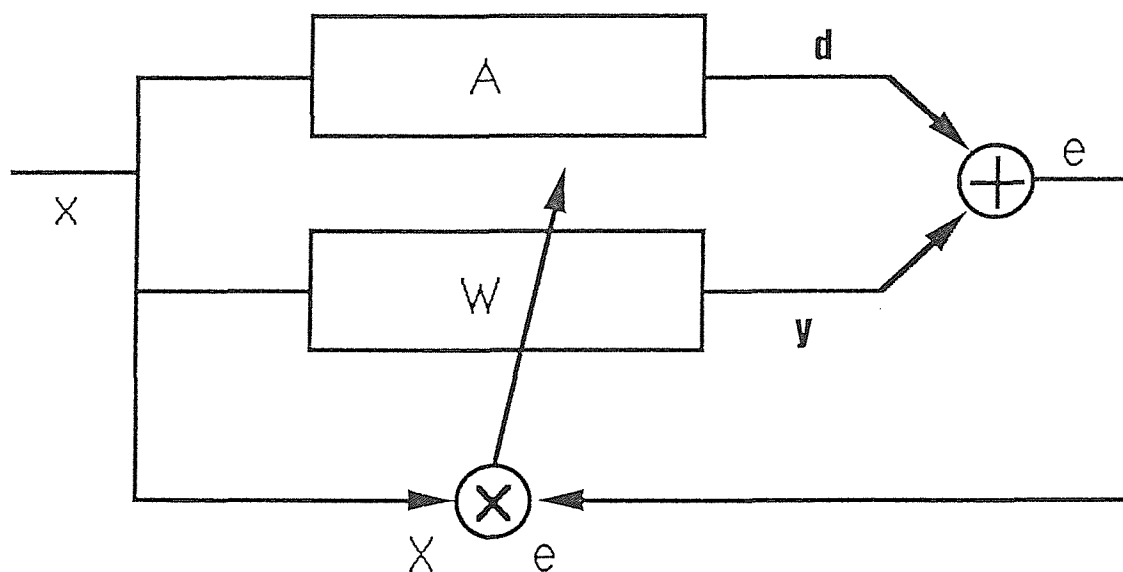
Figure 5.2 Schematic description of the LMS algorithm : The product of the input vector X by the error is used to update the filter W.

If W is an FIR filter, we have seen in chapter IV that the expectation of the square of the error is a quadratic function of the W coefficients. The LMS algorithm uses an iterative procedure based on an approximate steepest decent method to seek the error surface bottom. The principle is as follows :

The vector coefficient of the filter W at instant n is denoted

$$\mathbf{w}(n) = (w_0(n), w_1(n), ..., w_N(n))^T$$

the instantaneous error gradient vector at instant n is then

$$\Phi(n) = (\phi_0(n), \phi_1(n), ..., \phi_N(n))^T = (\frac{\partial e^2(n)}{\partial w_0(n)}, \frac{\partial e^2(n)}{\partial w_1(n)}, ...,\frac{\partial e^2(n)}{\partial w_N(n)})^T$$

Similarly, the input vector at instant n is defined as

$$\mathbf{x}(n) = (x(n), x(n-1), x(n-2),...,x(n-N))$$

The update equation for the filter at the step n+1 is defined to be

$$\mathbf{w}(n+1) = \mathbf{w}(n) - \mu.\Phi(n) \tag{5.1}$$

and μ is a constant that regulates the speed and stability of adaption.

Fom the **figure 5.1**, we have

$$e(n) = d(n) + \mathbf{w}(n)^T\mathbf{x}(n) \tag{5.2}$$

and since

$$\frac{\partial e^2(n)}{\partial w_k} = 2.e(n).\frac{\partial e(n)}{\partial w_k} \tag{5.3}$$

Then equations (5.1) (5.2) and (5.3) can be combined together to show that each element of Φ can be expressed as :

$$\phi_k(n) = 2.e(n).\frac{\partial w(n)^T}{\partial w_k(n)} x(n)$$

or $\quad \phi_k(n) = 2.e(n).\left[0, 0,...0,\dfrac{\partial w_k(n)}{\partial w_k(n)}, 0, ...0\right]^T x(n)$

therefore

$$\phi_k(n) = 2.e(n).x(n-k) \qquad\qquad\qquad (5.4)$$

So, in vector notation, the LMS algorithm can be expressed as

$$w(n+1) = w(n) - 2\mu.e(n).x(n) \qquad\qquad\qquad (5.5)$$

This formula can be represented graphically (see **figure 5.2**)

We can see in (5.1) that the change of the filter coefficient vector **w** is proportional to the opposite of the instantaneous gradient. Since $\Phi(n)$ is only an approximate estimate of the local gradient of the error surface (the variation of the *mean* square error with the filter coefficients), the LMS algorithm, strictly speaking, does not follow exactly the steepest descent line of the error surface. Without averaging, the gradient component contains a large amount of noise (it is sometimes called the stochastic gradient), but the noise is attenuated with time by the adaptive process, wich acts as a low pass-pass filter.
The main advantage of the LMS algorithm is that it can be implemented in a practical system without squaring, averaging, or differentiation and is elegant in its simplicity and efficiency.

V.1.2 Use of LMS algorithm in active control.

We have so far examined the simplest case of identification, i.e. when the error is obtained directly by the addition of the plant output and the filter output. This block diagram does not directly apply to the active control problem for two main reasons :
1- There is an additional transfer function between the filter output and the summing junction. This transfer function, C(s), is referred to as the error path.
2- The existence of a feedback path F(s) from filter output to filter input which modifies the expression of the gradient.

The block diagram of a typical active control system with these two transfer functions included is illustrated in **figure 5.3**.

(1) Influence of the error path (feedback path assumed zero)

The use of a theorem of linear filtering allows us to solve the problem introduced by the error path. Assuming that W is fixed i.e. not adapting (which is a reasonable approximation if the the filter coefficients are changing slowly compared to delays in C(s)) we can commute C and W. The case is now exactly similar to V.1.1 and we can therefore apply the same theory.

If we define x(n) filtered by C to be r(n), the filtered reference signal, i.e.

$$r(n) = \sum_{j=0}^{\infty} c_j . x(n-j) \qquad (5.6)$$

Where c_j are the coefficients of the impulse reponse of C, the update equation corresponding to the LMS algorithm for the filter coefficients in **figure 5.4** becomes

$$w(n+1) = w(n) - 2\,\mu . e(n) . r(n) \qquad (5.7)$$

This algorithm is sometimes called the filtered-x LMS (see **figure 5.4**) and is described in [24] as well as in [11].

(2) Influence of the feedback

We have seen in chapter IV that the presence of a feedback loop between the secondary transducer and the detection sensor makes the error surface non quadratic. Studying an IIR adaptive filtering algorithm in a similar case Flockton has shown in [25] that the expression of the instantaneous gradient has to be modified in order to take the feedback into account. The details of such a calculation will not be given here (see Appendix B.2 for more details), but we shall use the results of such an analysis. We will assume that althougth the error surface is non-quadratic it is at least unimodal so that a gradient descent method converges to a unique minimum.

From (B.2.14) the modified instantaneous gradient is :

$$\left(\frac{\partial e(n)^2}{\partial w_i}\right) = \phi_i(n) = e(n).h(n)*u(n-i) \tag{5.8}$$

where h(n) is now the filter whose z transform is

$$H(z) = C(z)\frac{1}{1 - F(z).W(z)} \tag{5.9}$$

which includes the effects of both error and feedback paths. u(n) is the signal which is fed to the filter **W** (**figure 5.3**), so that

$$U(z) = \frac{1}{1 - F(z).W(z)} X(z)$$

Finally if we define the modified filtered input signal as

$$r(n) = \sum_{j=0}^{\infty} h_j.u(n-j)$$

The updating formula is identical to (5.7),

$$w(n+1) = w(n) - 2 \mu.e(n).r(n) \tag{5.10}$$

but note that the definition of the filtered reference signal has been generalised.

(3) on line identification of H(z)

The algorithm described in (5.10) is different from the filtered-x LMS in the fact that the input signal has to be prefiltered by a modified error path filter

$$H(z) = C(z)\frac{1}{1 - F(z).W(z)}$$

The recursive component of H(z) comes from a modification given to the instantaneous gradient in order to take the feedback path into account. For this reason we propose to call this algorithm (originally put forward in [25]) the *modified-gradient filtered-x LMS algorithm*.
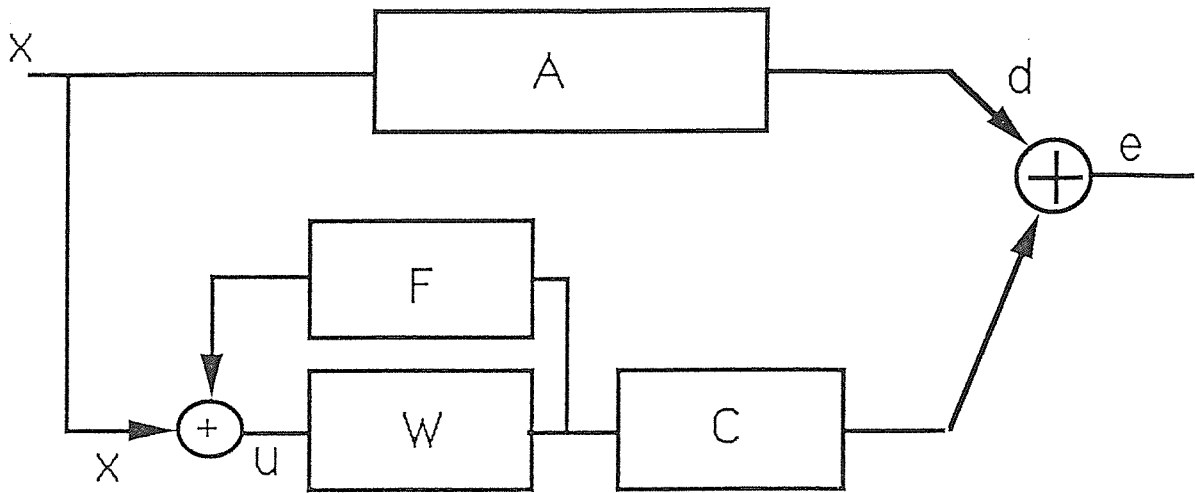
Figure 5.3 Error path and Feedback path
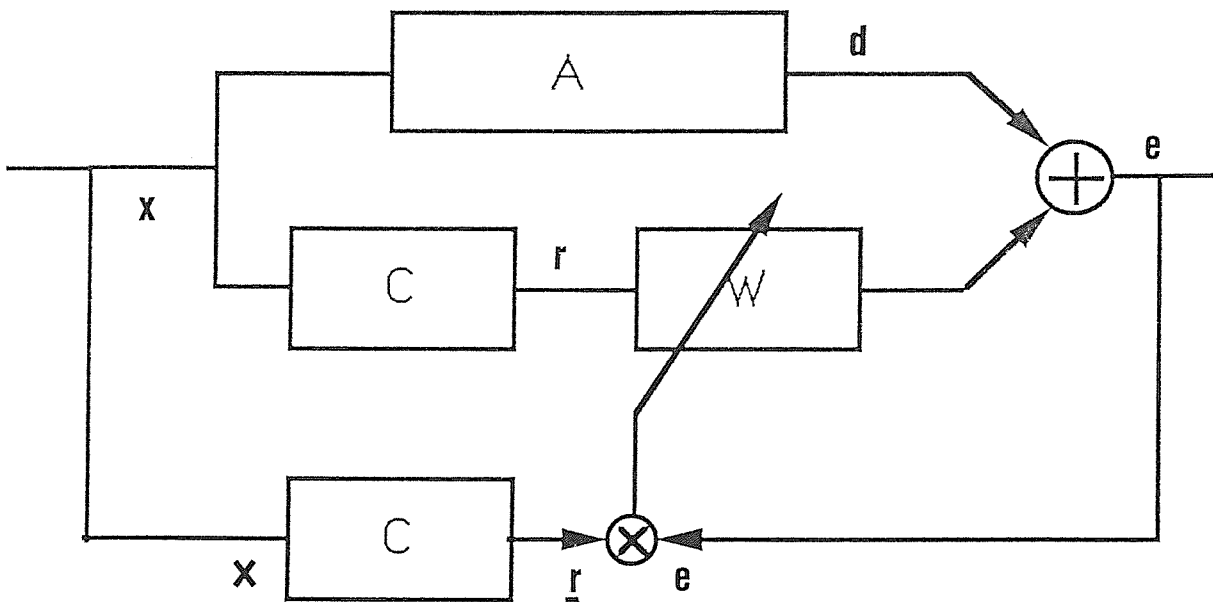
Figure 5.4 Filtered-x LMS   The product of the filtered-x vector and the error updates the filter W.

An interesting feature of the modified-gradient LMS is that the modified error path H can be identified simultaneously with noise control. If we look carefully at (5.9) we find that H is the transfer function experienced by a signal (x_1) injected at the output of the control filter to the error sensor (see **figure 5.5**). **Figure 5.6** describes the principle of such an on-line identification. Using as an input signal such as white noise, introduced at x_1 and the noise pressure detected at the error microphone as an error signal , a classical LMS algorithmcan be used to identify the modified error path. The error microphone will detect the sum of two signals : the response of the modified error path to the additional white noise excitation on one hand, the residual error signal of the control system on the other hand. Since the additive white noise and the residual error signal are uncorrelated, the latter signal can be considered as measurement noise for the error path identification system. We know from reference [24] that the LMS algorithm is not biased by measurement noise at output. Then the error path identification system will converge to the least square estimate of H(z).

V.1.3. Required filter length

We know from discussion of II.4 that the ideal controller a very long impulse response. If there is no dissipation in the duct then the controller has undamped poles and never decays. However there is always some kind of dissipation in a practical duct. If we make the reasonable assumption that duct dissipation causes 1% loss, so $\mu = \sqrt{0.99}$ in equ. (2.29). Then we can calculate the number of coefficients necessary to contain 99 percent of the ideal controller energy. (20 dB of attenuation).

If there is 1% loss over l_2 meter of pipe ($l_2 = 1.224$m) the ideal controller impulse response energy decays of 1% every 0.0036s. Therefore the time necessary to decay of 99 percent is :

$$t_0 = 0.0036N$$

with

$$(0.99)^N = 0.01$$
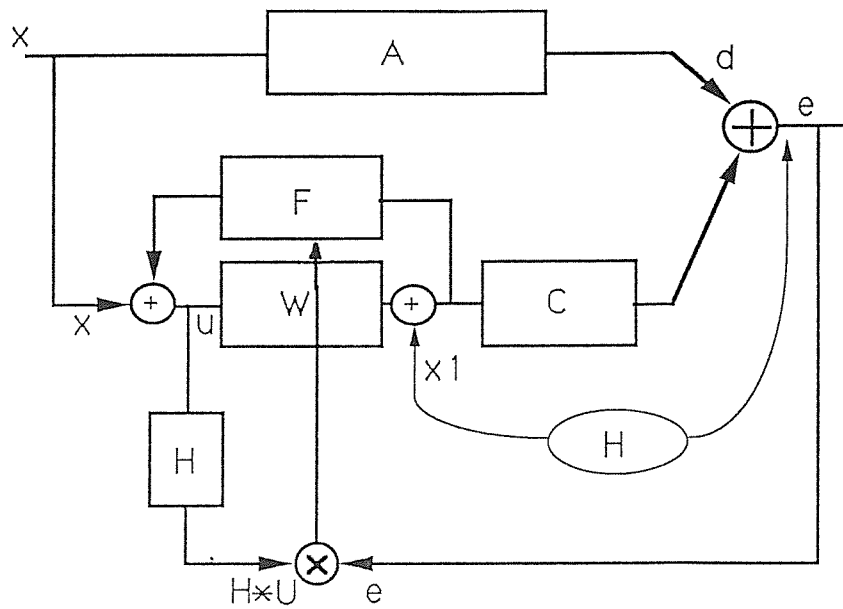
Figure 5.5 Modified-gradient filtered-x LMS. The product of the error by the vector U filtered by the modified error path H updates the filter W. H is the transfer function between x1 and e.
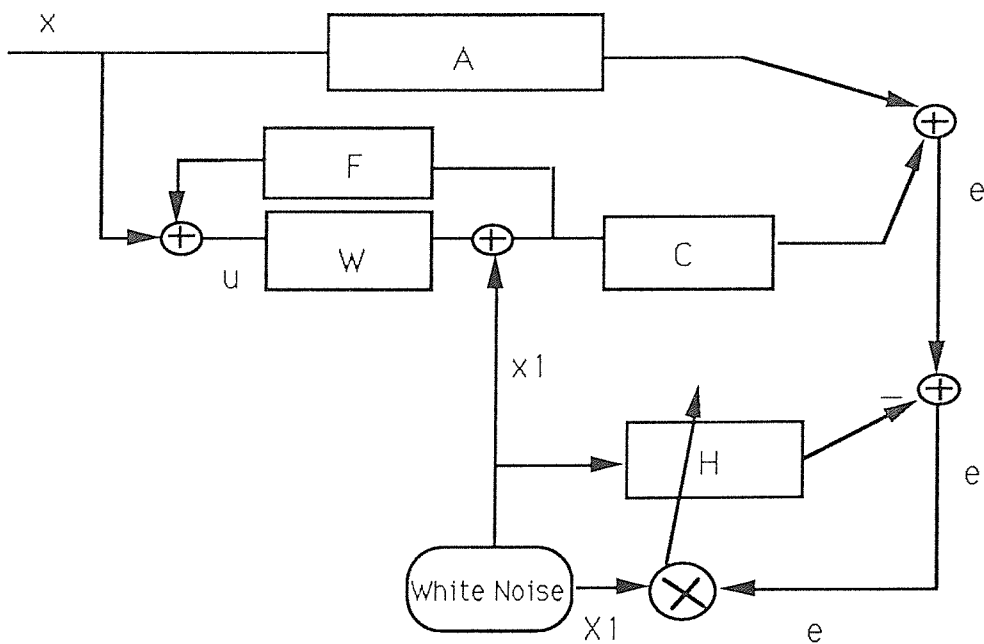
Figure 5.6 On-line identification of the modified error path

then

$$N = \frac{\ln(0.01)}{\ln(0.99)} = 458$$

and

$$t_0 = 2.75\text{s}$$

with a sampling frequency of 2500 Hz the required number of coefficient will be 6873. In practice the number of coefficient is less than 250. Then the performances of such an active control system will be severely limited by practical requirements.

V.2. The LMS algorithm with feedback cancellation

In order to avoid some of the problems inherent with using the LMS algorithm with a single FIR filter in the controller, a modified version is now presented . A filter F' such as F' ≈ –F is now implemented in parallel with F. The object is to cancel the feedback at the error microphone. The signal u(n) is therefore very close to the primary noise x(n) if F' is a close match to -F. The ANC system then becomes purely feedforward. Such a structure (already described in chapter IV) has been succesfully implemented to perform noise cancellation by Poole et al. [16].

V.2.1. Gradient expression

If we consider the feedback to be perfectly cancelled we do not have to consider it in the calculation of the gradient. Consequently the system is equivalent to the simple structure described by the formula (3.8). The formula for the gradient is then :

$$\Phi(n) = 2.e(n).r(n-k) \tag{5.11}$$

with r(n) equal to u(n) filtered by the filter C

$$r(n) = \sum_{j=0}^{\infty} c_j.u(n-j)$$

and therefore, the updating equation is

$$w(n+1) = w(n) - 2\mu.e(n).r(n-k) \tag{5.12}$$

Figure 5.7 gives a graphic representation of (5.12)

Without feedback the error is directly proportional to the input and so the error surface is quadratic. This is one of the main advantages of the feedback cancellation structure ; the convergence of the algorithm is guaranteed provided the convergence coefficient is reasonably small, and a good model of the feedback path is maintained.
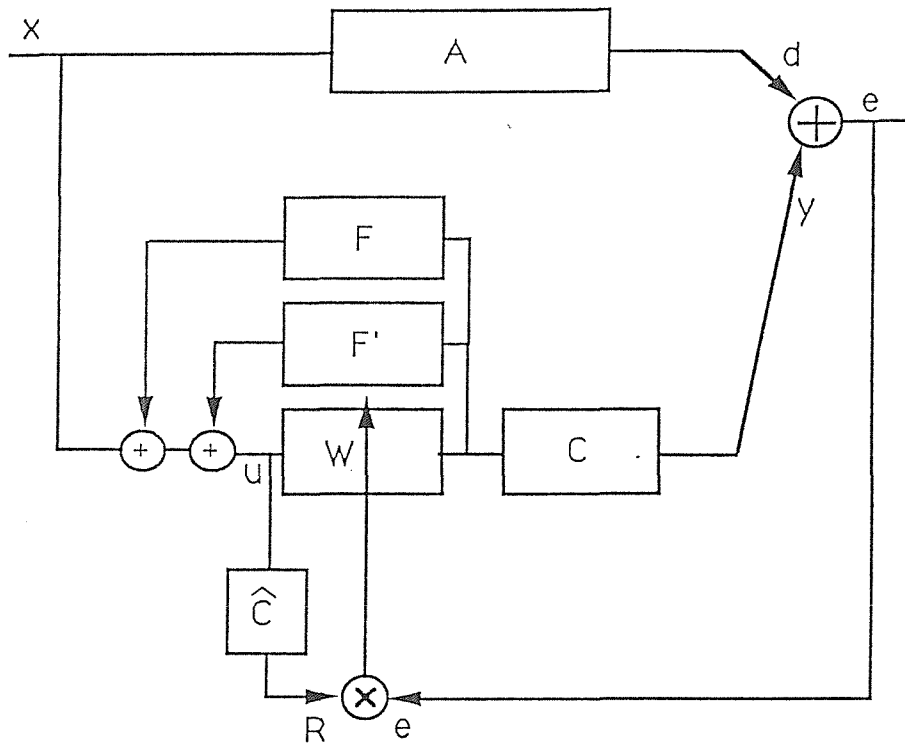
Figure 5.7 LMS algorithm with feedback cancellation. The product of the vector R and the error e updates the filter W. F′ is an estimate of -F, feedback path between the secondary source and the detection sensor.

V.2.2. Theoretical form of the feedback cancellation controller

With the introduction of F', the controller (a parallel combination of F' and W) is now recursive. We could expect the W filter to require a smaller number of coefficients than the single transversal filter used in the simple LMS algorithm. This is not true, however (as pointed out in [18]), the number of coefficients required turns out to be infinite, as we will now demonstrate.

From (2.7) and since $F(j\omega) = 0$ (perfect feedback cancellation)

$$\text{Wopt } (j\omega) = \frac{-A(j\omega)}{B(j\omega).C(j\omega)}$$

if we replace $A(j\omega)$, $B(j\omega)$, $C(j\omega)$ by their theoretical expressions (2.16), (2.17), (2.18), we have :

$$\text{Wopt } (j\omega) = -\frac{e^{-kl_2}-R_1R_2e^{-k(l+l_2)}}{H_s(f)\left(1+R_2e^{-2k(l_2+l_3+l_4)}\right)\left(1+R_1e^{-2k(l_0+l_1+l_2)}\right)} \tag{5.13}$$

We can easily develop this formula and take an inverse Fourier transform leading to the required impulse response for the w filter in this case.

$$w_{opt}(t) \quad =$$

$$\left(h_s^{[-1]}(t-\tfrac{l_2}{c})-R_1R_2h_s^{[-1]}(t-\tfrac{l+l_2}{c})\right) * \sum_{n=0}^{\infty}R_2^{(n)}\delta(t-\frac{2n(l_2+l_3+l_4)}{c}) * \sum_{n=0}^{\infty}R_1^{(n)}\delta(t-\frac{2n(l_0+l_1+l_2)}{c})$$

$$\tag{5.14}$$

The structure of $w_{opt}(t)$ appears complicated at first sight but turns out to be quite simple.

$$h_1(t) = h_s^{[-1]}(t - \tfrac{l_2}{c})-R_1R_2h_s^{[-1]}(t - \tfrac{l+l_2}{c}) \text{ gives two impulses (\textbf{figure 5.8.a}).}$$

The terms

$$h_2(t) = \sum_{n=0}^{\infty} R_2^{(n)} \delta(t - \frac{2n(l_2+l_3+l_4)}{c})$$

and

$$h_3(t) = \sum_{n=0}^{\infty} R_1^{(n)} \delta(t - \frac{2n(l_0+l_1+l_2)}{c})$$

are two Dirac sequences attenuated by R_2 and R_1 factors respectively, and so the convolution of these two terms gives a pseudo-periodic sequence of Diracs with a decay rate equal to the slowest decay of the two terms $R_1^{tc/(2(l2+l3+l4))}$ and $R_2^{tc/(2(l0+l1+l2))}$ (see **figure 5.8.b**).

Finally $w_{opt}(t)$ is a pseudo-periodic repetition of two impulses and its amplitude decreases in proportion to th maximum of $\{R_1^{tc/(2(l2+l3+l4))}, R_2^{tc/(2(l0+l1+l2))}\}$. (see **figure 5.8.c**)

V.2.3. Number of coefficients for W

Since $R_1^{tc/(2(l2+l3+l4))}$ is non zero for any finite t, $w_i(t)$ should have an infinite number of coefficients to contain all the information about the controller. It is interesting to determine a practical value for the number of coefficients. A sensible criterion is to consider the w(t) impulse response containing 99 percent of the energy. (20dB of attenuation)

Figure 5.8.a

and

Figure 5.8.b

etc ...
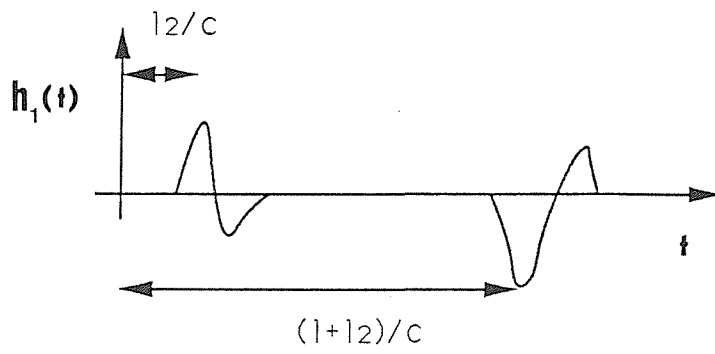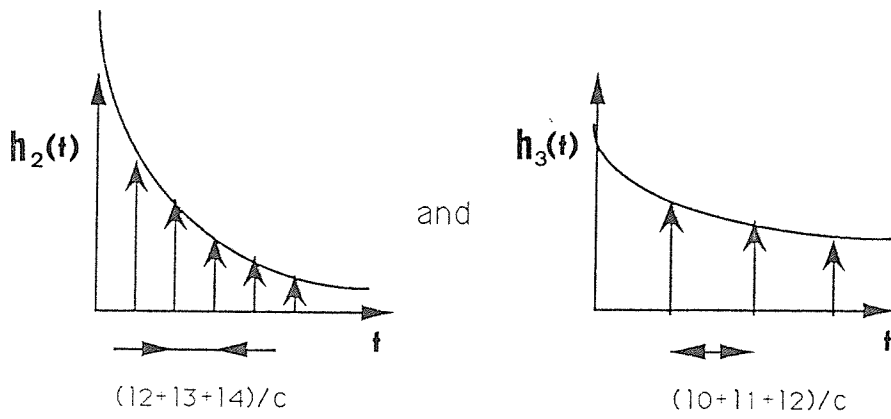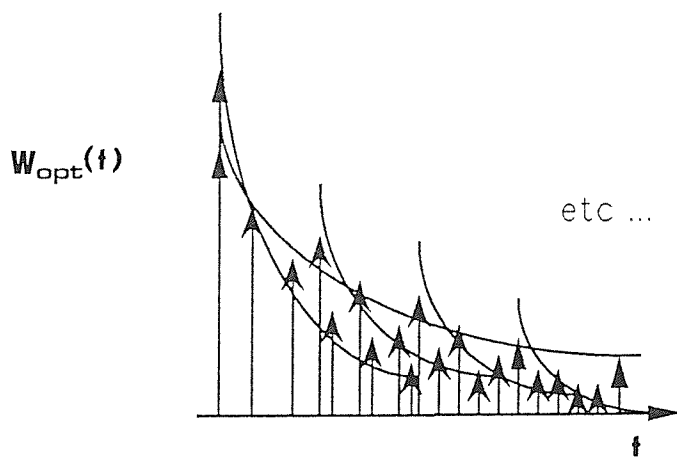
Figure 5.8.c

Figure 5.8 Shape of the controller W derived from the feedback cancellation structure

- 74 -

In the case considered here we have c = 340m/s ; R_2 = −0.83 ; R_1 = 0.39 ; $l_0+l_1+l_2 \approx l_2+l_3+l_4 \approx$ 2m

Since $R_2^{tc/(2(l0+l1+l2))}$ >> $R_1^{tc/(2(l2+l3+l4))}$ we have only to consider the left hand term.

The time t_0 ,corresponding to when this term has decayed by the criterion above is given by the solution to :

$$\frac{\int_{t_0}^{\infty} e^{-15.83t}dt}{\int_{0}^{\infty} e^{-15.83t}dt} = 0.01 \qquad (5.15)$$

which implies

$$e^{-15.83t0} = 0.01$$

so that

$$t_0 = \frac{\ln(0.01)}{-15.83} = 0.29 \text{ s}$$

With a sampling frequency of 2500 Hz the number of coefficients required is n = 0.29 X 2500 = 725. In practice, for computational reasons the number of coefficients cannot be more than 250. This demonstrates that the performances of such an active noise control system will be limited by the length of the W filters which can be implemented in practice.

V.2.4. Number of coefficients for F

The same calculation can be performed on F'. Since F' will be an FIR filter supposed to model F as well as possible, we have to determine the number of coefficients necessary to contain 99 percent of the energy. From (2.19) we deduce that f(t) decreases as $R_1 R_2^{tc/(2l)}$ which gives :

$$t_0 = \frac{\log(0.01)}{-56.39} = 0.08 \text{ s}$$

The requirement on this filter is not so stringent as that on W. With a sampling frequency of 2500Hz the number of coefficients required is 200. In practice we use 250 coefficients. Consequently the feedback cancellation should remove most of the effects of the feedback provided the system is not changing.

V.2.5. Adaptivity

It is very important for an Active Noise Control system to track the nonstationary behaviour of the duct. Any temperature and humidity changes may induce dramatic variations in a(t), b(t), c(t). The system should be able to follow such a change since the W filter is constantly updated. However there is a part in the controller in the system previously reported which is never updated : the F' filter. The feedback canceller is supposed to be determined before the adaptation and is kept in this configuration. Suppose the physical feedback path F changes when the system is running, the F' filter is therefore no longer a good estimate of -F ; this introduces number of drawbacks : bad feedback cancellation, non quadaraticity of the error surface and potential instability. There is no simple way to identify F' when the system is on line. In effect the transfer function between the loudspeaker and the detection microphone is not just F but a parallel filter including F', F, W. The influence of an F' misadjustment will thus be an important feature in the experimental study.

V.3. The recursive LMS algorithm

In the active control of sound in ducts, both simple LMS and feedback cancellation LMS algorithms requires very long filter lengths. Moreover the latter algorithm is not even fully adaptive if the changes in the feedback and error path are not tracked. We now describe a structure which is fully adaptive and requires only short filters : the recursive LMS.

V.3.1. Description of the structure

The idea of using a recursive controller with a transfer function similar to (2.26) is not new [26] but the difficulty of building such a filter with analog equipment and the lack of an efficient algorithm to update IIR filters delayed the first succesful application of this approach until 1987 [27].

The structure of an IIR control system is illustrated on **figure 5.9**. The controller comprises a two part filter (W, V). The filter W models the direct path (mainly a delay) and the recursive filter V cancels the effects of the direct feedback. An alternative interpretation of the action of the filter is that W identifies the zeros whereas V identifies the poles of the required controller. Both W and V are simultaneously updated and this is the principal change from the feedback cancellation structure. In practical realisations both W and V are implemented as separate FIR filters. If N is the number of W coefficients and M is the number of V coefficients we have :

$$y(n) = \sum_{i=0}^{N-1} w_i.u(n-i) + \sum_{i=0}^{M-1} v_i.y(n-i) \tag{5.16}$$

The problem of continously updating an IIR filter is extensively described in [28] by Shynk as well as in [29] by Widrow. In the next paragraph we describe an algorithm based on the calculation of the instantaneous error gradient as originally derived by Flockton [25] [36] . It is the equivalent of the LMS algorithm for an IIR filter, and so from now it will be designed as IIR LMS algorithm.

V.3.2. Gradient expression

This time we have to determine two gradient vectors :
the gradient vector of the transversal component of the controller

$$\Phi(n) = (\phi_0(n), \phi_1(n), ...,\phi_N(n))^T = (\frac{\partial e^2(n)}{\partial w_0}, \frac{\partial e^2(n)}{\partial w_1}, ..., \frac{\partial e^2(n)}{\partial w_N})^T$$

and the gradient vector of the recursive component of the controller

$$\Psi(n) = (\psi_0(n), \psi_1(n), ...,\psi_M(n))^T = (\frac{\partial e^2(n)}{\partial v_0}, \frac{\partial e^2(n)}{\partial v_1}, ..., \frac{\partial e^2(n)}{\partial v_M})^T$$

The calculation of these instantaneous gradient vectors is complicated because of the feedback path and the recursive nature of the controller. These calculations are fully fully discussed in Appendix B.2

Given the previous conventions and according to Appendix B.2 .11 & B.2 .12

$$\phi_i(n) = e(n).h(n)*u(n-i) \tag{5.17}$$

$$\psi_j(n) = e(n).h(n)*y(n-j) \tag{5.18}$$

with h(n) is now the impulse response of the filter whose Z-transform is

$$H(z) = \frac{C(z)}{1 - F(z).W(z) - V(z)} \tag{5.19}$$

If we define the filtered input $r_w(n)$ and the filtered output $r_v(n)$ as

$$r_w(n) = \sum_{j=0}^{\infty} h_i.u(n-i) \tag{5.20}$$

$$r_v(n) = \sum_{j=0}^{\infty} h_i.y(n-i) \tag{5.21}$$

and update the direct and recursive filter coefficients by an amount proportional to the negative of the gradients defined by equations (5.21) and (5.22), we obtain :

$$w(n+1) = w(n) - 2 \mu.e(n).r_w(n) \tag{5.22}$$

$$v(n+1) = v(n) - 2 \mu.e(n).r_v(n) \tag{5.23}$$

Where $r_w(n)$ and $r_v(n)$ are vectors of N and M past values of $r_w(n)$ and $r_v(n)$.

We see from (5.22) and (5.23) that the IIR LMS algorithm can be considered as two LMS algorithms applied simultaneously to W and V. Hence , the computational burden associated with implementing this algorithm is of the same order. In this case however, both u(t) and y(t) must be prefiltered by H(z) to generate $r_w(n)$ and $r_w(n)$. Fortunately, in this case, H can now be estimated on line, since as in § V.1.3, H(z) is the transfer function between the controller output and e and a simultaneous identification process can be performed at the same time as

implementing active control. (see **figure 5.10**). Then, the IIR LMS algorithm will be able to be fully adaptive. Interestingly , by making V = 0 in (5.17), (5.18), (5.19), (5.20), (5.21) we obtain the formulae (5.9) and (5.10). It proves that the IIR LMS is an extension of the LMS algorithm.

V.3.3. V and W for the ideal controller

The recursive controller (W, V) has a frequency response given by

$$T(j\omega) = \frac{W(j\omega)}{1-V(j\omega)} \qquad (5.24)$$

We know from (2.26) that

$$T_{ideal}(j\omega) = \frac{-e^{-kl_2}}{Hs(j\omega)(1 - e^{-2kl_2})}$$

The similarity of structure between the two expressions is striking and explains and justifies fully the use of the IIR LMS algorithm. During the identification process $W(j\omega)$ could efficiently converge to $-e^{-kl_2} \times$ (poles of Hs) and $1-V(j\omega)$ converges to $(1 - e^{-2kl_2}) \times$ (zeros of Hs). If the inverse of the loudspeaker is nearly an impulse, w(t) mainly consists of an l_2/c delay and v(t) consists of an delay twice as long. In practice l_2 is about 1m-1.50m. The delay is then 1.5/340= 4.4ms. The corresponding number of coefficients with a 2500Hz sampling frequency is 11 for w(t) and 22 for v(t). This is considerably smaller than the number of coefficients required for the algorithms discussed above ($\approx$1000). Since we need about a factor of 30 fewer coefficients the computational power necessary to perform the same task is reduced dramatically. However there are several drawbacks to this approach. The first one is the non quadraticity of the error surface both due to the presence of the feedback and to the recursive structure of the controller. The second one is that while a FIR filter alone is always stable (feedback is not taken into account), an IIR may not be. As soon as the poles are outside the unit circle the filter diverges. When the IIR filter converges its frequency response gets closer to the ideal controller described in (2.26). Unfortunatly this controller is potentially unstable since in theory all its poles are on the unit circle (i.e it has infinite resonances, see

section II.4). An IIR filter will thus have a propensity to become unstable, and therefore a way to stabilise the controller will have to be considered when implemented in practice.
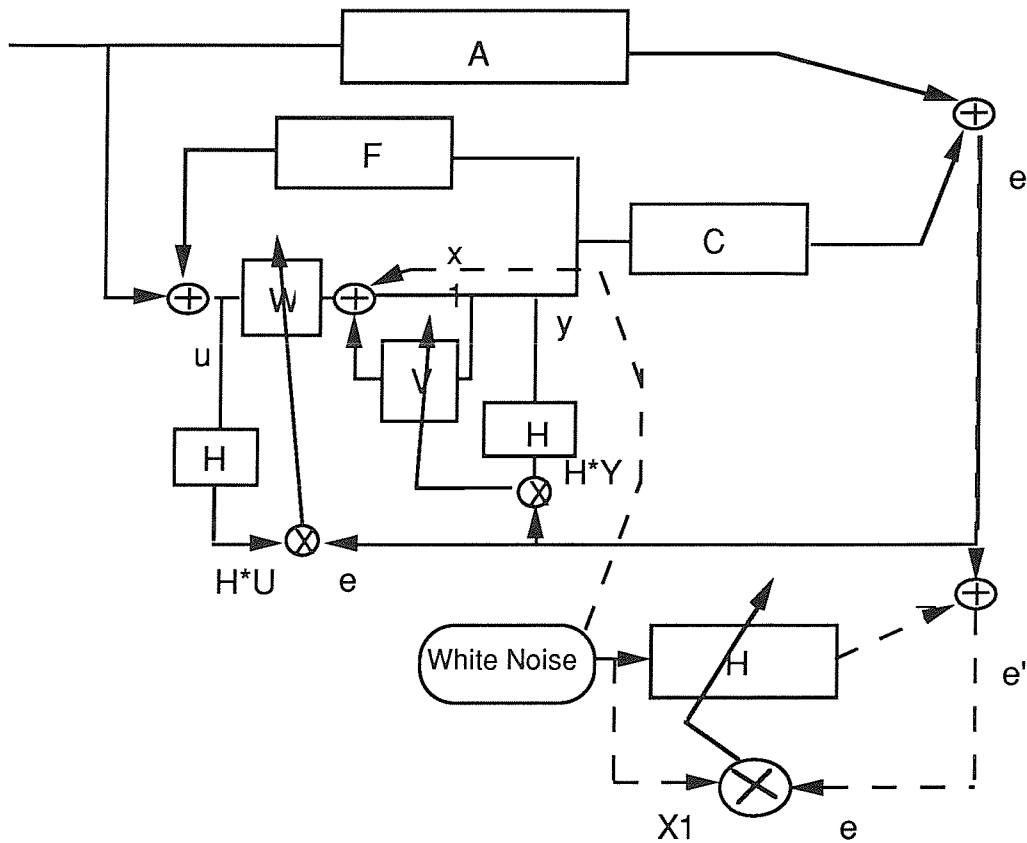
Figure 5.9 The IIR LMS algorithm with on-line identification of the error path

The product of the error by the input vector U filtered by the modified error path H updates the filter W

The product of the error by the output vector Y filtered by the modified error path H updates the filter V. H is the transfer function between x1 and e.

CHAPTER VI

Practical results (simulations and experiments)

In this chapter, the last one, we will study throught experiments and computer simulations, the three algorithms described in chapter V. As far as the experiment is concerned the various LMS algorithms were implemented on a TMS320C25 microprocessor with a sampling frequency of 2.5 kHz (the experimental setup has been described in chapter III). On the other hand, the software for the computer simulation (i.e the electro-acoustic model of chapter II and the three LMS algorithms) was programmed in the language C on a PC computer equiped with a 80386 microprocessor.

There is nothing better than the real experiment to juge the performance of an active control system. However, the importance of the computer simulation is not to be neglected. Its advantage is that physical features can be introduced one at a time to see the effects on the algorithm.

VI.1. Implementation of the LMS Algorithm

In order to simplify the language, each reference to the LMS algorithm in this section must be understood as modified-gradient filtered-x LMS.

This study of the LMS algorithm will be divided in three steps.

(1) anechoic duct with perfect transducers (simulated)

(2) influence of duct reverberation (simulated)

(3) experimental results and simulation of the experimental conditions

VI.1.1. Anechoic duct with perfect transducer

The first simulation has the following conditions :
    -perfect loudspeakers (i.e. impulse responses = $\delta(t)$)
    -$R_1=R_2=0$.
    -W has 250 coefficients.

The **figure 6.1** represents the impulse responses of the adaptive filter after 2 minutes of real time convergence (i.e. 120x2500 = 300 000 samples). We can notice a succession of peaks : the first one is delayed by 9 samples ans the next ones are delayed by 18 samples that is respectively by l_2/c and by $2l_2/c$ seconds.

In order to compare with the result of the generalized Yule-walker equations of chapter IV, we plot in **figure 6.2** the corresponding impulse response obtained by iterating equation (4.39). It is satisfying to notice that **figure 6.1** and **figure 6.2** are almost identical ; the modified-gradient LMS converges to the optimal least square solution. Interestingly, these impulse responses are not just truncated versions of (2.28).

The attenuation at the error sensor resulting from the controller reponse adapted using the LMS algorithm is given **figure 6.3**.
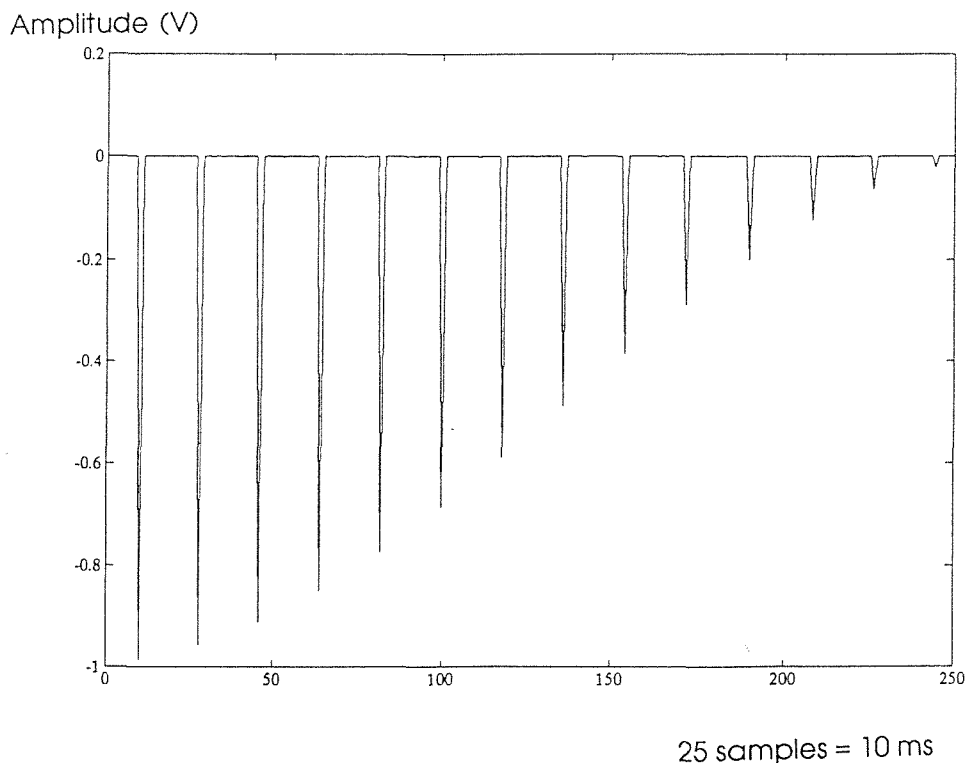
25 samples = 10 ms

Figure 6.1 Modified-gradient LMS,Simulation ; 250 coeffs ; R1=R2=0 ; perfect loudspeakers : Impulse reponse of the adaptive filter

Amplitude (V)
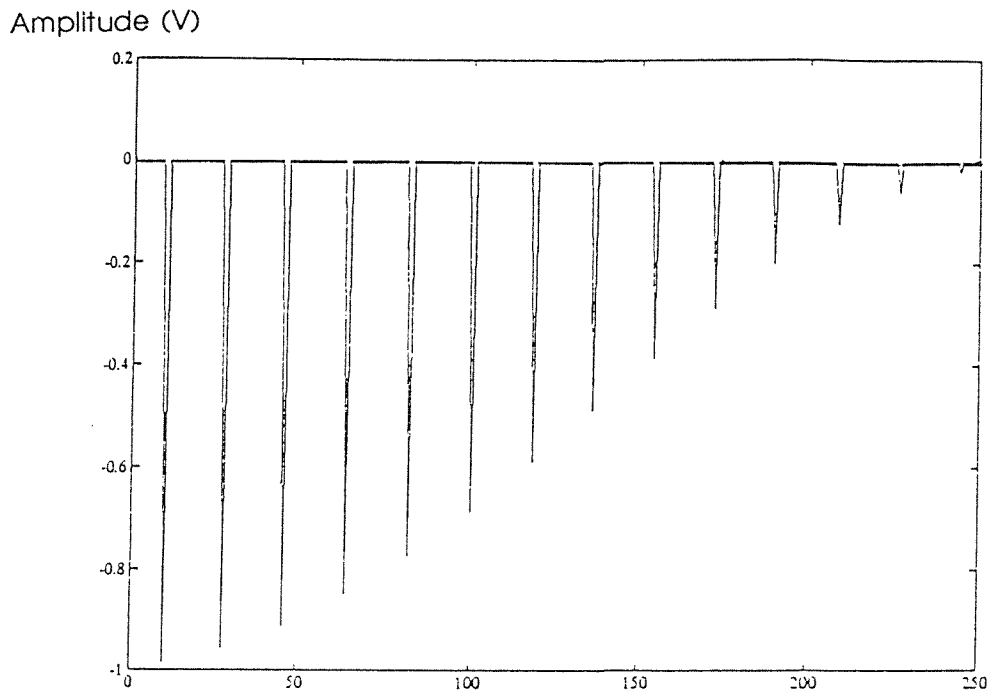
25 samples = 10 ms

Figure 6.2 Impulse response of the optimal least square FIR controller ; 250 coeffs.

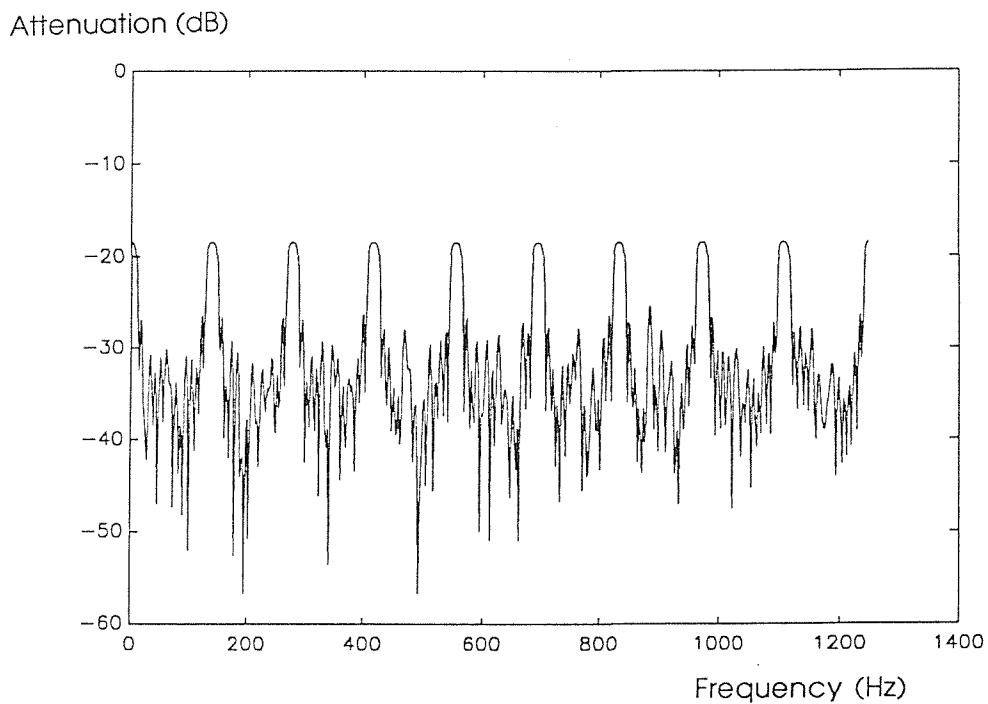Attenuation (dB)

Frequency (Hz)

Figure 6.3 Modified-gradient LMS,Simulation ; 250 coeffs ; R1=R2=0 ; perfect loudspeakers : attenuation at the error sensor

VI.1.2. Influence of the transducer.

Setting the reflection coefficients to zero again we now introduce a more realistic model for the transducers. The identification of the 50 coefficients FIR filter transducer model has been described in chapter III, this was used in the simulation of the adaption algorithm. Then, the LMS algorithm has been allowed to run for 2 minutes of real time. The right hand plot of **figure 6.4** is the error signal spectrum when the system is on and off. The attenuation is limited to 20 dB. Given the 9 sample delay between the detection microphone and the secondary loudspeaker, this is perfectly consistent with the conclusions of § 1.3 in chapter IV.

VI.1.3. Experimental results and simulation of the experimental conditions

The LMS algorithm has been used to control the sound in the experimental duct. The number of coefficients for the adaptive filter was 200. After various trials, the best value for the unnormalised updating coefficient was found to be 0.02. We have implemented two versions of this algorithm :

- an unmodified error path prefilter (filtered-x LMS)
- a continuously on-line identified error path (modified-gradient filtered-x LMS)

Flockton has shown in [25] that the first algorithm leads to a biased solution in presence of a feedback path whereas the second algorithm converges to the correct adaptive filter. Consistent with these conclusions, we have found the second algorithm to work better and we from now we will consider the latter only.

With the modified-gradient filtered-x LMS algorithm the overall reduction obtained at the error sensor was 10 dB. It took 2 or 3 minutes for the control algorithm to converge whereas the identification algorithm was much quicker (a few seconds to converge). However, the control algorithm was subject to divergence after few minutes of control. A better stability was obtained by decreasing the updating coefficent at the expense of a slower convergence rate (more than 10 minutes to converge satisfactorily) or by introducing a leak in the updating process (see VI.2.3 for more details). However all these remedies cannot compensate the main problem with the converged system : the number of coefficents is limited to 200 which is insufficient to achieve a good control.

Figure 6.5 shows both experimental and simulated impulse responses of the adaptive controller obtained after 10 minutes of real time control. They look very similar.

Amplitude (V)
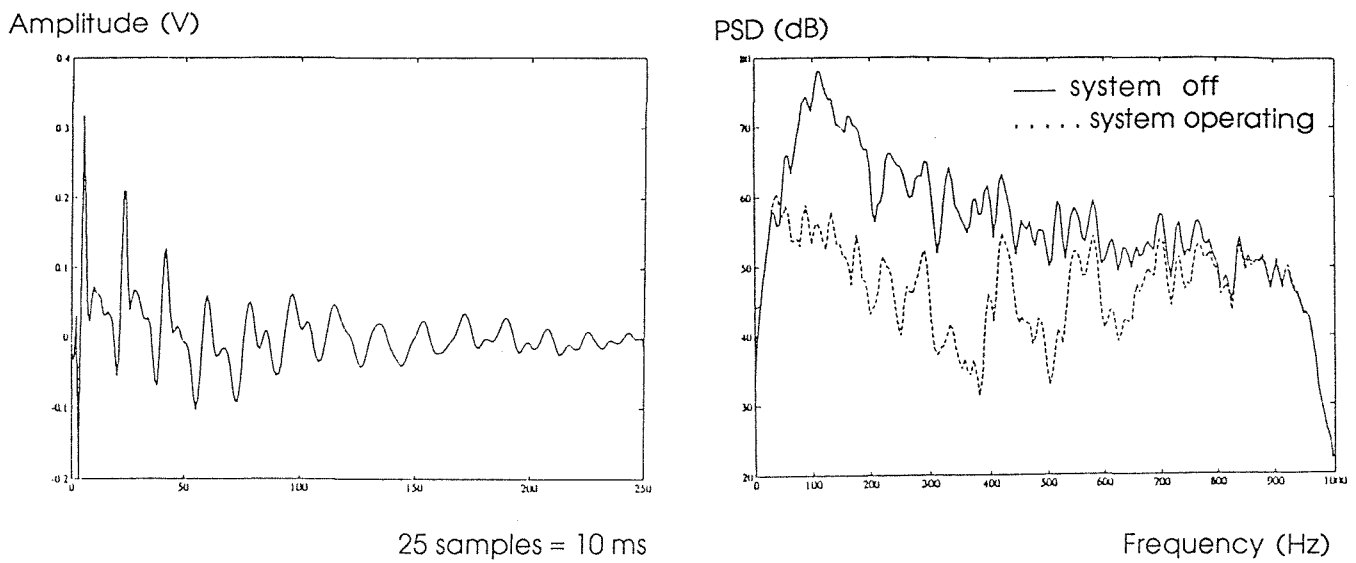
PSD (dB)

25 samples = 10 ms

Frequency (Hz)

Figure 6.4 Simple LMS, Simulation with realistic loudspeakers; 250 coeffs; R1=R2=0 : (left) W impulse response. (right) Power Spectral Density at the error microphone.
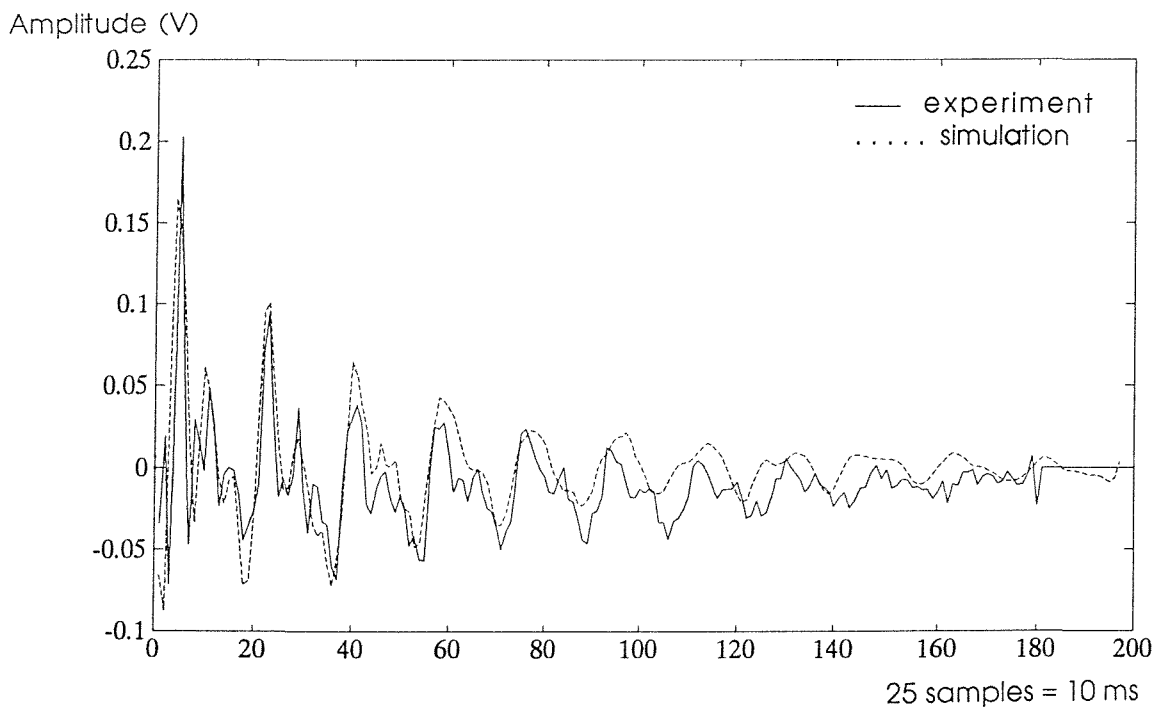
Amplitude (V)

25 samples = 10 ms

Figure 6.5 LMS algorithm. Controller impulse response after 10min of convergence. 200 coefficients, convergence coefficient = 0.02.

More interesting are the moduli of the corresponding frequency responses plotted on **figure 6.6**. We notice a periodic repetition of peaks every 140Hz which has already predicted by the study of the ideal controller (see figure 2.5). The fact that these peaks are not very sharp is a consequence of the FIR nature of the controller. Finally, **figure 6.7** is a display of the error signal spectrum when the system is operating (upper curve) and when off (lower curve). Again, simulated and experimental spectra are similar. On both residual error spectra there are peaks regularly spaced at frequencies F_1 = 148 Hz, F_2 = 222 Hz, F_3 = 296 Hz, F_4 = 370 Hz etc. These peaks cannot be related to interference at the detection of the downstream sound wave with the reflected one since the frequencies are not multiple of $c/(2.l_2)$=139 Hz and some time was spent tracking down where they came from. **Figure 6.8** and **figure 6.9** help answer this question. **Figure 6.8** is a plot of the (measured and simulated) frequency responses between the detection microphone and the primary source with no active control as denoted $B(j\omega)$ in **figure 2.2.** We distinctly notice anti resonances at 74Hz, 148Hz, 222Hz, 296Hz, 370Hz. These antiresonances indicate a bad coupling of the primary source with the detection microphone. This correspond to zeroes of $B(j\omega)$ in equ (2.23). When the primary source generates a sound in the duct at these frequencies, the detection microphone cannot detect it perfectly. Therefore, because of measurement noise, the coherence of the two signal is not perfect and the attenuation at these frequencies is reduced (see figure 6.6). **Figure 6.9** confirms this assumption. It represents the power spectral density at the detection microphone when the active noise control system is operating. We can see again that there is little signal at frequencies F1, F3, F4, F5 corresponding perfectly to the anti-resonances mentionned above. From these results we can predict that the performance of such an active noise control system will be related to the quality of the coupling between the primary source and the detection microphone. It is advisable to determine the distance between these two transducers in such a way that the frequency response $B(j\omega)$ is as uniform as possible.

VI.2. Implementation of the feedback cancellation algorithm

We have seen in chapter V.2 that the error path prefilter transfer function must be equal to C(z) and that the echo canceller transfer function has to be equal to -F(z). Several attemps were made to utilise a training signal on a off-line basis to determine the desired coefficients of the compensating filter F'(z) [16]. The principle was to utilise an LMS algorithm on an off-line basis with a training signal to determine the proper weights to cancel the acoustic feedback. However, Eriksson in his Ph. D thesis [31], pp. 36-42, has shown throught various computer
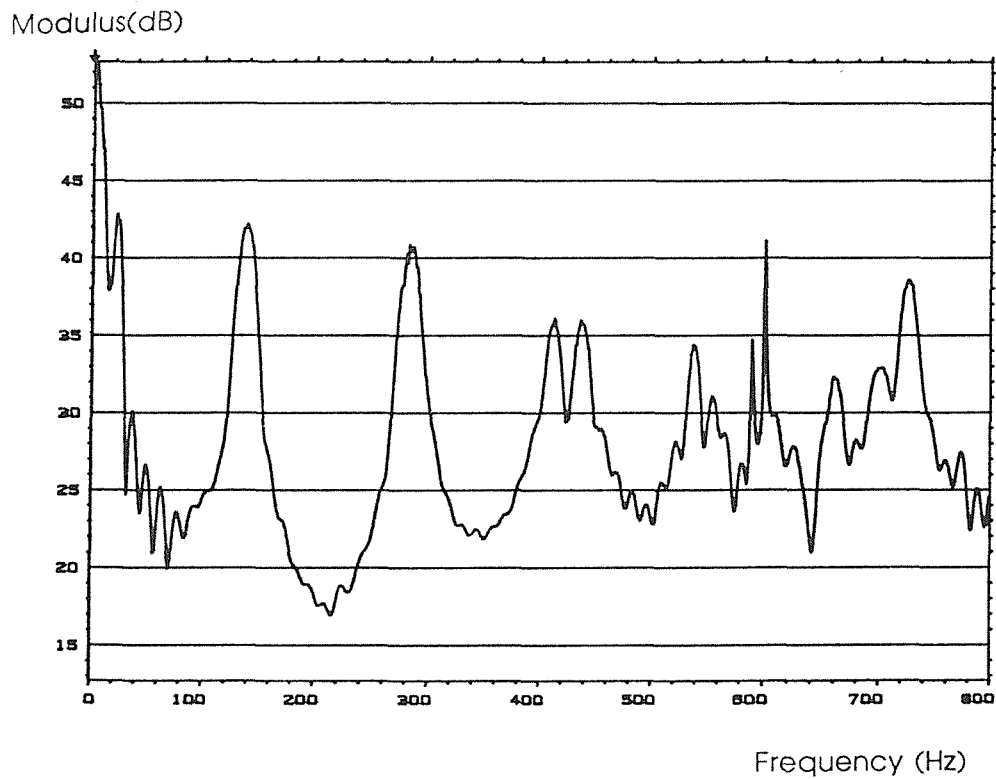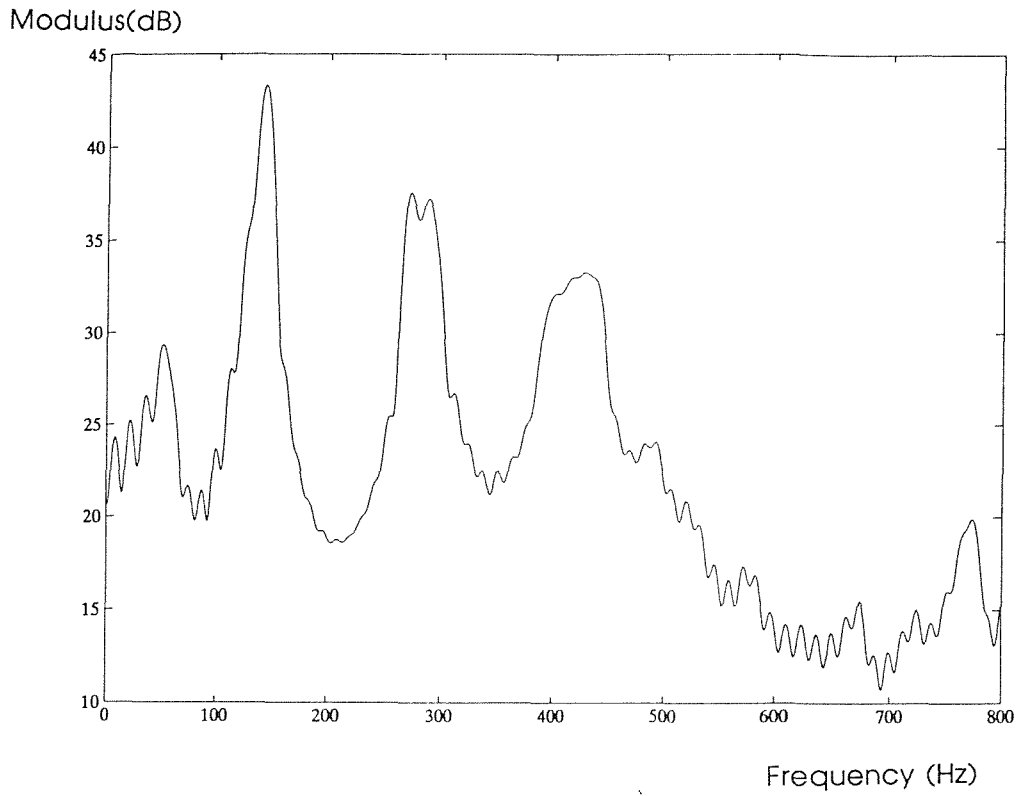
Figure 6.6 LMS algorithm. Frequency response of the controller after 10min of convergence. 200 coefficients, convergence coefficient = 0.02.
(top) simulation, (bottom) experiment

PSD (dB)

Frequency (Hz)

PSD (dB)

Frequency (Hz)
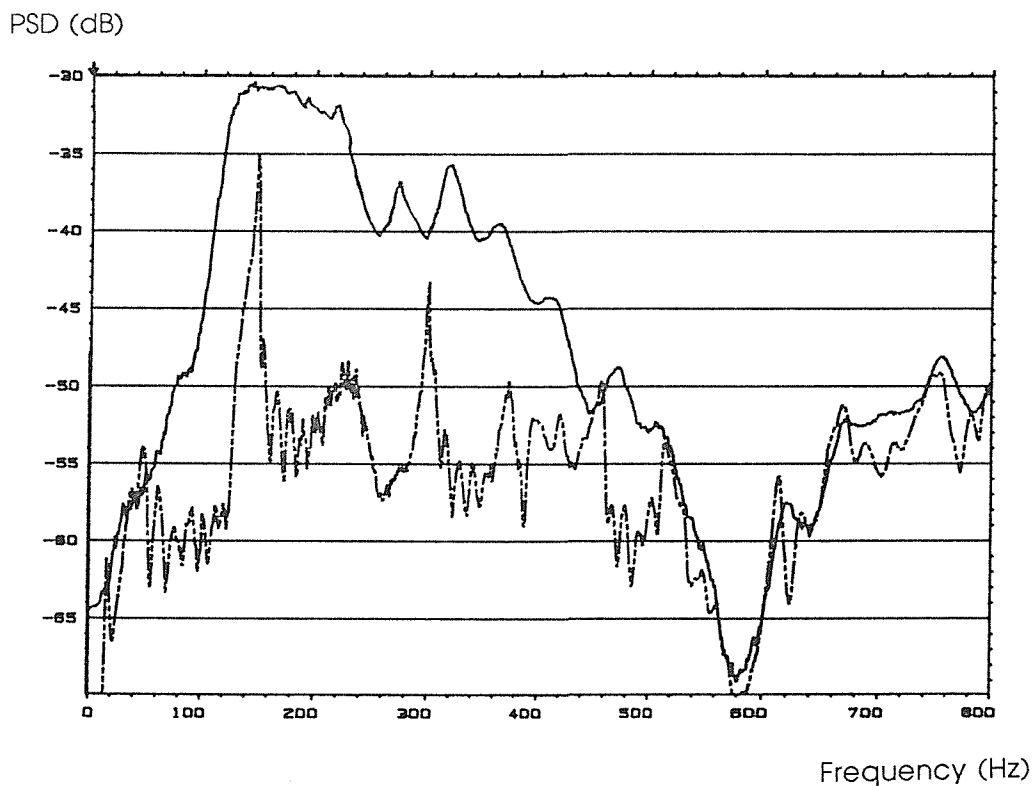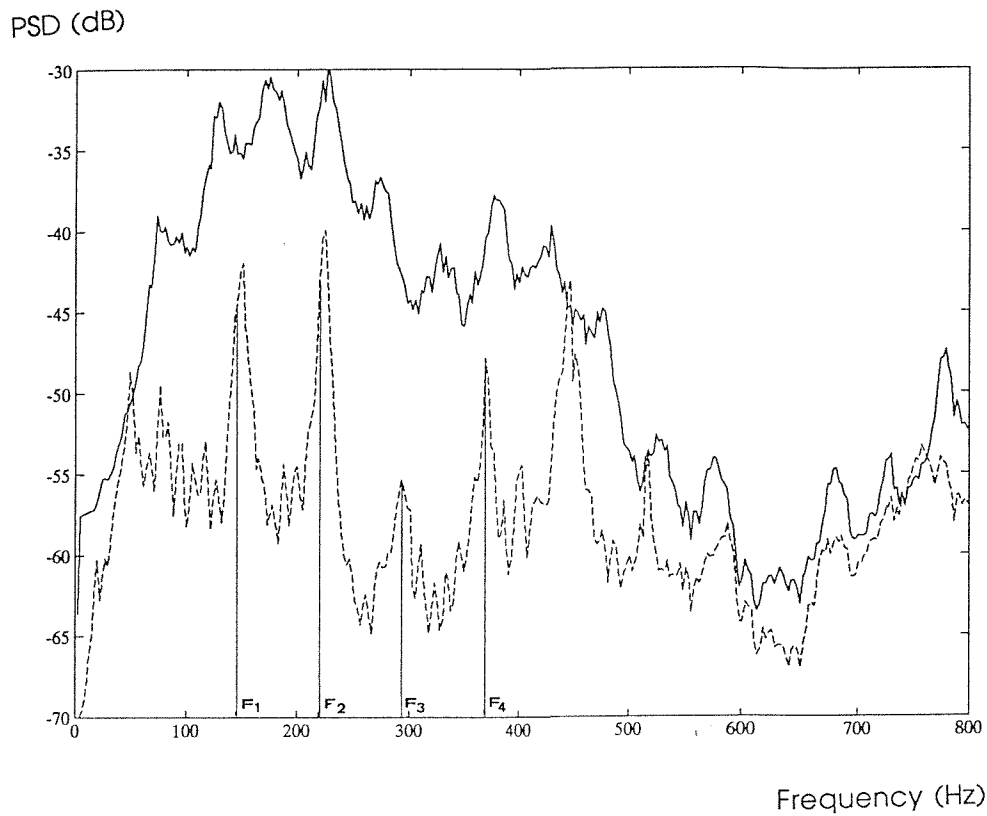
Figure 6.7 LMS algorithm. DSP at the error sensor after 10mn of convergence. 200 coefficients, convergence coefficient = 0.02.
(up) simulation, (bottom) experiment

- 88 -
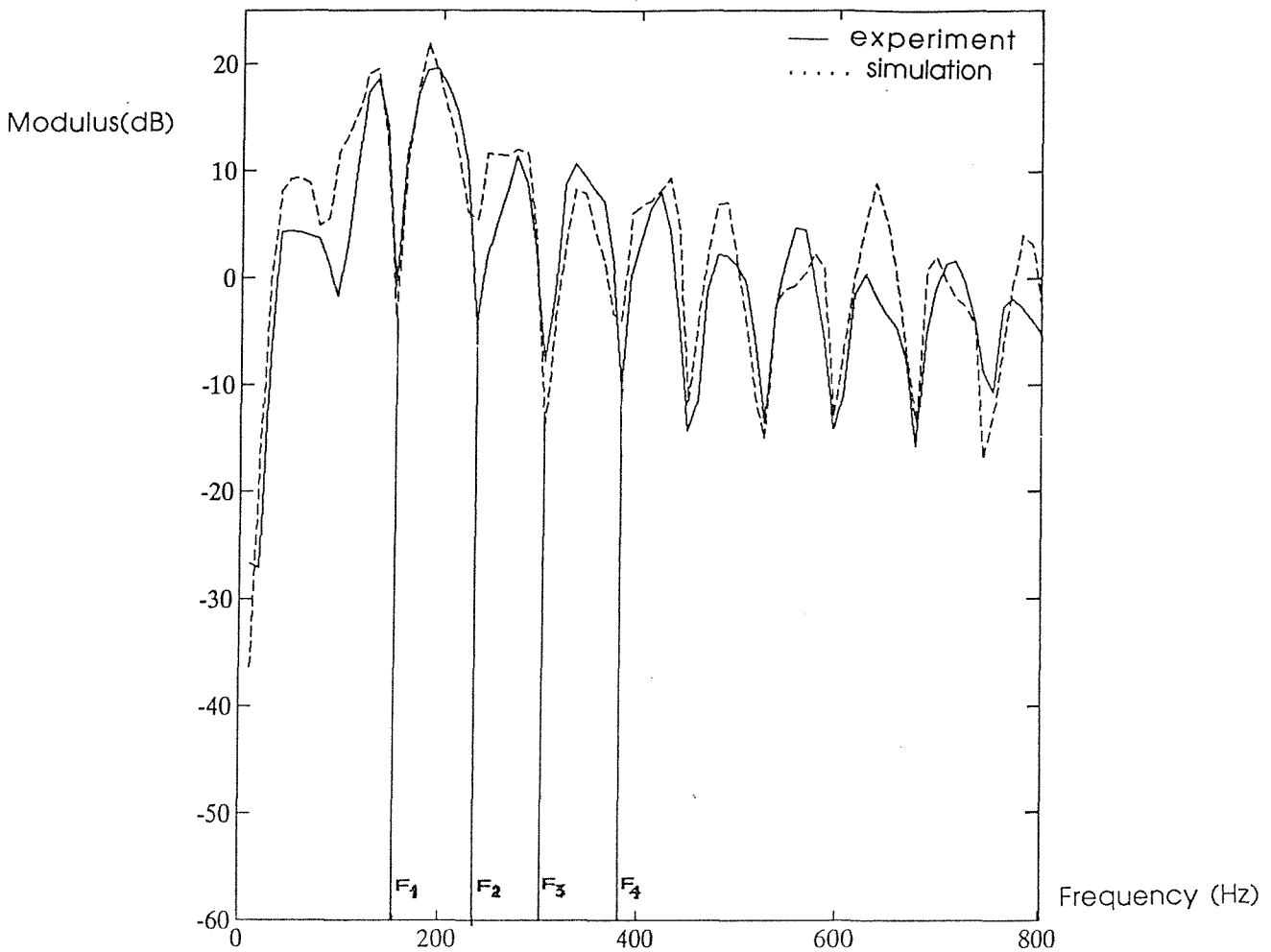
Figure 6.8 transfer function between the primary source and the detection microphone. The anti-resonances F1, F2, F3, F4 ... correspond to peaks F1, F2, F3, F4... in figure 6.7
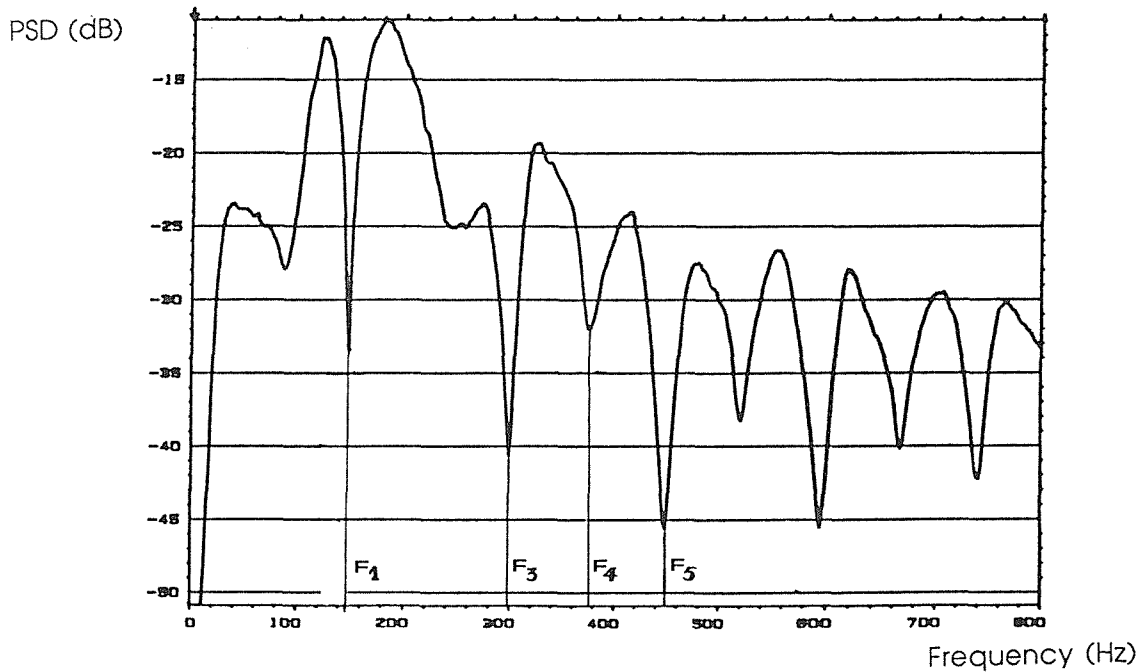
Figure 6.9 Experimental Power Spectral Density at the detection microphone when the ANC system (LMS algorithm) is operating.

simulations that this approach is only restricted to broadband primary input noise. It does not appear to be usable for sinusoidal input signals on an adaptive basis. Therefore, in order to use this approach on any kind of input signals, it will be necessary to initialy train the system with random noise and then not allow the feedback canceller to change. This is a important limitation since the feedback path continuously varies with time, then, it becomes very important to know how such a fix algorithm will behave to physical perturbations in the duct. This is considered in the following paragraph.

V.2.1. Influence of a perturbation in the feedback path (simulation)

In order to study the influence of a mismatch between the echo canceller and the feedback path we have considered two kinds of perturbation. The first one is to corrupt the filter F' by adding to each of its coefficients, a random value. The misadjustment is then uniformely distributed over the whole filter response
We have run the algorithm and plotted the residual error for several levels of the perturbation in F' (**figure 6.10**). The mean square value of the perturbation (p) varies from 0 to 0.05 the latter corresponding to a root mean square amplitude equal to 0.25 time the highest coefficient of F' .The performances obviously decrease when the level of the perturbation increases but the simulation shows that the perturbation does not greatly affect the stability of the system.
The second kind of perturbation which was introduced into F' is a phase shift. By adding a filter we modified the echo canceller phase by the a fraction of a sample (**figure 6.11**). The genuine filter has been obtained by inverse Fourier transforming the following Z-tranform :

$$P(z) = (z)^{(i/n)} \tag{6.4}$$

Where i<n
Such a variation in phase is likely to occur when a change of the temperature modifies the sound speed or even the reponse of the louspeaker. The residual error has been plotted for several values of delay up to one sample. (**figure 6.12**). It appears that the algorithm is very sensitive to this factor. When the echo canceller is out of phase by one sample no attenuation is achieved and the convergence coefficient has to be substantially reduced to preserve stability. All these results are consistent with the conclusion derived in similar studies [37] [38], which are that the attenuation is much more sensitive to variation of the loop delay than to variation of the loop gain.

Attenuation (dB)
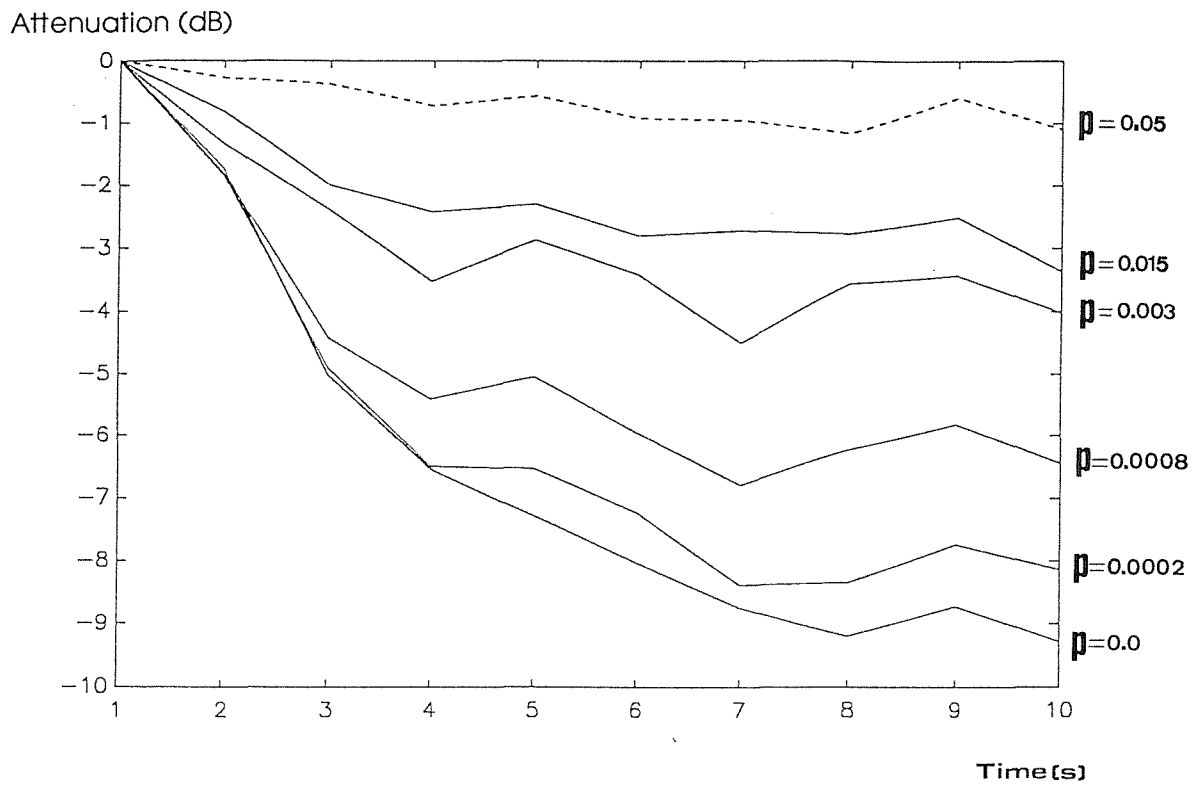
Figure 6.10 Feedback cancellation LMS. (Simulation) 250 coefficients . perfect loudspeakers. Robustness of the feedback canceller to a random misadjustment. P denotes the mean square value of the perturbation to F'
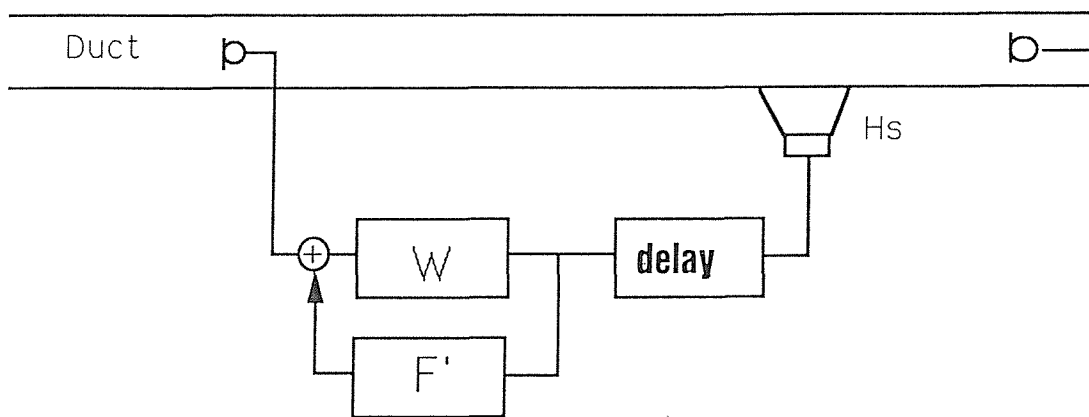
Figure 6.11 Feedback cancellation LMS (Simulation) Introduction of a phase delay.

Attenuation (dB)
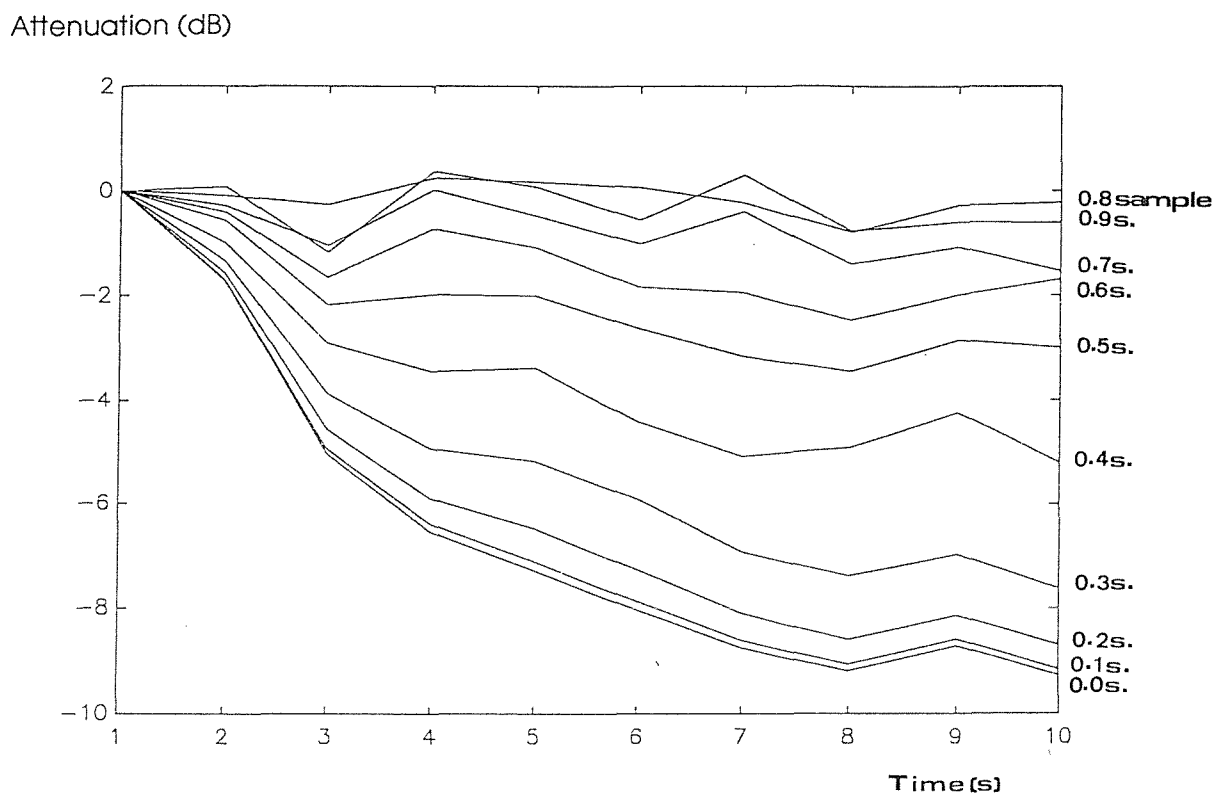
Figure 6.12 Feedback cancellation LMS (Simulation). 250 coeffs. Influence of a phase delay.

VI.2.2. Experimental results and simulation of the experimental conditions

In the experiment the number of coefficients used in the controller, the echo canceller and the error path filter was each 200. The convergence coefficient for the identification of F' and H was 0.1 which led to very quick convergence (1 second for a residual error of 2%). The value practically used for the convergence coefficient in the controller update is 0.02. This leads to steady and relatively quick convergence. Once converged this active noise control structure remains stable for a long time, we have to conclude that the mismatch between real feedback path and echo canceller was small.

However we have noticed that after several hours the controller slowly increases its gain at very low frequencies (0-20Hz). The controller appears to attempt to equalize the low frequency loudspeaker response which is very poor at these frequencies. This build up is very slow because of the absence of very low frequency

components of the sound pressure in the duct so the adaptive filter does not repond quickly at these frequencies. This phenomenon is damaging in the long run, the controller impulse response becomes distorted and the displacement of the secondary loudspeaker is too large to stay linear. Two solutions have been succesfully tested. The first one is to add an uncorrelated low-frequency noise to the input of the detection microphone. The effect is to decrease the coherence of the detection microphone signal and the error microphone signal. The system therefore reduces its gain at these frequencies in order not to amplify the uncorrelated noise. The attenuation remains the same for frequencies above 30Hz. This remedy is interesting in that it enables us to specifically modify the action of the algorithm in a particular frequency domain by introducing filtered noise into the detection sensor In a practical system in a duct with flow such low frequency measurement noise at the detection microphone would naturally be present due to turbulences. The other solution is to introduce a leak ρ in the formula (5.12) according to:

$$w(n+1) = \rho w(n) + \mu_w.u(n-i).e(n) \qquad (6.1)$$

Where ρ is required to be of the order of $1-10^{-6}$.

When the added noise from the first method is white, Widrow and Stearns show [27] that the two methods are identical. In practice, since it is impossible to compute ρ sufficiently close enough to 1.0 with the fixed point 16 bits precision of the TMS320C25 processor to implement the leak every sample as suggested in (6.1), we multiply the filter coefficients by 0.99 every p samples where p is generally equal to 10000. Such an operation is not perfectly linear but it does not seem to significantly modify the properties of the control system : the he amplification in low frequencies no longer occurs and the algorithm remains stable.

Figure 6.13 shows the impulse response of the W filter after 10 minutes of convergence, obtained by experiment and the simulation. Again the simulation is very close to the experiment. The measured and simulated transfer function $\frac{W(z)}{1 - W(z).F'(z)}$ is plotted in **figure 6.14**. Notice that, compared to the simple LMS algorithm spectrum, the peaks are much sharper and much closer to those of the ideal controller. Consequently is the attenution better as we can see on the **figure 6.15** . The peak at 296Hz is still present but has been reduced by 5 dB. Almost everywhere else the level of noise has been reduced. Moreover there is again a noticeable similarity between the measured graphs and the simulated graphs.

Figure 6.13 Feedback cancellation LMS. Feedforward controller impulse response after 10min of convergence. 200 coefficients, convergence coefficient = 0.02.
(left) simulation, (right) experiment

Figure 6.14 Feedback cancellation LMS. Frequency response of the controller after 10min of convergence. 200 coefficients, convergence coefficient = 0.02. (up) simulation, (bottom) experiment
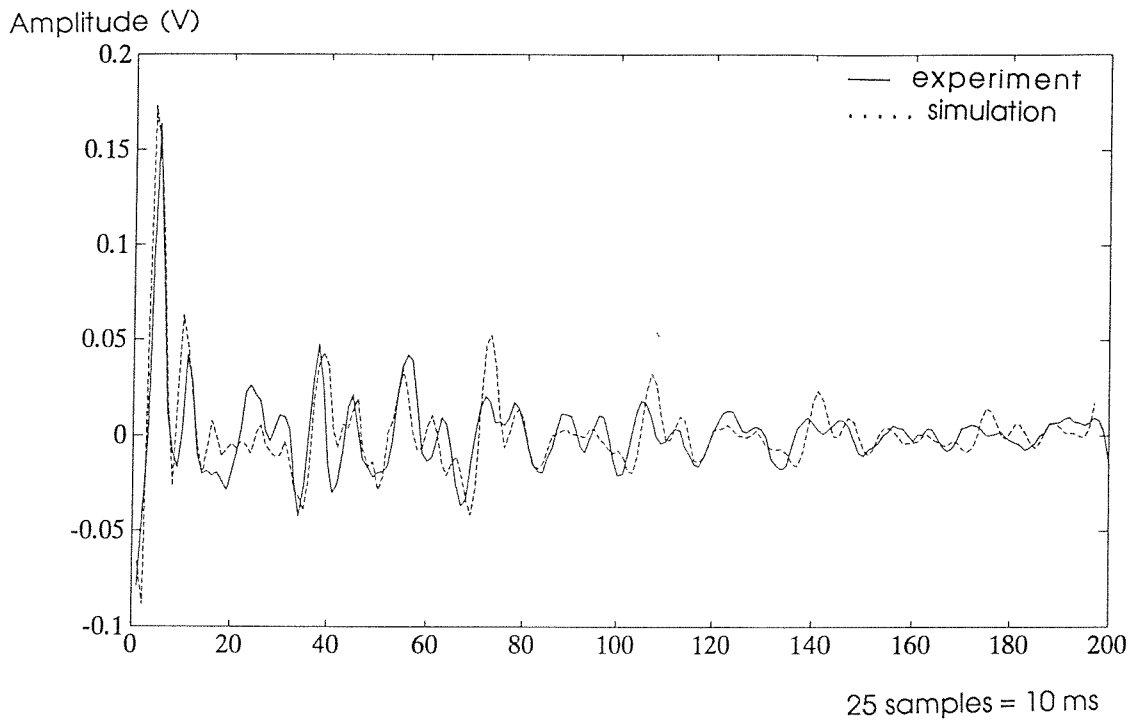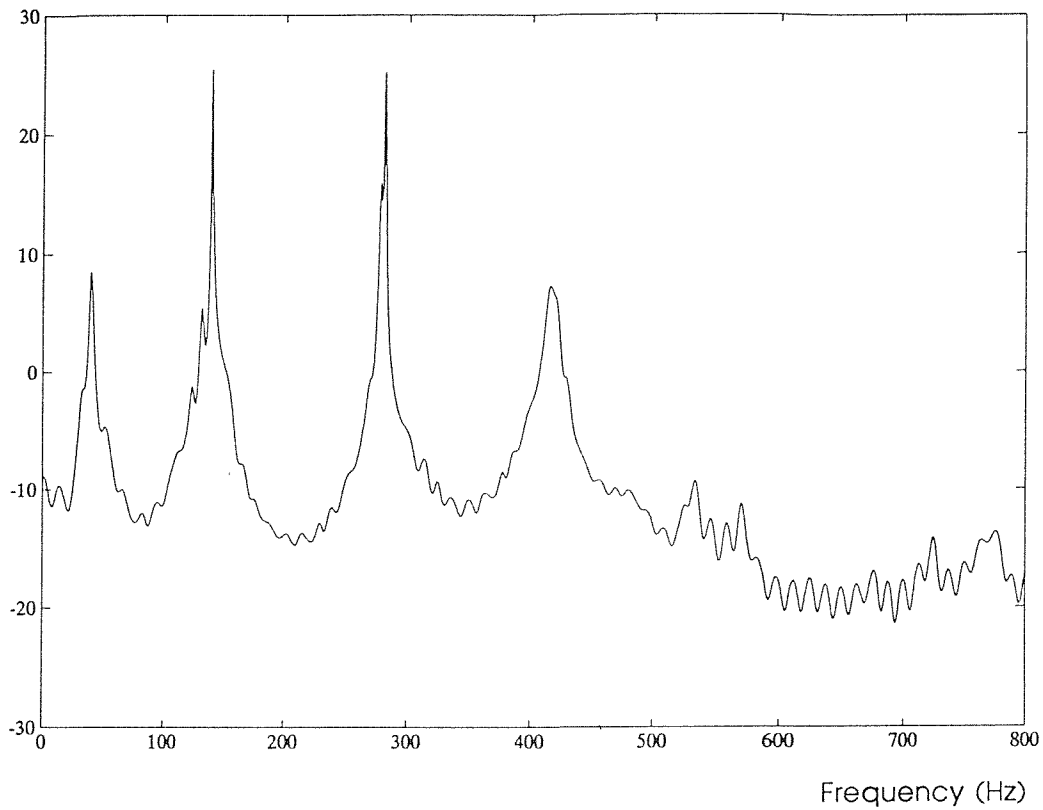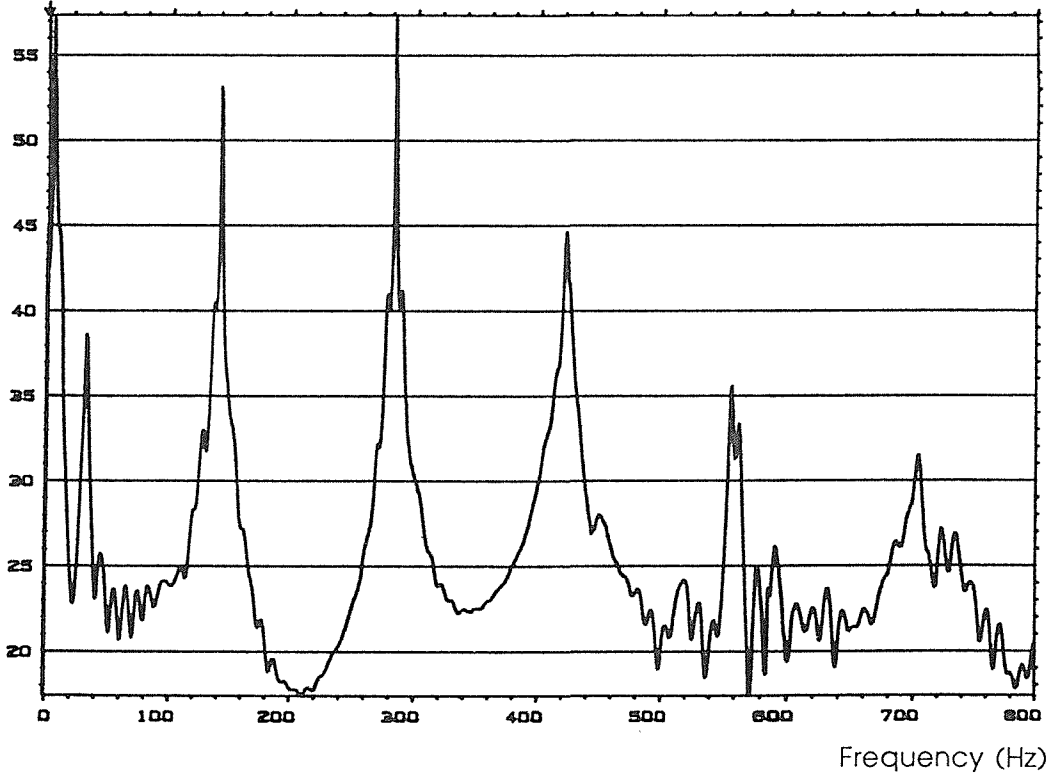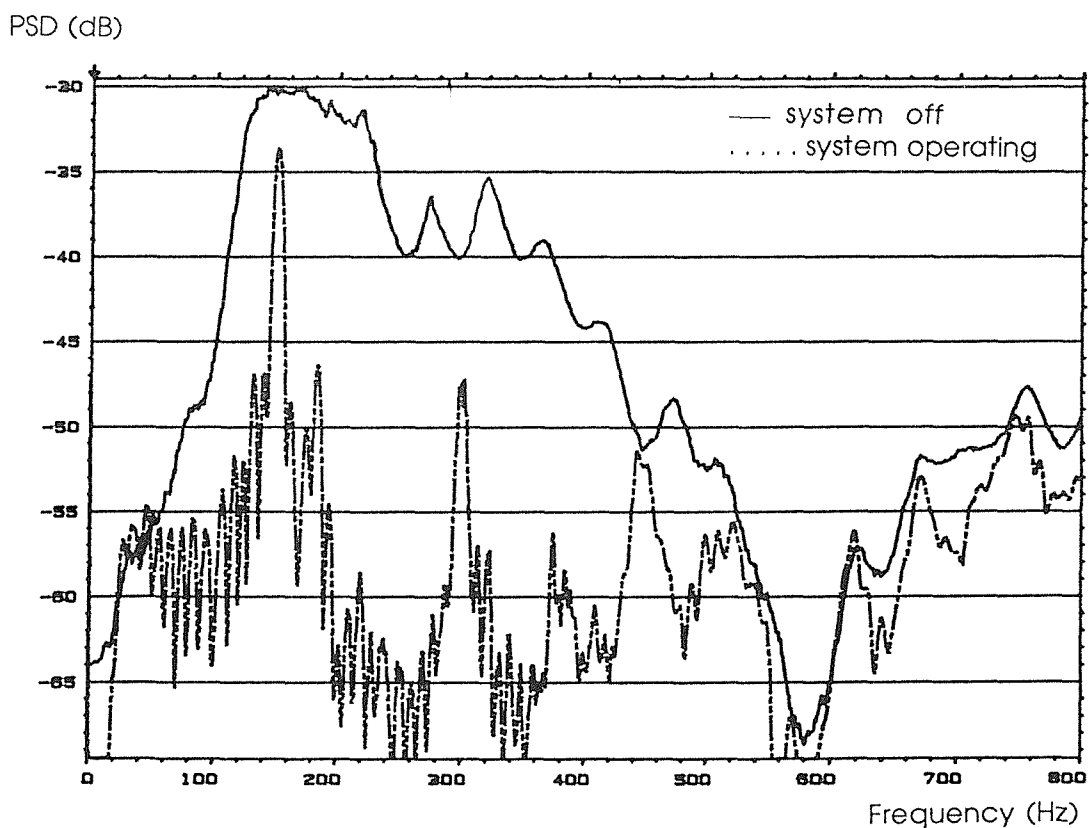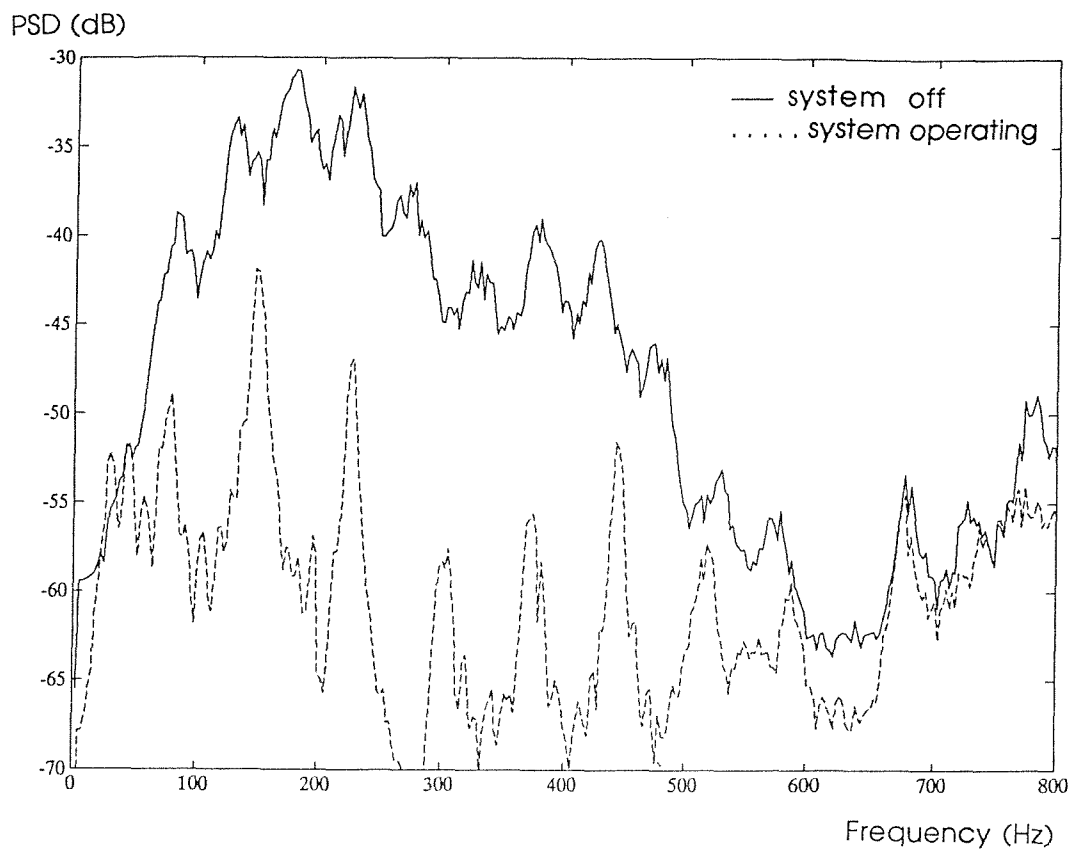
Figure 6.15 Feedback cancellation LMS. DSP at the error sensor after 10min of convergence. 200 coefficients, convergence coefficient = 0.02. (up) simulation, (bottom) experiment

VI.3. Implementation of the recursive LMS algorithm

We have seen in V.3.2 that this structure can be fully adaptive. The on-line identification of the error is identical to the one described in V.1.2. The only difference is that instead of using the prefilter H for the error path once, we now also need to use it twice, once to prefilter the input signal to update the FIR part of the controller and once to prefilter the output signal to update the recursive part.

VI.3.1. Which expression for the gradient?

There has been a kind of polemic over the correct expression to use for the instantaneous gradient for the IIR LMS algorithm. In 1976 Feintuch suggested [32] using a recursive LMS algorithm to perform system identification or active noise control. His derivation to obtain the updating equation is as follow :

the recursive filter is specified by

$$y(n) = w^T x(n) + v^T y(n) \tag{6.2}$$

the error is the difference between the desired response d(n) and the actual response y(n)

$$e(n) = d(n) - w^T x(n) + v^T y(n) \tag{6.3}$$

He then take the expected value to obtain the mean square error

$$E\{e^2(n)\} = w^T [A_{xx}] w + v^T [A_{yy}] v - 2w^T [A_{dx}] - 2v^T [A_{dy}]$$

$$+ 2w^T [A_{xy}] v \tag{6.4}$$

where $[A_{xy}]$ is the correlation matrix between x(n) and y(n).
Then, differentiating (6.4) Feintuch argues that the correlation terms $[A_{xy}]$, $[A_{dy}]$ and $[A_{xy}]$ are constant when differentiated with respect to the feedforward and the feedback weights w and v. Given this assumption he obtains two updating equations which do not require prefiltering of, x(n) and y(n) by $\dfrac{1}{1 - W(z).V(z)}$

In [33] and [34], Jonhson and Larimore on one hand and Widrow and Mc Cool on the other hand reply that Feintuch calculation is incorrect since the mentionned

- 97 -

correlation terms are obviously non constant when differentiated. Therefore the correct algorithm should prefilter x(n) and y(n) by $\frac{1}{1 - W(z).V(z)}$.

However, Widrow admits that Feintuch's algorithm even if it does not perfectly converge to the least square solution " has the extraordinary property of remaining stable even though noise in the feedback weight may occasionnally push the pole outside the unit circle. The feedback of the adaptive process interacts favorably with the feedback of the filter itself to produce a 'superstability' that will pull the poles back in beyond the brisk of instability". This point is further aknowledged by Flockton [25] and Shink [28].

In our case this fact is important. If the correct gradient IIR LMS algorithm is potentially unstable, it may be worthwhile to implement the more robust Feintuch algorithm instead. Then we have decided to study both of them through computer simulation. First, we have tried the two structures assuming the following conditions: perfect loudspeakers and R1=0.39, R2= -0.83. **Figure 6.16** is a plot of the square of the residual error during the converging process. As expected the algorithm with the true gradient estimate is better in term of convergence rate. However, after 260 seconds the error levels off and the algorithm finally diverges whereas the other structure continues to converge steadily. This is consistent with the conclusion of Widrow et. al. However, the previous conditions were perhaps too ideal. We have repeated the simulation with a practical loudspeaker model (**figure 6.17**). This time both algorithms remained stable during convergence. The practical loudspeaker by decreasing the optimal attenuation appears to prevent the IIR controller to become unstable. Therefore, it will be possible to use the modified gradient algorithm (see discussion in V.3.2).

VI.3.2. Experimental results and simulation of the experimental conditions

In the experiment we tried both Feintuch and correct-gradient IIRLMS. Both of them became unstable after about a quarter of an hour of convergence. This was surprising for the Feintuch algorithm given the conclusions of §VI.3.1. However, we think that the secondary source non-linearity at high input level combined with the fixed-point arithmetic may be responsible of such an unstability. Considering that the Feintuch algorithm was less efficient that the correct-gradient algorithm and did not allow to identify the error path on line, it was rapidly abandonned. From now we will only describe the modified-gradient IIRLMS.

Attenuation (dB)

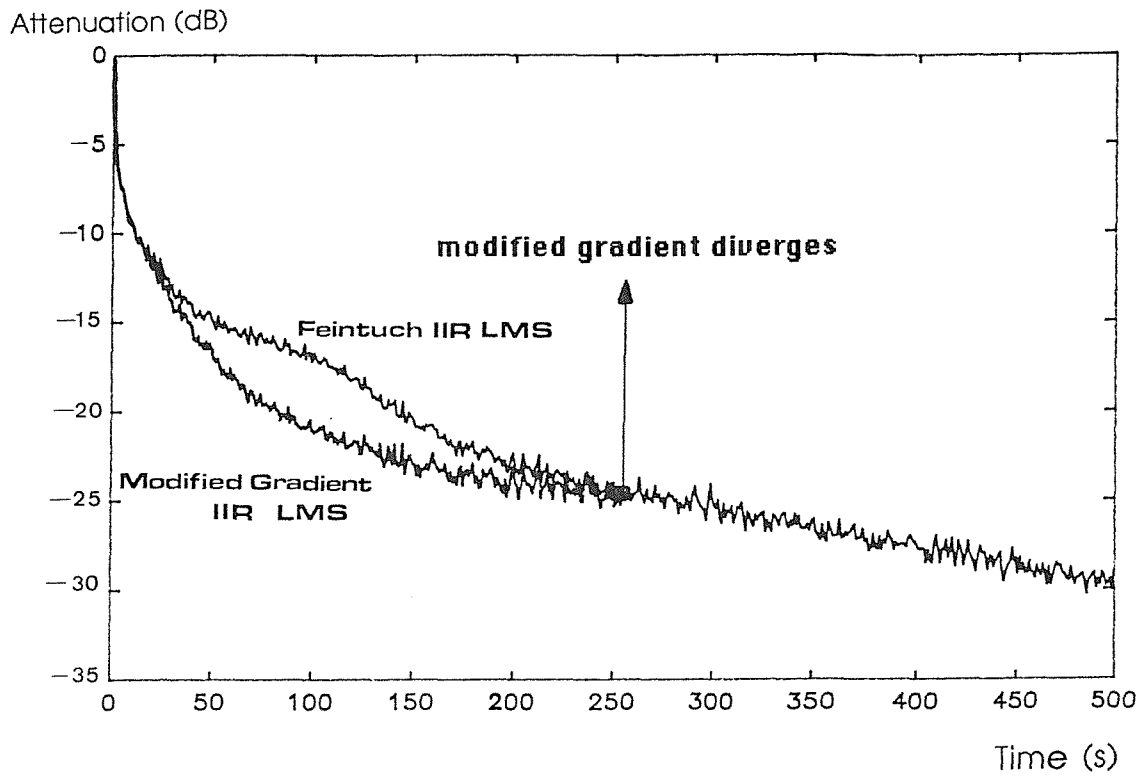**Figure 6.16** IIR LMS (Simulation) W = 200 coeff, V=200 coeffs. R1 = 0.39, R2 = -0..83. ideal loudspeaker. Comparison of the convergence of the Feintuch algorithm and the modified-gradient IIRLMS algorithm
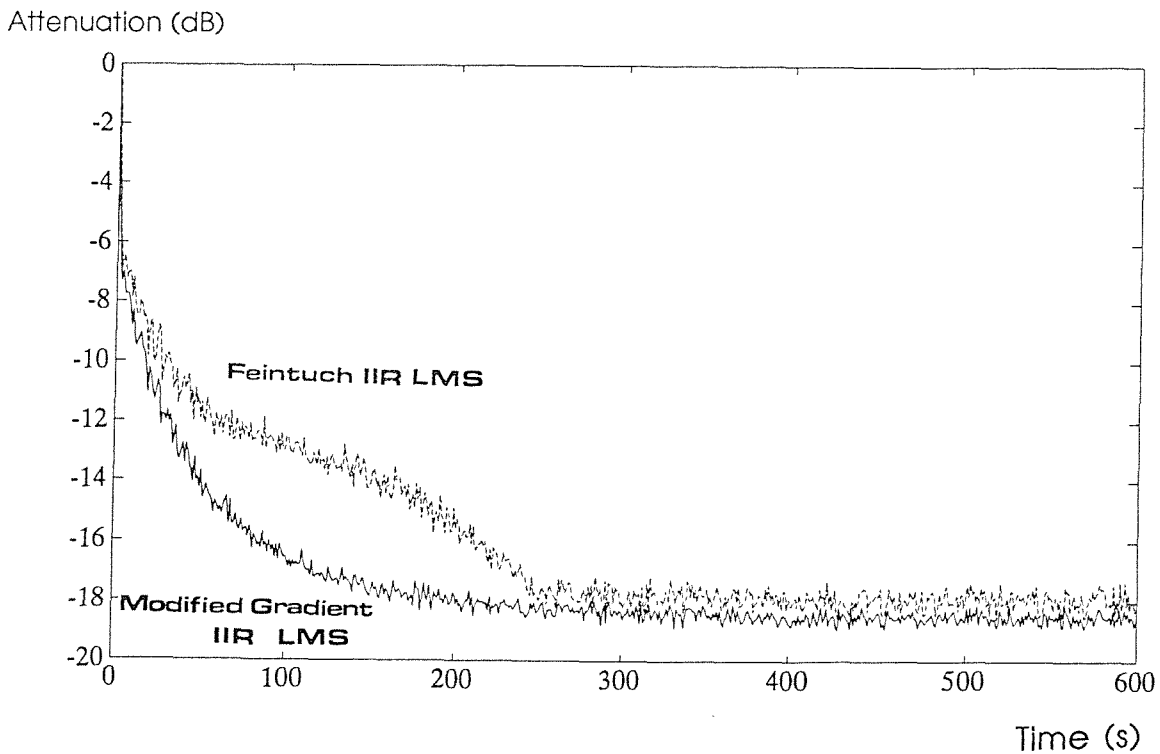
Attenuation (dB)

Figure 6.17 IIR LMS (Simulation) W = 200 coeff, V=200 coeffs. Experimental conditions. Comparison of the convergence of the Feintuch's algorithm and the modified-gradient IIR-LMS algorithm.

The number of coefficients for the forward adaptive filter the feedback adaptive filter and the error path filter were respectively 20, 40 and 200. μ_v was equal to 0.003 whereas μ_w was equal to 0.005. These are empirical values which, as we think, depend strongly of the experimental hardware. The system has been launch without prior indentification, all the adaptive filters had coefficients initially zero. In order to have a quick convergence of the overall system, it was experimentally found that the error path filter must be the fastest filter to be identified. Consequently the coefficient μ_h has to be large (0.4 is a practical value). The process of convergence is as follow : the error path filter is very quickly identified (1 or 2 seconds), then the feedforward filter starts to build itself and finally so does the feedback filter. The feedback filter is identified last because, at the begining, the update is proportional to the feedforward filter output and this one is necessarily very small. During the convergence of W and V the error path prefilter is slightly modified by the presence of the controller. Moreover, to ensure a good performance, the power of the uncorrelated noise added at the secondary source output is proportional to the power of the residual error (10 dB below is a reasonable value). As a consequence the convergence speed of identification will be dependant of the error but we do not think this is an inconvenient because the error path filter converges very quickly when the error is still important. As we stated above, the experimental trials have proved that the IIRLMS algorithm is rather difficult to handle properly. Its propensity to become unstable is as strong as the simple LMS controller. It was clear than a stabilisation had to be found. Again we have chosen to introduce a small leak in the update of the recursive controller (a stabililisation of the error path LMS does not seem to be necessary). Once introduced, such a leak gives good results. The system can admit reasonable perturbation without diverging. It is therefore possible to increase the convergence coefficients μ_v and μ_w if we want to improve the tracking properties. However a compromise has to be found between the correct value for the leak and the updating coefficients: a large leak leads to a lower attenuation and a large convergence coefficient makes the system less damped. As far as the number of coefficient is concerned we found that it is detrimental to use more filter coefficients than are necessary to implement the ideal controller. For example, we found that 20 and 40 coefficients for W and V leads to a better performance than say, 40 and 80. This is somehow surprising, since it is generally aknowleged (Widrow and Stearns in ref [29], as well as Shink in [28) that the more poles and zeroes we use to identify the controller the more unimodal is the error surface. However, it is possible that in this case, the error surface is unimodal and well behaved even with a minimal set of coefficients. This important problem should

requires further investigation. An interesting start in this direction has been made by Flockton in ref. [39].

Figure 6.18 shows the feedforward filters and feedback filter impulse responses derived from experiment and simulation after 10 minutes of real time convergence. Both filters are very close to simple delays but nethertheless they include the inverse of the secondary transducer. The small number of coefficients required to achieve a proper attenuation confirms that the IIR structure is the most suitable for this kind of active noise control. The experimental and simulated frequency response of the controller is plotted in **figure 6.19**. The extreme sharpness of the peaks at low frequencies as well as at high frequencies allows us to predict fairly good attenuation. Indeed when we look at **figure 6.20** the results are very good. The big peak at 148 Hz has decreased by more than 10 dB and the improvement over the feedback cancellation system is around 10 dB at high frequencies. Moreover it is interesting to notice that the simulated results match very well the experimental ones.
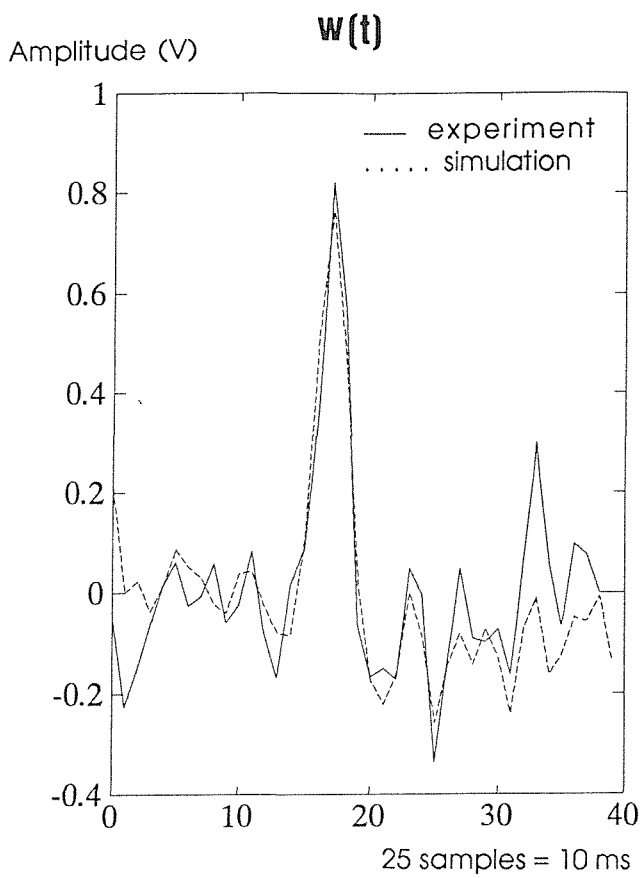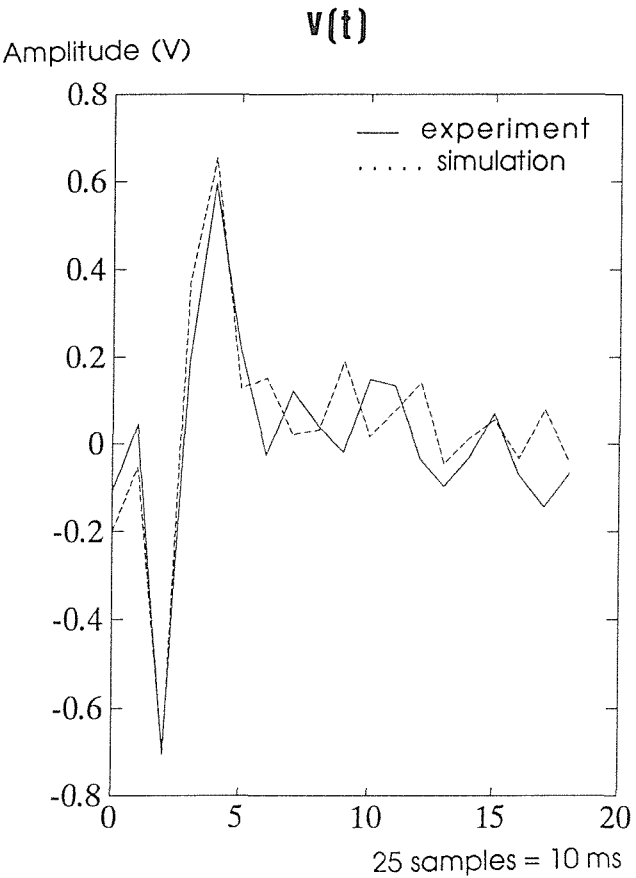
Figure 6.18 I IR LMS. Controller filter coefficients after 10min of convergence. 20 coefs for feedforward coefficients W, 40 coefs for recursive coefficients V, convergence coefficient = 0.003 and 0.005 for W and V.
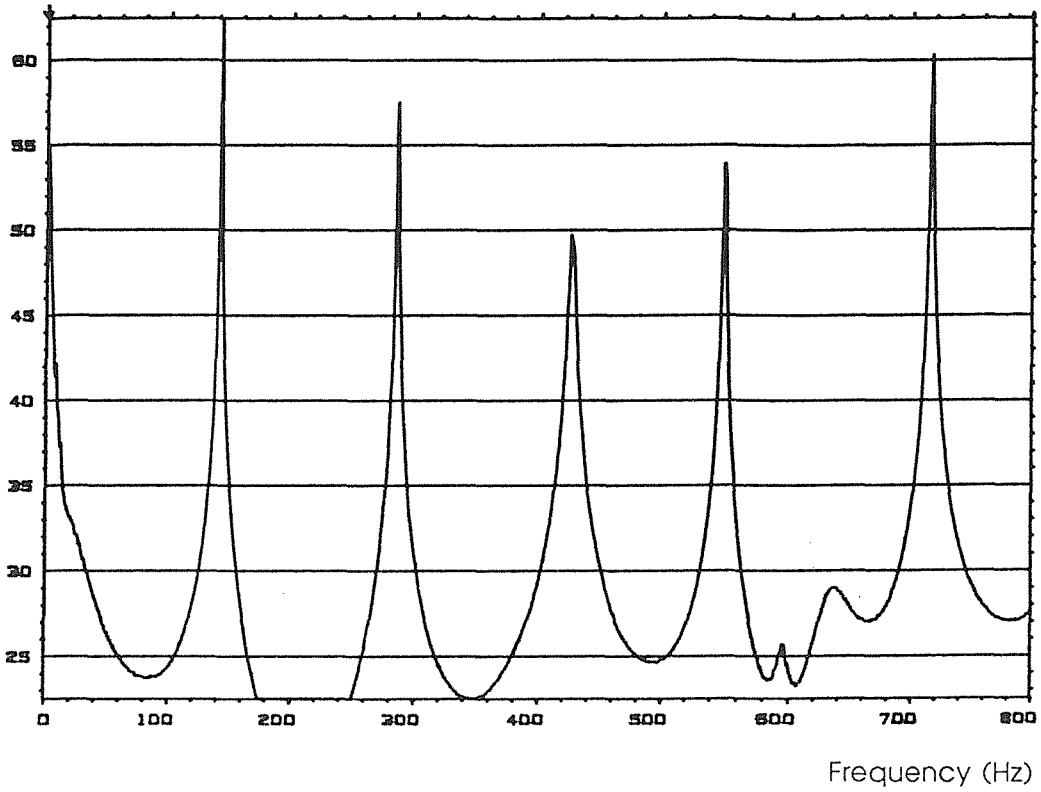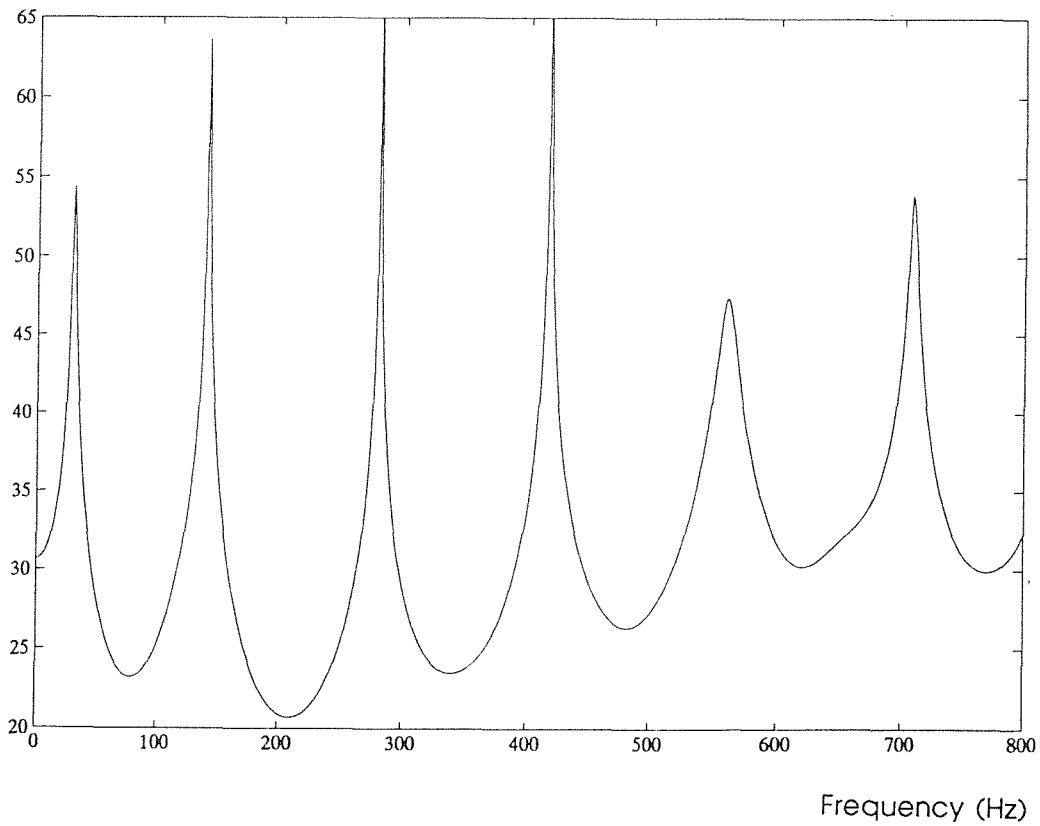
Figure 6.19   IIR LMS. Frequency response of the controller after 10mn of convergence. 20 coefs for W, 40 coefs for V, convergence coefficient = 0.003 and 0.005 for W and V.

(top) simulation, (bottom) experiment
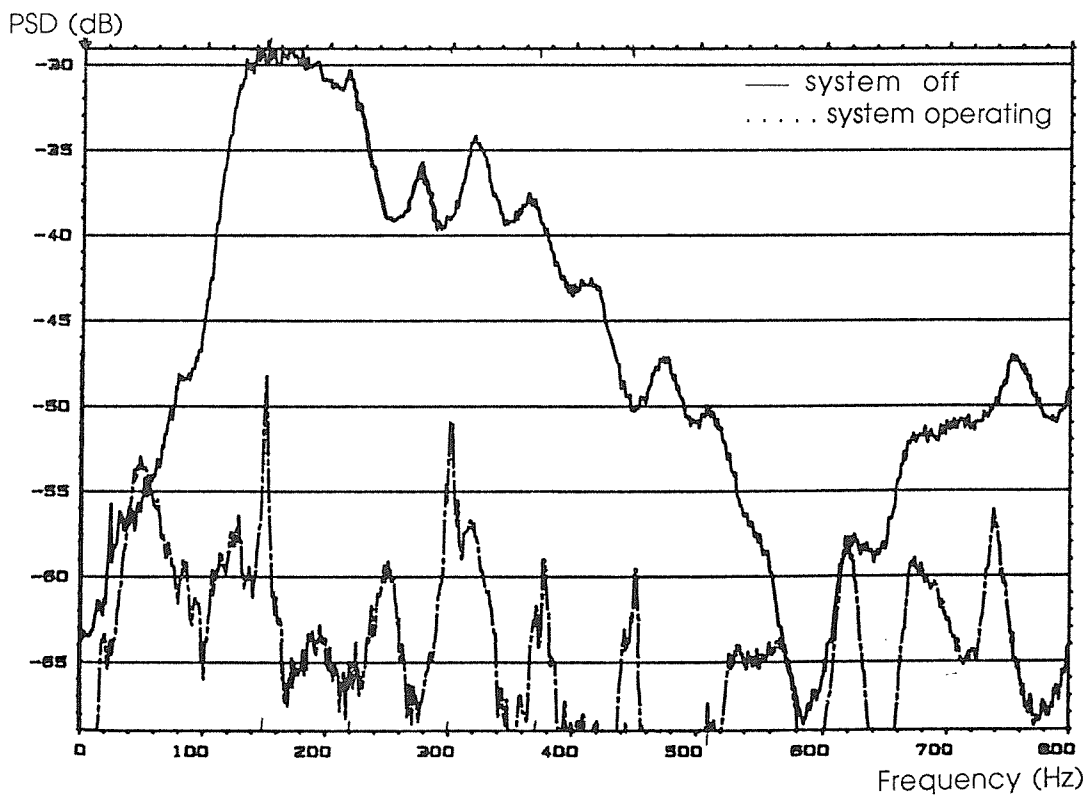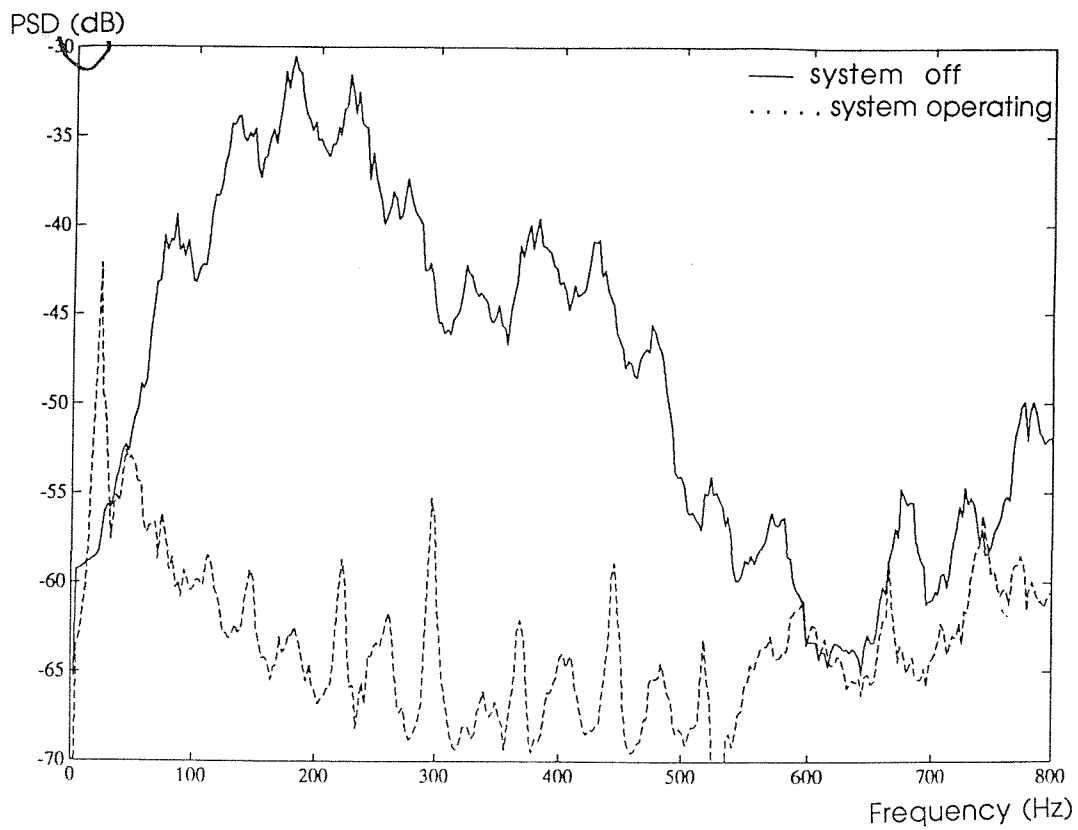
Figure 6.20 IIR LMS. PSD at the error sensor after 10mn of convergence. 20 coefs for W, 40 coefs for V, convergence coefficient = 0.003 and 0.005 for W and V. (up) simulation, (bottom) experiment

VI.4   Overall comparisons

A comparison of the performance of the three different structures are shown in
figure 6.21 & 6.22 . **Figure 6.21** shows the square of the residual error as a function
of time during the convergence process. The convergence coefficients were those
given previously in this chapter in the descriptions of the experiments. The
hierarchy is as follow : the IIRLMS algorithm achieves the best attenuation then
the LMS with feedback cancellation and last the simple LMS algorithm. The rates
of convergence are however similar for the three structures (20 seconds). **Figure
5.22** shows the compared residual error spectral densities after complete
convergence. As we have seen previously the main difference between the IIR
algorithm and two other ones is that it eliminates the 140 Hz peak and improves
significantly the attenuation at high frequencies.
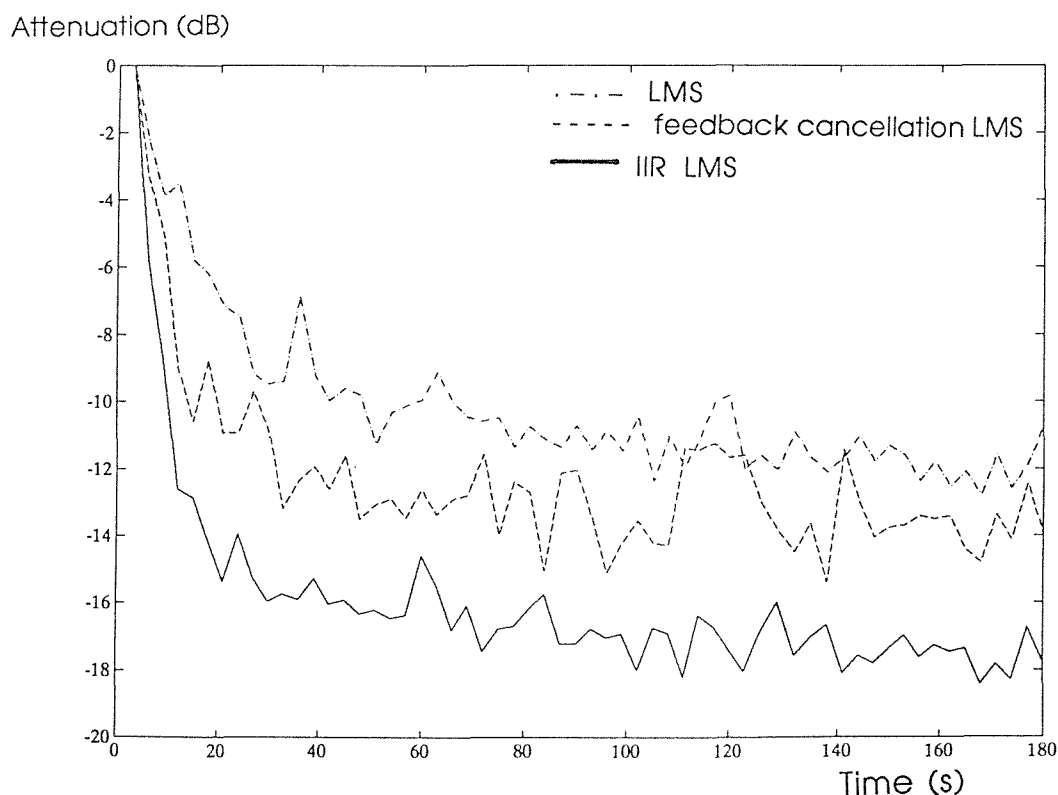
Figure 6.21 Comparison of the convergence for all three algorithms.
(Experiment)
Simple LMS algorithm: W=200 coeffs, Feedback cancellation Algorithm : W=200
coeffs, IIR LMS algorithm : W=20coeffs : V=40 coeffs.

Figure 6.22 Comparison of the attenuation for all three algorithms (Experiment)
Simple LMS algorithm : W=200 coeffs, Feedback cancellation Algorithm : W=200
coeffs, IIR LMS algorithm : W=20coeffs; V=40 coeffs.

VI.5 Active noise control system using a piezo-electric transducer

We saw in IV.1.3 and in various simulations of the present chapter that the quality of the transducers has a large influence on the active noise control performance. A particularly crucial point, not studied in this thesis, is that usually, the detection of the sound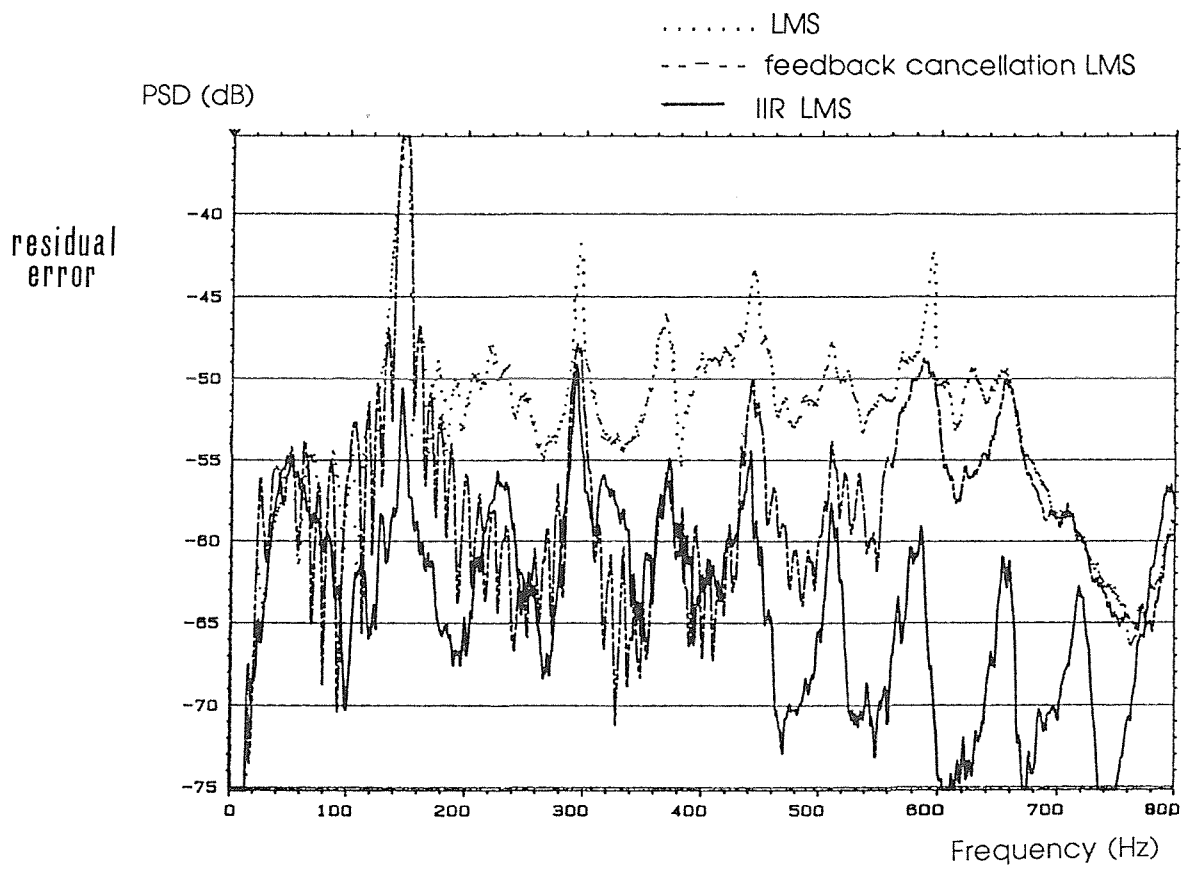 signal in ducts is done in the presence of air flow, producing turbulence at the microphones. This turbulence generates noise which is incoherent with the original sound wave and then, according to equation (4.27), the attenuation is often limited for this reason. Several methods are used to solve this problem. The one generally used in practical realisations is to encapsulate the microphone in a long tube, the tube having the effect of averaging the pressure field around the microphone position which eliminates some of the turbulent signal. However, this does not give complete satisfaction.

The solution we propose to examinate here is inspired from a method developed at the ISVR [40], to measure power flow in a pipe by using a piezo-electric wire coiled up around the pipe. The piezo-electric wire can be considered as a transducer which converts non-turbulent sound waves into electric signals. Then it can be used as a sensor in an active noise control system. However, this paragraph will not be an extensive study on this subject, we will only demonstrate briefly that active noise control is feasible with such a sensor, leaving the door open to further investigations.

VI.5.1 Principle of the sensor

The piezoelectric wire is made of PVDF, a material which has the preperty of beeing electrically polarized when stretched. The stretching converts a neutral cristal form into a highly polar cristal form of the material. As a result, a voltage, proportional to the applied stress, appears between the two end of the wire. **Figure 6.23** explains how a sound wave in the duct can be detected when the wire is coiled up around the pipe. Because the sound wave are plane (a major assumption of this thesis) they are invariant by rotation around the pipe axis. Therefore they tend to excite preferentially the first cylindrical mode of the pipe (the mode which modifies only the diameter of the pipe). When a positive sound pressure comes into the area delimited by the wire the duct diameter slightly increases creating a stretching of the wire which produces a voltage change between the two ends of the wire. Of course, a negative sound pressure generates a voltage change of opposite sign. The interest of this system is that, if the wire is wrapped around

many times, it completely integrates the small pressure fluctuation in the duct over a section. Therefore the turbulences have little influence on the measurement. Moreover, since the flexural modes do not change the diameter of the duct to a first approximation they are not detected.
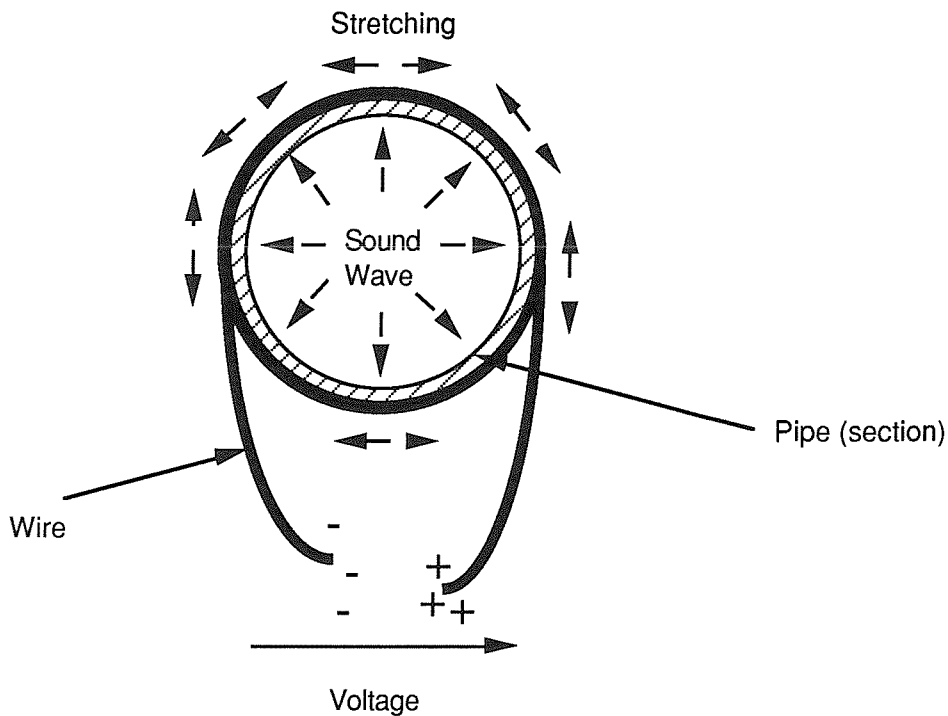
FIGURE 6.23 Principle of the piezo-electric wire. The sound pressure modifies locally the diameter of the duct causing a stretching of the wire. The stretching finally produces a voltage proportionnal to sound pressure.

Figure 6.24 shows how four turns of the wire was coiled up around the PVC duct used in the experiments above.
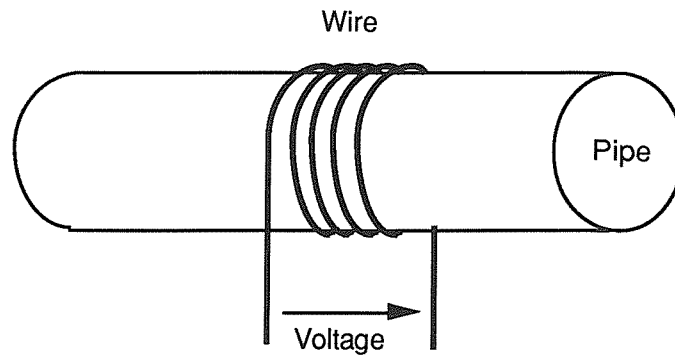
Wire

FIGURE 6.24 Description of the piezo-electric sensor

VI.5.2 Experimental results.

We modified the experimental setup described in section III.1 by replacing the error microphone by the piezoelectric wire. The three adaptive algorithms described above were then used to achieve active noise control. In order to make the comparison possible with the previous structures, we used the same number of coefficients as used previously. Power spectral densities of the residual error for each algorithm before and after convergence are plotted on **figures 6.25, 6.26, and 6.27**. At first sight we can say that the performance in each case is generally worse than that obtained with an error microphone in sections VI.1, VI.2 and VI.3 (fig 6.7 to 6.15). However, a noticeable reduction is achieved. We again see a bad attenuation at 148Hz and 296Hz, frequencies corresponding to antiresonances in the duct at the detection sensor. Surprisingly, the IIR LMS is not performing very well in the middle of the spectrum (around 100Hz and 250Hz) compared to the LMS algorithm and the feedback LMS algorithm. In practice the IIR LMS cycled all the time between an efficient state of noise control and a poor one. It is thought that when the algorithm had converged some vibration generated by the secondary source was propagating along the duct wall to the piezo-electric wire thus causing a cycle of instability. A structural coupling of the actuator with the sensors does probably exist and may have a destabalising effect in this system. Even so, given the limited amount of time available to realise this experiment these results are encouraging. They encourage a more carefull study of the properties of this approach in presence of air flow, an experiment we did not have the proper equipement to realise.

Figure 6.25 LMS algorithm. The error sensor is a piezo-electric wire. W=200 coeffs. Convergence coefficient = 0.02. PSD at the error sensor before convergence and after 10 mn of convergence.

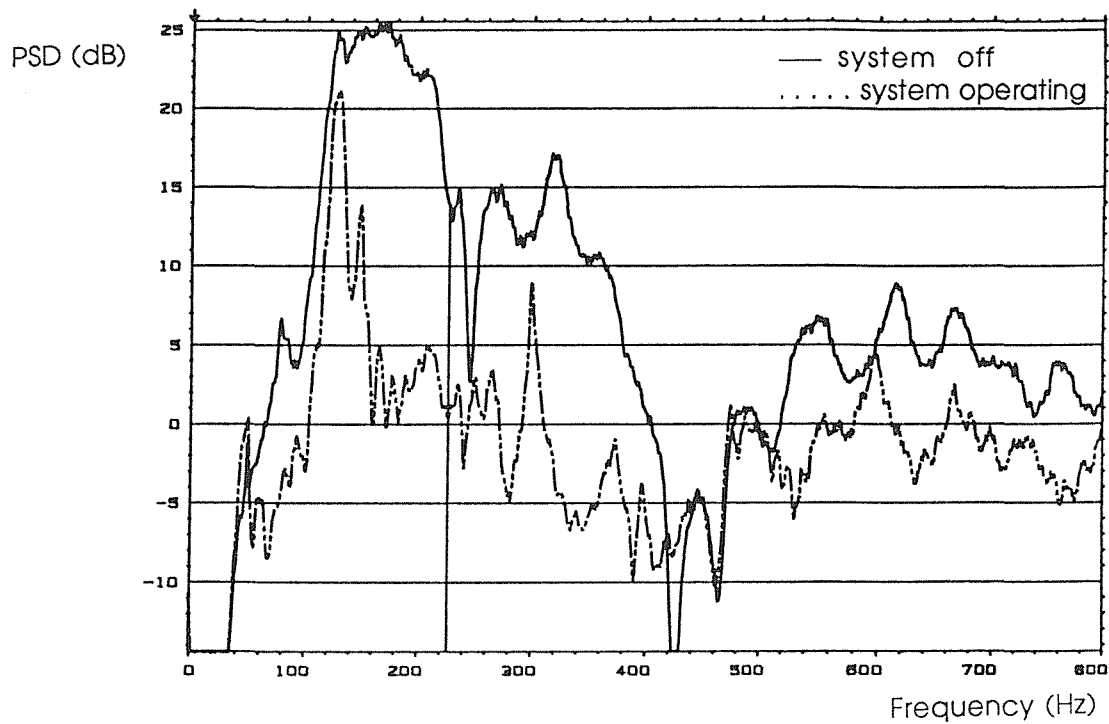**Figure 6.26** Feedback cancellation LMS. The error sensor is a piezo-electric wire. W=200 coeffs. Convergence coefficient = 0.02. PSD at the error sensor before convergence and after 10 mn of convergence.

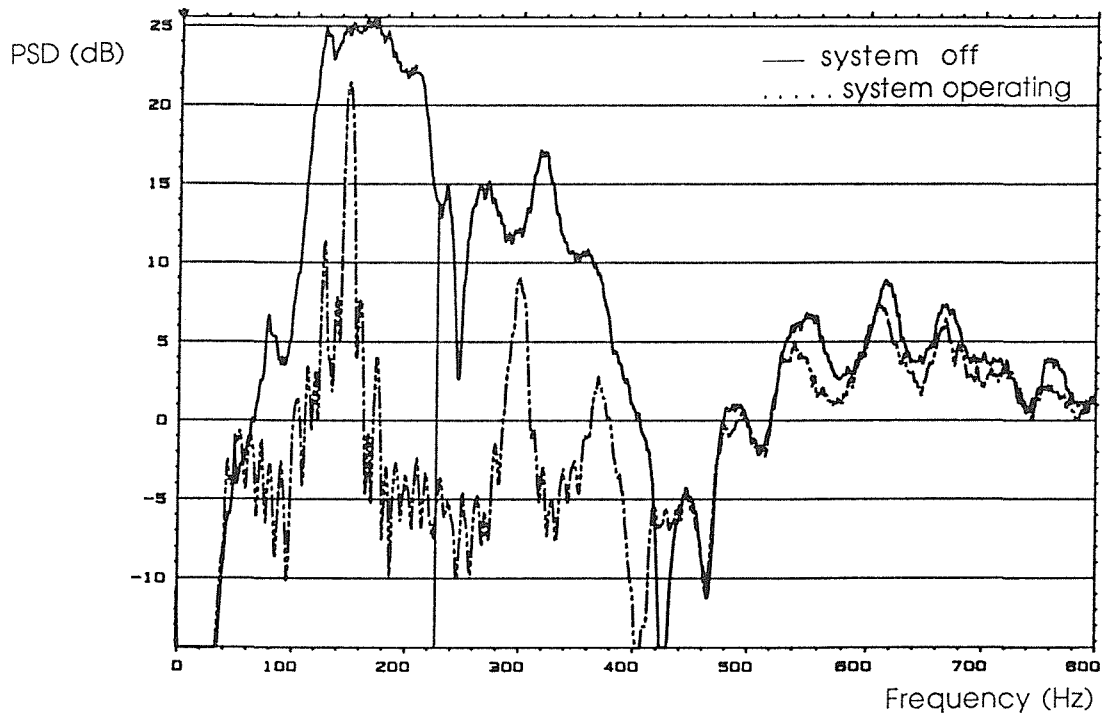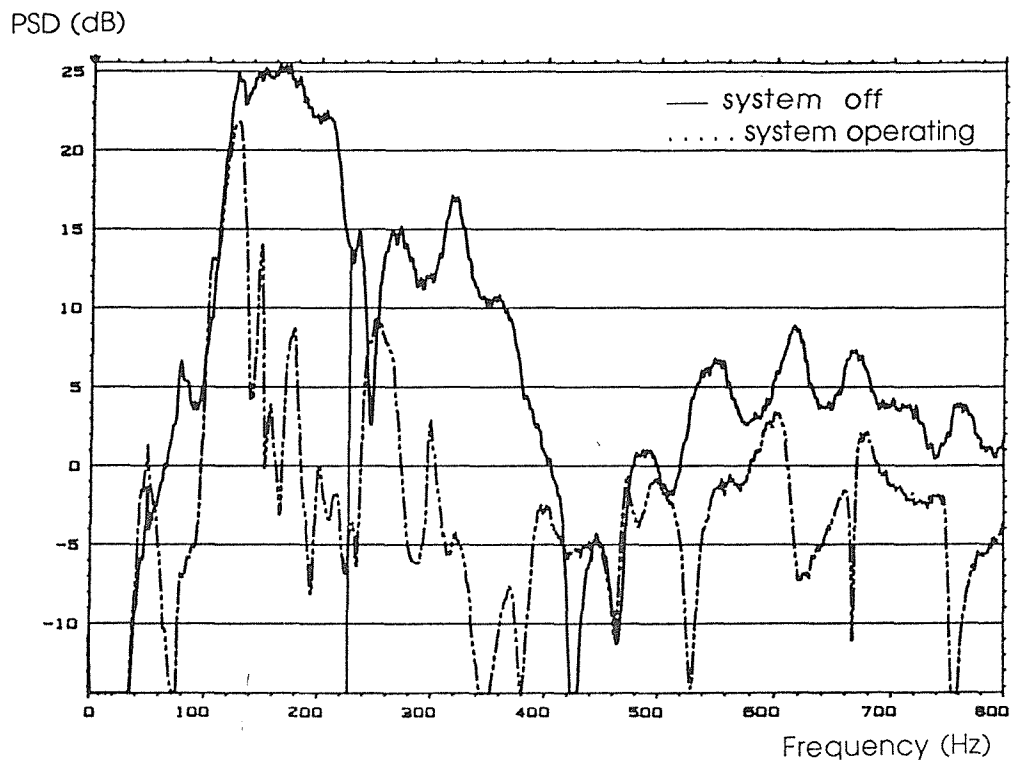PSD (dB)

Figure 6.27 IIR LMS. The error sensor is a piezo-electric wire. W=20 coeffs. V=40 coeffs. Convergence coefficients are 0.003 and 0.005 for W and V. PSD at the error sensor before convergence and after 10 mn of convergence.

VII CONCLUSION

The purpose of this study was to compare three adaptative time domain algorithms currently used in the active control of sound in ducts : the LMS algorithm, the LMS algorithm with feedback cancellation and the Infinite Impulse Response LMS algoritm. Here are the conclusions of our tests :

The LMS algorithm is mainly interesting because of its simplicity. It can reduce the broadband noise in the duct by up to 10 dB under the usual conditions investigated here. Its main limitation is that it requires a very large number of coefficients in the presence of a feedback path and also can be difficult to stabalise under certain conditions.

The LMS algorithm with feedback cancellation is a reliable structure as long as the duct parameters remains stationary (this unfortunately is a very restrictive condition in practical applications). The convergence is generally steady and stable and global attenuation of broadband noise in the duct of up to 15 dB was achieved under the conditions investigated here.

The IIR LMS algorithm is the more powerful structure. Attenuation of broadband noise in the duct was up to 20 dB for the practical realisation investigated here. The algorithm can work in a fluctuating environment with a tracking time of about 20 seconds. Because this algorithm is potentially unstable, however, some leak must be introduced to prevent the poles from going out the unit circle.

Another interesting point of this thesis is the use of a realistic computer model of the complete active noise control system which was used to test the different algorithms. This approach enabled us to reinforce and to understand better the experimental results. In particular, we have demonstrated the imperfect frequency response of the transducers was responsible for most of the limitation of the system.

We have been concerned in this thesis with only some of the aspects of a single channel active noise control system in ducts. A number of other aspects remain

open even in this restricted field of active control. Particularly worthy of further study is the nature of the error surface of an IIR controller in presence of a feedback path, following Flockton's approach [39]. The point is of importance since the convergence properties of LMS type algorithms depend on the unimodality and the quadraticity of the error surface. One could also develop a more robust IIR controller. Lattice filters, for instance, have straightforward stability monitoring features and could be used either on-line to implement the controller or in parallel to check the stability. Besides the Gray and Markel algorithm which converts an IIR filter into a lattice one [42], various adaptive IIR lattice filter algorithm are available [43] [44]. We tested one of them [43] through simulation without great success but we still consider this approach as promising.

Finally, given the early results obtained with an piezo-electric transducer we recommend continued research in this direction in order to design a active noise control system less sensitive to air flow turbulence.

APPENDIX

A.1 Simple LMS : Updating Equations :

(see figure A.1)

$$y(n) = \sum_{i=0}^{N_w} w_i(n).u(n-i) \qquad (A.1.1)$$

$$r(n) = \sum_{i=0}^{N_h} h_i(n).u(n-i) \qquad (A.1.2)$$

$$y_1(n) = \sum_{i=0}^{N_h} h_i(n).x_1(n-i) \qquad (A.1.3)$$

$$e_1(n) = e(n) - y_1(n) \qquad (A.1.4)$$

$$w_i(n+1) = w_i(n) - \mu_w.r(n-i).e(n) \qquad (A.1.5)$$

$$h_i(n+1) = h_i(n) + \mu_h.x_1(n-i).e_1(n) \qquad (A.1.6)$$
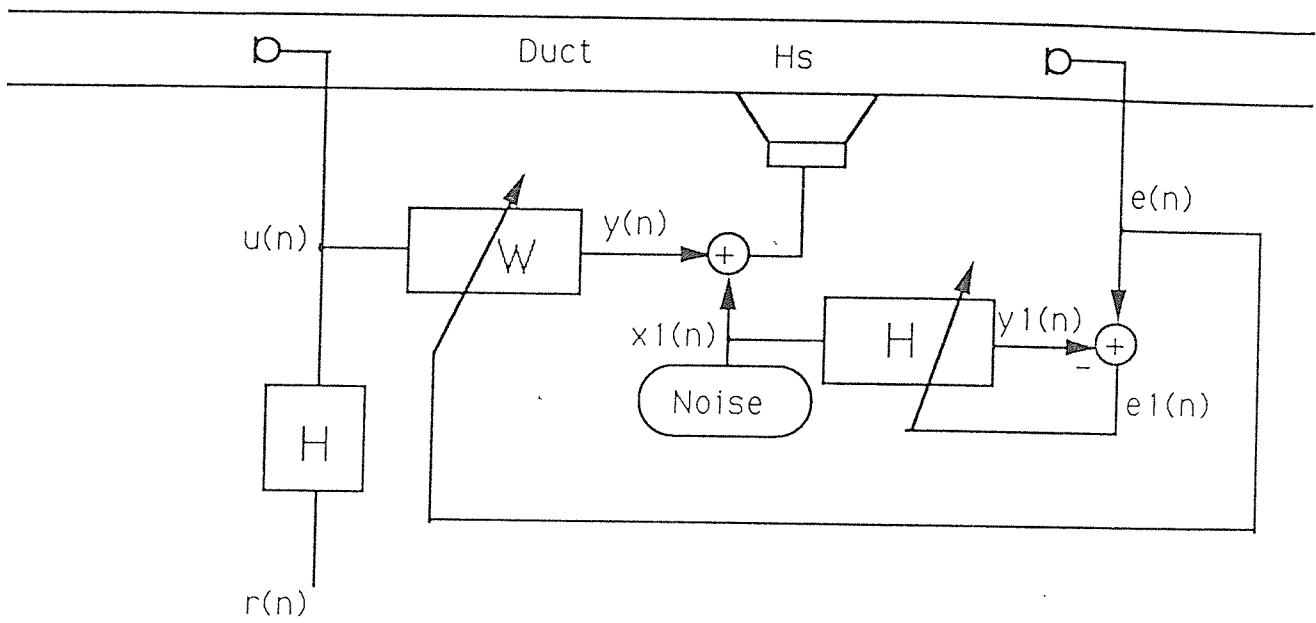
Figure A.1 Simple LMS algorithm : Updating equations

A.2 Feedback Cancellation LMS : Updating Equations :

(see figure A.2. (top))

SYSTEM CANCELLING

$$y(n) = \sum_{i=0}^{N_w} w_i(n).u(n-i) \qquad (A.2.1)$$

$$u(n) = x(n) - f_1(n-1) \qquad (A.2.2)$$

$$r(n) = \sum_{i=0}^{N_h} h_i(n).u(n-i) \qquad (A.2.3)$$

$$f_1(n) = \sum_{i=0}^{N_h} f'_i(n).y(n-i) \qquad (A.2.4)$$

$$w_i(n+1) = w_i(n) - \mu_w.r(n-i).e(n) \qquad (A.2.5)$$

H IDENTIFICATION   (see figure A.2. (bottom))

$$x_1(n) = b(n) \text{ (noise)} \qquad (A.2.6)$$

$$y_1(n) = \sum_{i=0}^{N_h} h_i(n).x_1(n-i) \qquad (A.2.7)$$

$$e_1(n) = d(n)-y_1(n) \qquad (A.2.8)$$

$$h_i(n+1) = h_i(n) + \mu_h.y(n-i).e(n) \qquad (A.2.9)$$

F' IDENTIFICATION   (same principle as with H)

$$x_1(n) = b(n) \text{ (noise)} \qquad (A.2.10)$$

$$y_2(n) = \sum_{i=0}^{N_h} f'_i(n).x_1(n-i) \qquad (A.2.11)$$

$$e_2(n) = d(n)-y_2(n) \qquad (A.2.12)$$

$$f'_i(n+1) = f'_i(n) + \mu_f.y(n-i).e(n) \qquad (A.2.13)$$
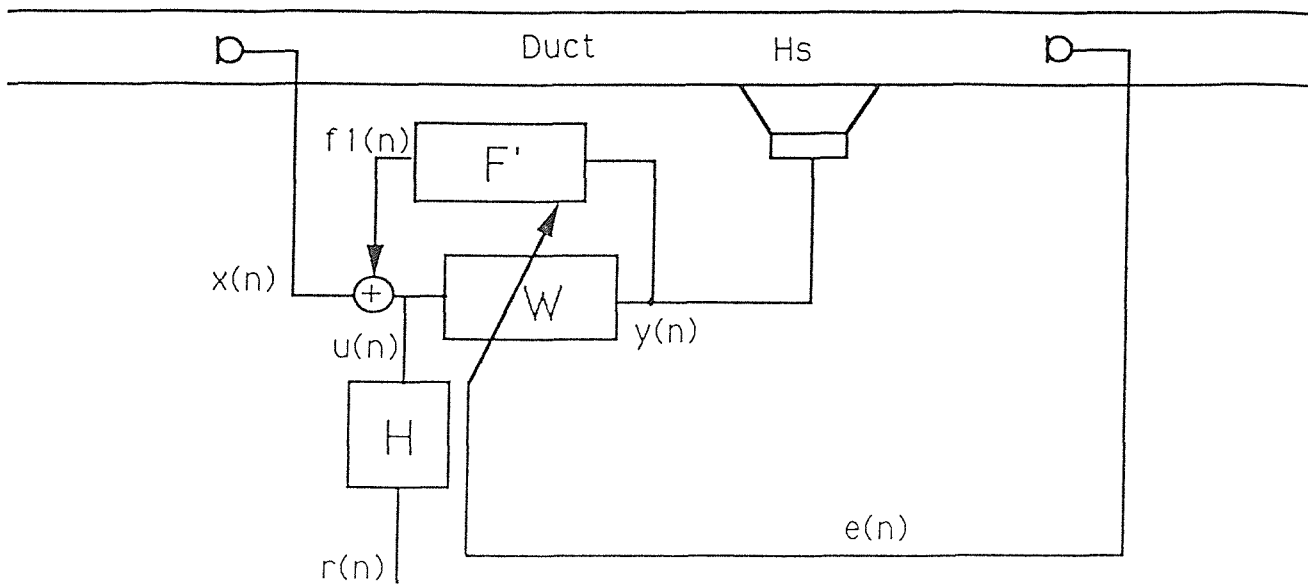
Figure A.2 Feedback cancellation LMS algorithm : System Cancelling
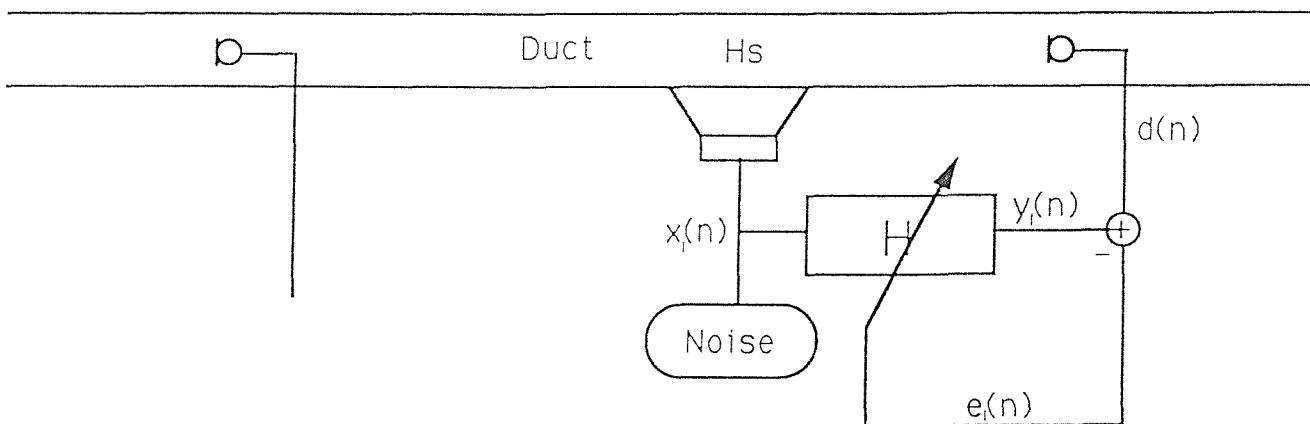
Figure A.2 Feedback cancellation LMS algorithm : Identification of H

A.3 IIR LMS : Updating Equations :

(see figure A.3)

$$y(n) = \sum_{i=0}^{N_w} w_i(n).u(n-i) + \sum_{i=1}^{N_v} v_i(n).y(n-i) + x_1(n) \qquad (A.3.1)$$

$$r_u(n) = \sum_{i=0}^{N_h} h_i(n).u(n-i) \qquad (A.3.2)$$

$$r_y(n) = \sum_{i=0}^{N_h} h_i(n).y(n-i) \qquad (A.3.3)$$

$x_1(n)$ is identification noise

$$y_1(n) = \sum_{i=0}^{N_h} h_i(n).x_1(n-i) \qquad (A.3.4)$$

$$e_1(n) = e(n) - y_1(n) \qquad (A.3.5)$$

$$w_i(n+1) = w_i(n) - \mu_w.r_u(n-i).e(n) \qquad (A.3.6)$$

$$v_i(n+1) = v_i(n) - \mu_v.r_y(n-i).e(n) \qquad (A.3.7)$$

$$h_i(n+1) = h_i(n) + \mu_h.x_1(n-i).e_1(n) \qquad (A.3.8)$$
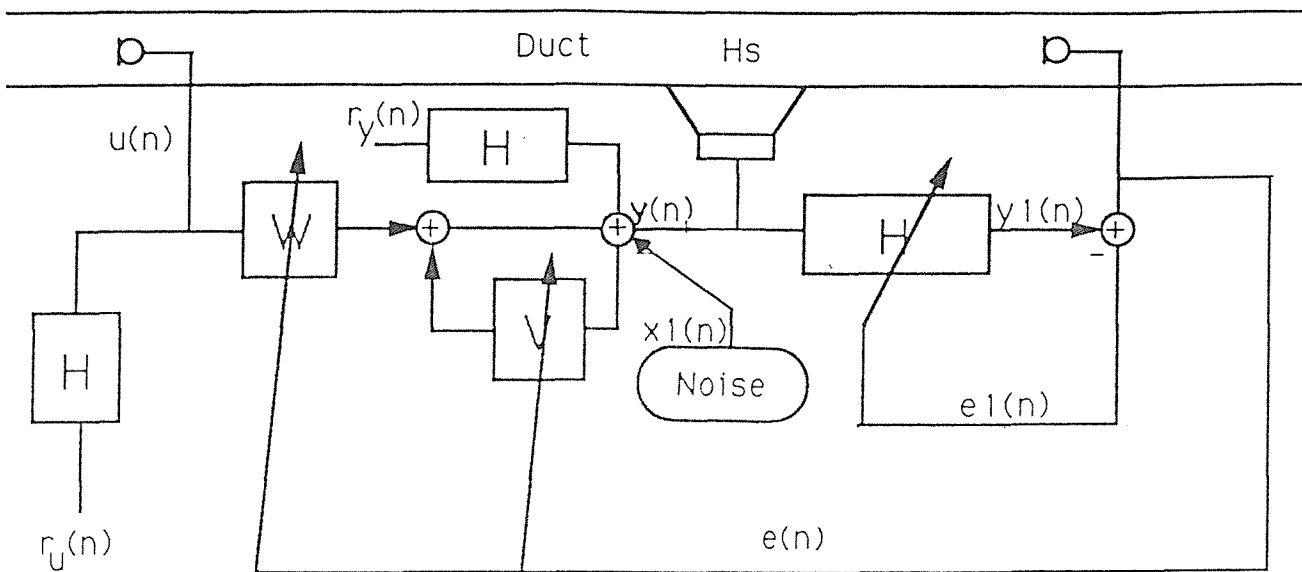
Figure A.3 IIR LMS algorithm : Updating equations

A.4 Technical characteristics

LOUDSPEAKERS

      Primary : *REALISTIC* 8Ω, 4" WOOFER. CAT No. 40-1022A. 55Hz-5kHz
      Secondary : *RS* 8Ω, 6 1/2" BASS LOUDSPEAKER Ø 16.2cm

MICROPHONES

      Detection and Error : *WM-063* omninidirectional electret microphone.

ANTI-ALIASING FILTERS

      KEMO VBF 23 - cutoff frequency : 1000Hz

RECONSTRUCTING FILTERS

      KEMO VBF 23 - cutoff frequency :   1000Hz (primary source)
                                         800Hz(secondary source)

PIEZO-ELECTRIC WIRE

      RAYCHEM (connected to charge amplifier B&K 2635)

DIGITAL SIGNAL PROCESSOR

      TMS320C25 Texas Instrument microprocessor

DIGITAL-ANALOG CARD

      12 bits *LOUGHBOUROUGH Sound Image PCS25 and PC4i2o* cards

B.1 Calculation of the inverse of the ideal controller

The objective of this section is to calculate the impulse response corresponding to the following frequency response :

$$W_i(j\omega) = \frac{-e^{-j\omega l_2/c}}{H_S(j\omega)M_d(j\omega)(1 - e^{-2j\omega l_2/c})}$$ (B.1.1)

Assuming that $H_S(j\omega)$ and $M_d(j\omega)$ are inversible, the impulse response corresponding to $\dfrac{-e^{-j\omega l_2/c}}{H_S(j\omega)M_d(j\omega)}$ is

$$s(t) = h_S^{(-1)}(t) * m_e^{(-1)}(t)) * \delta (t - \frac{l_2}{c})$$ (B.1.2)

It is more difficult to calculate the impulse response corresponding to :

$$R(j\omega) = \frac{1}{1 - e^{-2j\omega l_2/c}}$$ (B.1.3)

This frequency response is periodic and can be rewritten as :

$$R(j\omega) = \frac{1}{1 - e^{-j\omega/\omega_0}}$$ (B.1.4)

with $\omega_0 = c/2l_2$

$R(j\omega)$ can be seen to be as the same as the frequency response of a signal sampled at the angular frequency ω_0 and whose z transform is :

$$R(z) = \frac{1}{1 - z^{-1}} \text{ for } |z| > 1$$ (B.1.5)

Therefore, our problem is to find r(n), the inverse z transform of R(z) .
We know from the literature [41] that the inverse z-transform can be calculated as follows :

$$r(n) = \frac{1}{2\pi j} \int_{(\Gamma)} R(z).z^{n-1}\, dz \qquad\qquad (B.1.6)$$

where (Γ) signifies that we must integrate anti-clockwise on a closed contour in the complex plane around the origin. Using the Cauchy Theorem we can evaluate (B.1.6) by the residues method.

$$r(n) = \frac{1}{2\pi j} \int_{(\Gamma)} R(z).z^{n-1}\, dz = \Sigma \text{ (residues of } R(z).z^{n-1}) \text{ in } (\Gamma) \qquad (B.1.7)$$

We remember that the residue at a pole $z = a$ of order q of the function $R(z).z^{n-1}$ is given by :

$$\text{Res}_a{}^q = \lim_{z \to a} \frac{1}{(q-1)!} \frac{d^{q-1}}{dz^{q-1}} [R(z).z^{k-1}(z-a)^q] \qquad (B.1.8)$$

For a pole of order 1 this expression can be simplified into :

$$\text{Res}_a{}^1 = \lim_{z \to a} [R(z).z^{k-1}(z-a)] \qquad\qquad (B.1.9)$$

We can now calculate the inverse of $R(z)$. Substituing (B.1.5) into (B.1.6) we obtain:

$$r(n) = \frac{1}{2\pi j} \int_{(\Gamma)} \frac{z^{n-1}}{1-z^{-1}}\, dz = \frac{1}{2\pi j} \int_{(\Gamma)} \frac{z^n}{z-1}\, dz \qquad (B.1.10)$$

where (Γ) can be a circle around the unit circle.
For $n \geq 0$ (Γ) contains only a pole of order 1 at $z=1$. Using (B.1.9) we obtain the residue for this pole.

$$\text{Res}_1{}^1 = \lim_{z \to 1} [\frac{z^n}{z-1}(z-1)] = 1 \qquad\qquad (B.1.11)$$

Then, for all $n \geq 0$ $r(n) = 1$

When $n < 0$ the function $\frac{z^n}{z-1}$ has two poles : a pole of order n at $z = 0$ and a pole of order 1 at $z = 1$. The calculation of the residue for the pole of order 1 is identical to (B.1.8) :

$$\text{Res}_1{}^1 = \lim_{z \to 1} \left[\frac{z^n}{z-1} (z-1) \right] = 1 \qquad (B.1.12)$$

The calculation of the residue for the pole of order n is less obvious.

$$\text{Res}_0{}^n = \lim_{z \to 0} \frac{1}{(n-1)!} \frac{d^{n-1}}{dz^{n-1}} \left[z^n \frac{z^{-n}}{z-1} \right] \qquad (B.1.13)$$

$$\text{Res}_0{}^n = \lim_{z \to 0} \frac{1}{(n-1)!} \frac{d^{n-1}}{dz^{n-1}} \left[\frac{1}{z-1} \right] \qquad (B.1.14)$$

since $|z| \ll 1$ we can expand $\frac{1}{z-1}$ into a Taylor series

$$\text{Res}_0{}^n = \lim_{z \to 0} \frac{1}{(n-1)!} \frac{d^{n-1}}{dz^{n-1}} [-(1 + z + z^2 + \ldots + z^n +)] \qquad (B.1.15)$$

Then differentiating the series n-1 times

$$\text{Res}_0{}^n = \lim_{z \to 0} \frac{1}{(n-1)!} [-(n-1)! . - (n)(n-1)(n-2)(\ldots)(2).z - \ldots] = -1 \qquad (B.1.16)$$

Finally for all $n < 0$

$$r(n) = \text{Res}_1{}^1 + \text{Res}_0{}^n = 0 \qquad (B.1.17)$$

and to summarise :

$r(n) = 1$ for all $n \geq 0$

$r(n) = 0$ for all $n < 0$

Then converting the sequence r(n) into the equivalent continouous waveform, we have :

$$r(t) = \sum_{n=0}^{\infty} \delta(t - \frac{2nl_2}{c}) \qquad (B.1.18)$$

and since

$$w_{ideal}(t) = r(t)*s(t)$$

(B.1.18) and (B.1.2) imply that

$$w_{ideal}(t) = (h_s^{(-1)}(t)*m_e^{(-1)}(t)) * \sum_{n=0}^{\infty} \delta(t - \frac{l_2}{c} - \frac{2nl_2}{c}) \qquad (B.1.19)$$

B.2 Instantaneous gradient of the recursive controller In presence of a feedback path.

We seek to establish the expression of the gradient of the instantaneous squared error with respect to the recursive controller weight coefficients. An important assumption to obtain this result is that the controller does not change with time. Such an hypothesis is necessary if we want that the z-transforms to maintain their validity. In practice this assuption is counter to the fact that the controller is adaptive. However we can very often consider that the adaptive process so slow (quasi-static) that the gradient calculation is not affected too much by the dynamics of the adaptive process.

Since the controller has two components we will have two gradients :

$$\phi_i(n) = \frac{\partial e(n)^2}{\partial w_i} = 2.e(n)\frac{\partial e(n)}{\partial w_i} \tag{B.2.1}$$

$$\psi_j(n) = \frac{\partial e(n)^2}{\partial v_j} = 2.e(n)\frac{\partial e(n)}{\partial v_j} \tag{B.2.2}$$

Instead of differentiating the instantaneous error we differentiate the z-transform of the error and then take the inverse z-transform of the result. Because of the linearity of both z-transform and differentiation this is equivalent.

From the block diagram in **figure B.2.1** we can write the z transform of the error as :

$$E(z) = \frac{C(z).W(z)}{1 - F(z).W(z)-V(z)} X(z) + D(z) \tag{B.2.3}$$

so that

$$\frac{\partial}{\partial w_i}(E(z)) = \frac{C(z)(1-V(z))}{[1 - F(z).W(z)-V(z)]^2} z^{-i} X(z) \tag{B.2.4}$$

and since the input to the controller U(z) is related to the reference signal X(z) by :

$$U(z) = \frac{1-V(z)}{1 - F(z).W(z)-V(z)}.X(z) \tag{B.2.5}$$

(B.2.4) and (B.2.5) lead to

$$\frac{\partial}{\partial w_i}(E(z)) = \frac{C(z)}{1 - F(z).W(z)-V(z)} z^{-i} U(z) \tag{B.2.6}$$

similarly for the gradient with respect to the recursive coefficients we have

$$\frac{\partial}{\partial v_j}(E(z)) = \frac{C(z)}{1 - F(z).W(z)-V(z)} z^{-j} Y(z) \tag{B.2.7}$$

Then if we call H the filter whose z-transform is :

$$H(z) = \frac{C(z)}{1 - F(z).W(z)-V(z)} \tag{B.2.8}$$

(B.2.6) and (B.2.7) can be rewritten as :

$$\frac{\partial}{\partial w_i}(E(z)) = H(z). z^{-i} U(z) \tag{B.2.9}$$

$$\frac{\partial}{\partial v_j}(E(z)) = H(z). z^{-j} Y(z) \tag{B.2.10}$$

by taking the inverse z transform of the expressions and using B.2.1 and B.2.2 we have :

$$\phi_i(n) = 2.e(n).h(n)*u(n-i) \tag{B.2.11}$$

$$\psi_j(n) = 2.e(n) h(n)*y(n-j) \tag{B.2.12}$$

If there is no feedback filter v(n) the gradient is only

$$\phi_i(n) = \frac{\partial e(n)^2}{\partial w_i} = 2.e(n)\frac{\partial e(n)}{\partial w_i}$$

and making $V(z) = 0$ in (B.2.8) we have

$$H(z) = \frac{C(z)}{1 - F(z).W(z)} \qquad\qquad (B.2.13)$$

We can then calculate the instantaneous gradient for the transversal controller only :

$$\phi_i(n) = 2.e(n).h(n)*u(n-i) \qquad\qquad (B.2.14)$$
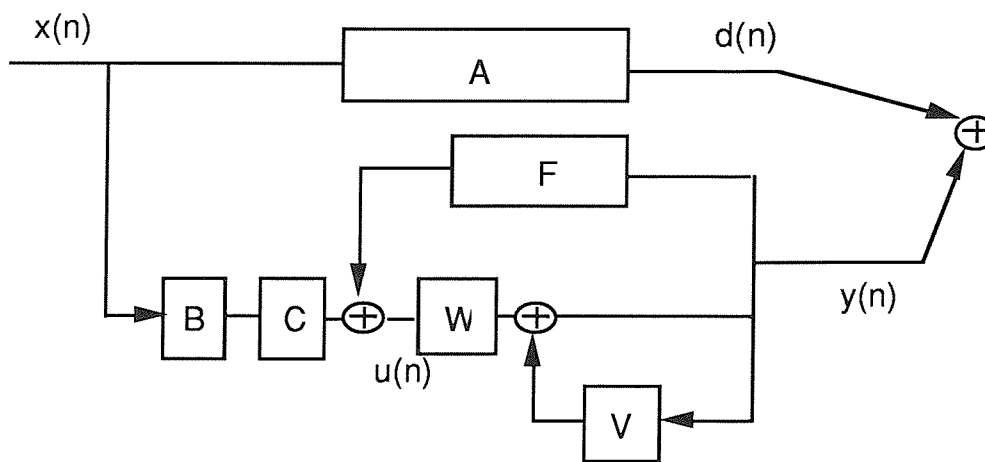

Figure B.2   Notation for the calculation of the instantaneous gradient

REFERENCES

[1]   C. HUYGENS : *"Traité de la lumière."* Leiden, 1690.

[2]   Th. YOUNG : *"Course on lectures on natural philosophy and mechanical arts."* 1807.

[3]   P. LUEG : *"Process of silencing sound oscillations."* U.S. patent 2 043 416, 1934.

[4]   M. JESSEL and G. MAGIANTE : *"Active sound absorbers in air ducts".* Journal of Sound and Vibration. 23-3, pp 383-390, 1972

[5]   J.H POOLE and H.G. LEVENTHALL : *"An experimental study of Swinbank's method of active attenuation of sound in ducts."* Journal of Sound and Vibration. 49-2, pp 257-266, 1976.

[6]   M.A. SWINBANKS : *"The active control of sound propagation in long ducts."* Journal of Sound and Vibration, 27-3, pp 411-436, 1973.

[7]   C.E. ROSS : *"An algorithm for designing a broadband active sound control system."* Journal of Sound and Vibration, 80-3, pp 373-380, 1982.

[8]   C.E. ROSS : *"An adaptive digital filter for broadband active sound control."* Journal of Sound and Vibration, 80-3, pp 381-388, 1982.

[9]   A. ROURE : *"Self-adaptive broadband active sound control system".* Journal of Sound and Vibration. 101-3, pp 429-441. 1985

[10]   R. LA FONTAINE and J. SHEPHERD : *"An experimental study of a broadband active attenuator for cancellation of random noise in ducts."* Journal of Sound and Vibration. 91-3, 351-362, 1983.

[11]   J.C. BURGESS : "*Active adaptive sound control in a duct : a computer simulation*". Journal of the Acoustical Society of America, 70-3, pp 715-726, 1981.

[12]   B. CHAPLIN : "*The cancellation of repetitive noise and vibration*". Proceedings of International Conference on Noise Control Engineering. G.C. Maling Ed, Noise Control Foundation, New York, 1980.

[13]   B. WIDROW and al. : "*Adaptive noise cancelling, principle and applications.*" Proceedings IEEE, 63-12, pp 1692-1716, 1975.

[14]   A. ROURE : "*Derniers developpements de l'attenuation acoustice active au LMA.*" Journées thématiques sur le contrôle acoustique et vibratoire. ENTPE, 16-17 oct 1990.

[15]   L.J. ERIKSSON : "*The development of the filtered-U-algorithm for active noise control.* " 119th meeting of the Acoustical Society of America, May 21-25, University Park, Pennsilvania, 1990.

[16]   L.A POOLE, G.A. WARNAKA, R.C. CUTLER : "*The implementation of digital filters using a modified Widrow-Hoff algorithm for the adaptive cancellation of acoustic noise.* " Proc IEEE, pp 21-7-3,21-7-4 , 1984.

[17]   S.J. ELLIOTT, I. STOTHERS, P. NELSON : "*A multiple error LMS algorithm ans its applications to the active control of sound and vibration.*" IEEE Trans. on acoustic, speech and signal processing. 10, pp1423-1424, oct 1987.

[18]   S.J. ELLIOTT and P. A NELSON : "*Model for describing active noise control in ducts.* " ISVR technical report No. 127 April 1984.

[19]   L.E. KINSLER, A.R. FREY : "*Fundamentals of acoustics,*" Wiley International Editions 1982, p 203.

[20]   D.J. DEFATTA, J.G. LUCAS, W.S. HODGKISS : "*Digital Signal Processing,*" Wiley International Editions 1988, p102.

[21]   M. BELLANGER : *"Traitement Numérique du Signal,"* Masson Editeur 1987 Paris, p362.

[22]   M. SONDHI and D. A. BERKLEY : *"Silencing echoes on the Telephone Network,"* Proc. IEEE, No 68, pp 948-963, 1980.

[23]   A. PAPOULIS : *"Probability, Random variable and Stochastic Processes."* Mc GRAW-HILL Book Company, pp 403-406, 1965.

[24]   B. WIDROW and S. D. STEARNS : *"Adaptive Signal Processing."* PRENTICE HALL : Signal Processing Series, pp 99-115, Chapter 6, 1985.

[25]   S.J FLOCKTON : *"The use of FIR and IIR adaptive filtering system in the active control of acoustic noise."* 32nd Midwest Symposiun on Circuits and Systems, Urbana, Illinois, Aug 1989.

[26]   Kh. EGHTESADI and H.G. LEVENTHALL : *"Active attenuation of noise the monopole system."* Journal of Acoustic Society of America, Vol 71 No-3 , pp 608-610, March 1982.

[27]   L.J. ERIKSSON : *"Active attenuation system with on-line modelling of speaker, error path and feedback path."* U.S. Patent No 4 677 676 (30 June 1987)

[28]   J. J SHYNK : *"Adaptive IIR Filtering."* IEEE ASSP Magazine : pp 5-21, April 1989.

[29]   B. WIDROW and S. D. STEARNS : *"Adaptive Signal Processing."* PRENTICE HALL : Signal Processing Series, pp 154-164, Chapter 8, 1985.

[30]   C.R. JOHNSON : *"Lectures on Adaptive Parameter Estimation,."* PRENTICE HALL : Advanced Reference Series, pp 16-21, 1988.

[31]   S. ERIKSSON : *"Active Sound Attenuation Using Adaptive Digital Signal Processing Techniques."* Ph. D thesis, University of WISCONSIN-MADISON, 1985.

[32]   P.L. FEINTUCH   : "*An adaptive recursive LMS filter.*" Proc IEEE, Vol 64, No-11, pp 1622-1624, Nov.1976

[33]   C. R. JOHNSON and M.G. LARIMORE   : "*Comments on and Additions to " An adaptive Recursive Filter""* Proc IEEE, Vol 65, No-9, pp 1399-1401, Sept. 1977

[34]   B. WIDROW and J. Mc COOL   : "*Comments on " An Adaptive Recursive LMS Filter" "* Proc IEEE, Vol 65, No-9, pp 1402-1404, Sept. 1977

[35]   M. A. SWINBANKS : "*The active control of low-frequency sound in a gas turbine compressor installation*". Proc. Inter-Noise 82, pp 423-426, 1982

[36]   S. J. FLOCKTON : "*Gradient-based adaptive algorithms for systems with external feedback paths.*", IEEE Proceedings-F, Vol. 138, No. 4, Aug. 1991

[37]   P. SJOSTEN and P. ERIKSSON: "*Efficient filter structure for active noise, LMS controllers*", Mechanichal Systems and Signal Processing,Vol. 5(1), pp. 45-50, 1991.

[38]   S. D. SNYDER and C. H. HANSEN : "*The influence of transducer transfer function and acoustic time delay on the implementation if the LMS algorithm in active noise control systems*", Journal of Sound and Vibration, Vol. 141(3), pp 409-424, 1990.

[39]   S. J. FLOCKTON : "*Error surfaces of adaptive noise controllers*", ICASSP Vol D10.5, pp 2081-2084, 1991.

[40]   A. R. BRISCOE and R. J. PINNINGTON "*Fluid Borne Vibration in Pipes*", ISVR internal Report No 89/20. May 1989.

[41]   M. KUNT "*Traitement numérique des signaux*", Traité d'électricité, d'électronique et d'électrotechnique. Editions DUNOD, 1981.

[42]   A. H. GRAY and J. D. MARKEL "*Digital lattice and ladder filter synthesis*", IEEE trans. Audio Electroacoust., vol. AU-21, pp. 492-500, Dec. 1973.

[43]   I. L. ALAYA *"On a new adaptive lattice algorithm for recursive filters"*,
         IEEE Transactions on acoustics, speech, and signal processing. Vol.
         ASSP-30, No. 2, pp.316-319, April 1982.

[44]   D. PARIKH, N. AHMED and S. D. STEARNS *"An adaptive lattice
         algorithm for recursive filtters*, IEEE Transactions on acoustics, speech,
         and signal processing. Vol. ASSP-28, No. 1, pp.110-111, Febr. 1980.